ORIGINAL RESEARCH

DNA Methyltransferase 1–Dependent DNA Hypermethylation Constrains Arteriogenesis by Augmenting Shear Stress Set Point

Joshua L. Heuslein, PhD; Catherine M. Gorick, BS; Ji Song, PhD; Richard J. Price, PhD

***Background*—**Arteriogenesis is initiated by increased shear stress and is thought to continue until shear stress is returned to its original "set point." However, the molecular mechanism(s) through which shear stress set point is established by endothelial cells (ECs) are largely unstudied. Here, we tested the hypothesis that DNA methyltransferase 1 (DNMT1)–dependent EC DNA methylation affects arteriogenic capacity via adjustments to shear stress set point.

***Methods and Results*—**In femoral artery ligation–operated C57BL/6 mice, collateral artery segments exposed to increased shear stress without a change in flow direction (ie, nonreversed flow) exhibited global DNA hypermethylation (increased 5-methylcytosine staining intensity) and constrained arteriogenesis (30% less diameter growth) when compared with segments exposed to both an increase in shear stress and reversed-flow direction. In vitro, ECs exposed to a flow waveform biomimetic of nonreversed collateral segments in vivo exhibited a 40% increase in DNMT1 expression, genome-wide hypermethylation of gene promoters, and a DNMT1-dependent 60% reduction in proarteriogenic monocyte adhesion compared with ECs exposed to a biomimetic reversed-flow waveform. These results led us to test whether DNMT1 regulates arteriogenic capacity in vivo. In femoral artery ligation–operated mice, DNMT1 inhibition rescued arteriogenic capacity and returned shear stress back to its original set point in nonreversed collateral segments.

***Conclusions*—**Increased shear stress without a change in flow direction initiates arteriogenic growth; however, it also elicits DNMT1-dependent EC DNA hypermethylation. In turn, this diminishes mechanosensing, augments shear stress set point, and constrains the ultimate arteriogenic capacity of the vessel. This epigenetic effect could impact both endogenous collateralization and treatment of arterial occlusive diseases. **(*J Am Heart Assoc*. 2017;6:e007673. DOI: 10.1161/JAHA.117.007673.)**

Key Words: endothelial shear stress • epigenetics • peripheral artery disease • collateral • vascular biology

Collateral arteriogenesis, the growth of existing arterial vessels to a larger diameter, is a fundamental adaptive response that is often critical for the perfusion and survival of tissues downstream of chronic arterial occlusion(s). Arterial occlusion(s) create steep pressure gradients and increased flow along collateral arterial pathways bypassing the occlusion(s). The resulting increase in shear stress acting on the endothelium initiates a highly coordinated signaling cascade, ultimately resulting in the outward growth of the collateral vessel.[1,2] Outward luminal growth is hypothesized to continue until normalization to the original shear stress level (ie, the shear stress "set point") has been achieved.[2–5]

In addition to shear stress magnitude, however, other hemodynamic factors can influence arteriogenesis. Indeed, we have recently demonstrated that collateral artery segments exposed to both a 2-fold increase in shear stress magnitude and reversed flow direction (ie, "reversed" flow segments) following femoral artery ligation (FAL; flow direction) in mice exhibit amplified arteriogenesis, whereas segments experiencing just a 2-fold increase in shear stress magnitude (ie, "nonreversed" flow segments) exhibit a substantially more constrained extent of arteriogenesis.[6] Furthermore, this difference in arteriogenic capacity was maintained up to 12 weeks following FAL. Importantly, these collateral artery segments start at the same basal diameter and shear stress magnitude before FAL, suggesting that shear stress set point may be altered because of differential hemodynamics post FAL.

From the Department of Biomedical Engineering, University of Virginia, Charlottesville, VA.

Accompanying Tables S1 through S6 and Figures S1 through S8 are available at http://jaha.ahajournals.org/content/6/12/e007673/DC1/embed/inline-supplementary-material-1.pdf

Correspondence to: Richard J. Price, PhD, Department of Biomedical Engineering, University of Virginia, Box 800759, Health System, Charlottesville, VA 22908. E-mail: rprice@virginia.edu

Received September 21, 2017; accepted October 23, 2017.

Clinical Perspective

What Is New?

- Collateral arterioles exposed to an increase in shear stress without a change in flow direction exhibit constrained arteriogenesis, an augmented shear stress set point, and DNA hypermethylation.
- In vitro, endothelial cells exposed to an increase in shear stress without a change in flow direction exhibit increased DNA methyltransferase 1 (DNMT1) expression, hypermethylation of gene promoters, and a DNMT1-dependent reduction in monocyte adhesion.
- Pharmacological inhibition of DNMT1 in vivo restores arteriogenic capacity and returns shear stress back to its original set point.

What Are the Clinical Implications?

- Modulation of the shear stress set point by DNMT1 inhibition could represent a therapeutic strategy for treating arterial occlusive diseases.
- By focusing on the molecular mechanisms regulating the maturation stage of arteriogenesis, as opposed to initiation and growth stages, such an approach could better account for the chronic nature of arterial occlusive diseases in humans.
- DNMT1 inhibition may avoid the so-called Janus phenomenon, which refers to the conundrum created by the fact that proarteriogenic therapies also tend to promote atherosclerosis.

Although critical in determining ultimate arteriogenic capacity, the molecular mechanism(s) involved in establishing and maintaining the shear stress set point remain unknown. Epigenetic mechanisms, such as DNA methylation, histone modifications, and noncoding RNA regulation, could be a way for local hemodynamics to regulate long-term gene expression changes.[7] Of these epigenetic mechanisms, DNA methylation is considered the most stable.[8,9] DNA is methylated at a cysteine base pair, most often at a CpG dinucleotide (CpG site).[9] Methylation of CpG sites in the promoter region of a gene is commonly associated with repression of gene expression.[10–12] DNA methylation occurs through the activity of DNA methyltransferases (DNMTs), particularly DNMT1 postdevelopment.[13–15] Recently, DNA methylation has been shown to differentially regulate flow-mediated endothelial gene expression through DNMT1,[16–19] although the role of DNA methylation in the regulation of arteriogenesis has not been explored. Here, using our previous observations of differential arteriogenic capacity within collateral artery segments in vivo as a basis, we tested the central hypothesis that an augmented shear stress set point constrains arteriogenic capacity via DNMT1-dependent endothelial cell (EC) DNA hypermethylation.

Materials and Methods

The authors declare that all supporting data are available within the article and its online supplementary files.

Mice

All animal protocols were approved by the Institutional Animal Care and Use Committee at the University of Virginia (protocol 3814) and conformed to all regulations for animal use outlined in the American Heart Association Guidelines for the Use of Animals in Research. Male C57BL/6 mice and Balb/c were purchased from Charles River Laboratory. All animals were housed in the animal facilities at the University of Virginia. C57BL/6 mice were used for all studies unless otherwise noted.

FAL Model

We used a previously detailed FAL scheme[6,20,21] that produces consistent arteriogenesis in the collateral arteries of the gracilis adductor muscles,[6,22–27] along with minimal heterogeneity in the baseline collateral structure and known changes in flow direction from baseline. Male mice (10 to 12, 20 to 21, or 70 to 80 weeks of age for C57BL/6, Balb/c, and aged Balb/c studies, respectively) were anesthetized (intraperitoneal [IP] 120 mg/kg ketamine, 12 mg/kg xylazine, and 0.08 mg/kg atropine), depilated, and prepped for aseptic surgery. On the left leg, an incision was made directly above and along the femoral artery, which was gently dissected from the femoral vein and nerve between the bifurcation of the superior epigastric artery and popliteal artery. Two 6.0 silk sutures were placed immediately distal to the epigastric artery, which served as the origin of the muscular branch artery in all mice, and the artery segment between the 2 ligatures was then severed with microdissecting scissors. The surgical site was then closed with 5.0 prolene sutures. A sham surgery, wherein the femoral artery was exposed but not ligated, was performed on the right hindlimb (ie, on the other leg). Animals received 1 injection of buprenorphine for analgesia at the time of surgery and a second dose 8 to 12 hours later.

Muscular Branch Ligation Model

Male mice were anesthetized (IP 120 mg/kg ketamine, 12 mg/kg xylazine, and 0.08 mg/kg atropine), depilated, and prepped for aseptic surgery. On the left leg, an incision was made directly above and along the femoral artery. The muscular branch artery was gently dissected from the paired vein and ligated with one 6.0 silk suture just distal to the epigastric artery. The surgical site was then closed with 5.0 prolene sutures. A sham surgery, wherein the muscular

branch artery was exposed but not ligated, was performed on the right hindlimb (ie, on the other leg). Animals received 1 injection of buprenorphine for analgesia at the time of surgery and a second dose 8 to 12 hours later.

5AZA Treatment

5-Aza-2′-deoxycytidine (5AZA) (#A3656; Sigma) was reconstituted in dimethyl sulfoxide (DMSO) to a stock concentration of 0.25 mg/μL. Each day immediately before use, stock 5AZA was diluted to 1.25 μg/μL and DMSO to 0.01% DMSO in sterile saline. Both solutions were then passed through a 0.22-μm sterile syringe filter. Mice were treated daily with an IP injection of 0.1 mg/kg 5AZA in sterile saline or 0.01% DMSO in a total volume of 100 μL.

Laser Doppler Perfusion Imaging

For monitoring blood flow recovery and postsurgical ischemia, mice were anesthetized via 1.5% isofluorane under constant oxygen. Mice were placed in a prone position and the soles of the feet were scanned (PeriCam PSI, PeriMed). Mean foot perfusion was used to calculate relative perfusion ratio (ligated/unligated).

Quantification of Global DNA Methylation by HRM

Methylation of genomic repeat elements, such as long interspersed nuclear element-1 (LINE1), have been used as markers of global genomic DNA (gDNA) methylation.[8,28,29] LINE1 methylation in the peripheral blood was therefore used as an indicator of the efficacy of our 5AZA treatment protocol on DNA methylation in vivo. Peripheral blood (100–150 μL) was collected retro-orbitally with heparinized capillary tubes from mice 7 days after beginning daily 5AZA or DMSO IP injections. gDNA was immediately extracted using the Quick-gDNA MiniPrep Kit (#D3006; Zymo Research) and gDNA (80 ng) underwent bisulfite conversion using the EZ-DNA Methylation-Gold kit (#D5005; Zymo Research) according to manufacturer's instructions. Polymerase chain reaction (PCR) and high-resolution melting (HRM) analysis were adapted from a previously determined protocol.[28] Briefly, modified DNA was diluted to 10 ng/μL with nuclease-free water. A 20-μL reaction mix of 20 ng bisulfite modified DNA and a final concentration of 1x EpiTect HRM Master Mix (#59445; Qiagen), 0.75 μmol/L LINE1 forward primer (5′-GTTGAGGTAGTATTTTGTGTGGGTT-3′), 0.75 μmol/L LINE1 reverse primer (5′-TCCAAAAACTAT-CAAATTCTCTAACAC-3′), and nuclease-free water. PCR cycling conditions for LINE1 were 95°C for 5 minutes followed by 40 cycles of 95°C for 20 seconds then 55°C for 30 seconds then 72°C for 20 seconds. Melt analysis occurred from 60°C to 90°C rising by 0.1°C/5 s. PCR and HRM were performed on a CFX96 Real-Time Detection System (Bio-Rad) and each sample was run in duplicate.

Differences in DNA methylation as detected by HRM were quantified by the net temperature shift as previously calculated.[28] Briefly, the net temperature shift was calculated as average distance between the normalized melt curves of experimental samples from a universal methylated positive control (#D5012; Zymo Research) where a more negative net temperature shift indicates a less methylated sample. For LINE1, the 2 normalization regions used were between 72°C and 73°C and 82°C and 83°C.

Tissue Harvesting for Whole-Mount Vascular Casting and Cross-Sectional Analysis

For analysis of luminal diameters in the gracilis collateral arteries and to enable sectioning at specific regions, vascular casting was performed using an opaque polymer that allows for accurate luminal diameter measurements.[24] At the determined point of harvest after FAL, mice were anesthetized (IP 120 mg/kg ketamine, 12 mg/kg xylazine, and 0.08 mg/kg atropine) and euthanized via an overdose of pentobarbital sodium and phenytoin sodium (Euthansol, Virbac), and then the abdominal aorta was cannulated. The lower body was then perfused with 7 mL of 2% heparinized saline with 2 mmol/L adenosine (16404; Fisher Scientific) and 0.1 mmol/L papaverine (P3510; Sigma-Aldrich) to clear and vasodilate the downstream vasculature at a constant rate of 1 mL/min (PHD2000; Harvard Apparatus). Once perfused, we waited 5 minutes to enable vasodilation. Tissues were then perfused with 3 mL of 4% paraformaldehyde solution (19943; Affymetrix) at 1 mL/min and allowed to fix for 10 minutes. The lower body was then perfused with 0.8 mL of Microfil casting agent (FlowTech, Inc) at a constant speed of 0.15 mL/min. Viscosity of Microfil was adjusted to minimize transport across capillaries. After curing for 1.5 hours at room temperature, gracilis muscles were dissected free and then cleared in 50% glycerol in PBS overnight. Cleared tissues were mounted between 2 coverslips using 500-μm thick spacers (645501; Grace Bio-Labs Inc) to keep constant thickness between muscles. Muscles were imaged using transmitted light at 4× magnification on a Nikon TE200 inverted microscope with a charge-coupled device camera (Quantifier, Optronics Inc). Individual fields of view were montaged together (Photoshop CS2; Adobe Systems Inc).

For analysis of luminal diameters from intact gracilis collateral whole mounts (ie, vascular casting), collateral entrance regions were defined according to the following method. A cropped portion (560 μm×560 μm) of the montaged image (previously randomized and deidentified) was taken of the collateral artery at the first visible branch point of a terminal arteriole from the primary collateral as it extended from either the muscular branch or saphenous artery as previously

described.[6] After each cropped image region was taken, all images were randomized and deidentified. The mean diameter was then taken from 4 or 5 separate diameter measurements along the length of the cropped portion of the collateral artery.

After imaging, muscles were rehydrated, cut, and then paraffin embedded for cross-sectional analysis at the muscular branch and saphenous artery entrance regions to the collateral arteries. Resulting cross-sections were rehydrated and immunolabeled for 5-methylcytosine (84 days post FAL) or hematoxylin-eosin stained for collateral artery structure analysis (day 28 post FAL).

Immunofluorescence Labeling of 5-Methylcytosine

Sections (5-μm thickness) of paraffin-embedded muscle from the muscular and saphenous regions were rehydrated and subjected to heat-mediated antigen retrieval for 20 minutes in a citrate-based antigen retrieval buffer (H-3300; Vector Laboratories). After cooling, tissues were encircled with a hydrophobic barrier pen and blocked with PBS+0.1% saponin+ 2% bovine serum albumin (Jackson Immunoresearch) for 1 hour at room temperature. Tissues were then incubated overnight at 4°C with anti-5-methylcytosine (1:100; BI-MECY, Eurogentec) and rat anti-CD31 (1:75; SZ31, Dianova). Following primary antibody incubation, slides were washed in PBS then incubated with DRAQ5 (a nuclear marker), a donkey-anti-mouse Cy3 F_{ab} (1:200; Jackson Immunoresearch), and a goat-anti-rat-488 secondary antibody (1:200; Jackson Immunoresearch) for 1 hour at room temperature. Following incubation, slides were washed again in PBS, mounted with Prolong Gold (Life Technologies) to minimize photobleaching, allowed to cure overnight, and imaged using a Nikon TE2000 C1 laser scanning confocal microscope with a 20× oil objective. All settings were held constant throughout imaging. Cropped fields of view (200 μm×200 μm) encompassing the collaterals in each region were randomized and deidentified. The collateral diameter, nuclear area, raw integrated density, and nuclear raw integrated density of 5-methylcytosine (5-mC) within an individual cross-section were determined in Fiji.[30] For each mouse, mean collateral diameter, nuclear 5-mC raw integrated density per nuclear area and 5-mC positive area per total nuclear area was calculated from the average of the 2 primary gracilis collateral arteries, with 2 immunolabeled sections per collateral artery for a total of 4 images per mouse.

Cross-Sectional Analysis of Collateral Artery Structure

Sections (5-μm thickness) of paraffin-embedded muscle from the muscular and saphenous regions were labeled for hematoxylin and eosin. Individual fields of view encompassing the collateral vessels were imaged with a 40× water objective on a Zeiss inverted microscope (Zeiss Axioskop) with a charge-coupled device camera (Quantifier, Optronics Inc). All images were randomized and deidentified before analysis. Luminal diameter, wall area, and wall thickness were determined using Fiji.[30]

Human Umbilical Vein Endothelial Cell Culture

Human umbilical vein ECs (HUVECs) purchased from VEC Technologies Inc. were thawed and maintained on 0.1% gelatin-coated flasks in M-199 medium (Lonza), supplemented with 10% fetal bovine serum (Life Technologies Inc), 100 U/mL penicillin-G + 100 μg/mL streptomycin (Life Technologies Inc), 2 mmol/L L-glutamine (Life Technologies Inc), 5 μg/mL EC growth supplement (Biomedical Technologies), and 10 μg/mL heparin (Sigma-Aldrich). HUVECs are both phenotypically consistent and one of the most extensively used cell culture models for study of flow-mediated EC signaling, including numerous studies of flow responses of the arterial system[17,31–41] (eg, atheroprone versus atheroprotective waveforms) and DNMT1-dependent DNA methylation.[17,18] For each set of experimental comparisons, cells were used from the same cell line between subculture passages 2 to 3.

In Vitro Exposure of Endothelial Cells to Biomimetic Shear Stress Waveforms

HUVECs were plated on cell culture–grade plastic dishes coated with 0.1% gelatin and grown to confluence. A cone and plate flow apparatus,[39] which maintains cells at 5% CO_2 and 37°C, was used to induce a shear stress protocol. The applied shear stress protocol consisted of a 24-hour preconditioning period at a steady shear stress of 15 dyne/cm^2, which was then either increased to 30 dynes/cm^2 (nonreversed flow) or increased to 30 dynes/cm^2 and reversed in direction (reversed flow) to simulate relative hemodynamics previously quantified in our in vivo FAL model.[42] Fresh culture media consisting of M199 with 4% dextran from *Leuconostoc* spp (Sigma-Aldrich, M_r ≈500 000), 2% fetal bovine serum, 100 U/mL penicillin-G + 100 μg/mL streptomycin, 2 mmol/L L-glutamine, 5 μg/mL EC growth supplement, and 10 μg/mL heparin was added to cells before exposure to shear stress and was continuously exchanged throughout the duration in the cone and plate apparatus.

HUVEC RNA Isolation and Quantitative Reverse Transcriptase PCR

Total RNA was extracted with the PureLink total RNA purification system using the on-column DNase protocol (Life Technologies Inc) according to manufacturer's instructions.

RNA concentration and purity were determined with a NanoDrop spectrophotometer (Thermo Fisher Scientific) in duplicate. For quantitative reverse transcriptase PCR, 500 ng of total RNA was reverse transcribed using the iScript cNDA synthesis kit (Bio-Rad). A reaction mixture of 12.5 ng of reverse-transcribed cDNA, DNMT1 forward primer (TGCCAGCTGAGCGTGGTGGT), DNMT1 reverse primer (GCATGCGGGCAGCCACCAAT), and FastStart SYBR Green (Roche Applied Sciences) underwent quantitative reverse transcriptase PCR on a CFX96 Real-Time Detection System (Bio-Rad). Expression was normalized to β2-microglobulin (forward 5′-AGCATTCGGGCCGAGATGTCT-3′, reverse 5′-CTGCTGGATGACGTGAGTAAACCT-3′), which is endogenously expressed and is not altered by many stimuli including shear stress.[36] Normalized expression was quantified using the comparative $2^{\Delta\Delta Ct}$ method.

RRBS and mRNA-Seq

Total gDNA and total RNA were extracted from flow-exposed HUVECs using the Quick-gDNA MiniPrep Kit (#D3006; Zymo Research) and the Quick-RNA MiniPrep Kit (#R1054; Zymo Research) according to manufacturer's instructions. Total gDNA and total RNA concentration and purity were determined with a NanoDrop spectrophotometer in duplicate. Both gDNA and RNA were isolated from the same plate of cells for each condition within an experiment. Purified gDNA and purified total RNA isolated from flow-exposed HUVECs were pooled from 2 independent flow experiments. Pooled gDNA samples were sent to Zymo Research where DNA fragmentation, library preparation, bisulfite conversion, next-generation sequencing, and bioinformatics were performed. Pooled RNA samples were also sent to Zymo Research where they performed mRNA sequencing (mRNA-Seq). HiSeq 50 bp singleton reads from RNA-Seq were first adaptor trimmed and then analyzed using TopHat and Cufflinks software. TopHat (version 2.2.0) was used for alignment of short read to the human genome hg19. Cufflinks (version 2.2.0) was used to transcript assembly and differential expression. CommeRbund (version 2.0.0) was used for visualization of differential analysis. Default parameters were used in all instances.

RRBS Analysis

Reduced representation bisulfite sequencing (RRBS) next-generation sequencing reads were mapped to the "Feb. 2009 (GRCh37/hg19)" genome assembly by Zymo Research. The % CpG methylation was calculated as the percent of methylated CpG sites per total CpG sites in a given differentially methylated region (DMR) with ≥10x CpG coverage in a given DMR. Significance was determined using a Fisher exact test then applying a Benjamini-Hochberg procedure to find false discovery rate. DMRs with ≥10× CpG coverage in their promoter regions (transcription start site ±1 kb) were considered significant if the false discovery rate was <0.1 and the absolute value of %CpG methylation of a DMR in N minus the %CpG methylation of a DMR in R was ≥10%. We then compared this list of significant DMRs with our mRNA-Seq data set to determine genes with relative gene expression changes that correspond to their methylation status between shear stress conditions, ie, identify genes upregulated in N conditions that also have a significantly hypomethylated promoter region as well as genes that are downregulated in N conditions that have hypermethylated promoter regions compared with in R conditions. Only genes demonstrating this relative gene expression-methylation correlation were used for gene ontology analysis using MSigDB[43] from the Broad Institute.

Transillumination Laser Speckle Imaging and Shear Stress Analysis

Transillumination laser speckle imaging was performed as previously described.[42] Briefly, 28 days after FAL, mice were anesthetized (IP 120 mg/kg ketamine, 12 mg/kg xylazine, and 0.08 mg/kg atropine), depilated, and prepped for aseptic surgery. On the left leg (ligated leg), an incision was made above and along the femoral artery such that a window of skin was dissected free and retracted directly above the superficial adductor muscles. Exposed tissue was superfused throughout the procedure and during imaging with a warmed solution of Tris-$CaCl_2$ (0.1 g/L $CaCl_2$) with 2 mmol/L adenosine (16404; Fisher Scientific) and 0.1 mmol/L papaverine (P3510; Sigma-Aldrich). To image the gracilis muscle, the mouse was placed supine on an intravital microscope stage (Zeiss Axioskop). A 30mW, 658-nm laser diode (LPM658-30; Newport Corporation) was coupled to a fiber optic cable and placed beneath the mouse in a transillumination orientation. A cooled, monochrome charge-coupled device camera (Optonics Quantifier) was used to acquire the raw speckle images using a 4× air objective (Zeiss Acroplan LD NA=0.1). The objective and camera were chosen to ensure satisfaction of the Nyquist sampling criteria of at least 2 pixels per individual speckle.[27] An objective mounted fiber optic light guide allowed for brightfield imaging to enable luminal diameter measurements (A08650; Schott Inc). For each field of view, a sequence of 20 12-bit raw speckle images was acquired with a 5-ms exposure time to capture average velocity over multiple cardiac cycles.

All processing of raw speckle images was performed using Fiji[30] as previously described.[42] Briefly, raw speckle images were converted to laser speckle flow index maps, removing any images with excessive motion artifact. To then account for the influence of whole background tissue variations, the processed flow images were normalized to median

background intensity. Individual flow images were then merged into larger 2-dimensional maps using Adobe Photoshop (CS2, Adobe Systems Inc). Finally, to allow for comparison of velocity change across experiments, vessel speckle intensity was normalized to the background tissue according to equation 1 to obtain the normalized speckle index.

$$\text{normalized speckle index} = \frac{\text{speckle intensity}_{\text{vessel}}}{\text{speckle intensity}_{\text{background}}} - 1 \quad (1)$$

Blood velocity analysis of laser speckle images was limited to defined muscular branch and saphenous collateral artery regions and assumed Poiseuille flow. The mean speckle shear rate in each region was calculated using the normalized speckle index and vessel diameter according to equation 2:

$$\text{speckle shear rate} \propto \frac{\text{normalized speckle index}}{\textit{diameter}} \quad (2)$$

Small interfering RNA Transfection in HUVECs

Twenty-four hours before exposure of HUVECs to flow conditions, HUVECs were plated without antibiotics on 0.1% gelatin-coated plates in serum-free M199 (Life Technologies) supplemented with 10% fetal bovine serum, 2 mmol/L L-glutamine, 5 μg/mL EC growth supplement (Biomedical Technologies), and 10 μg/mL heparin (Sigma-Aldrich). After cells were allowed to adhere for 2 hours after plating, cells were transfected with either 120 pmol of ON-TARGETplus SMARTpool human DNMT1 small interfering RNA (L-004605-00-0005; GE Dharmacon) or 120 pmol of ON-TARGETplus nontargeting small interfering RNA (D-001810-10-05; GE Dharmacon) in 52 μL of Oligofectamine transfection reagent (Life Technologies) and 6.8 mL Opti-MEM media (Life Technologies) for 5 hours at 37°C. After 5 hours, plates were flooded with 8 mL of M199 media without antibiotics supplemented with 10% fetal bovine serum + L-glutamine + 5 μg/mL EC growth supplement (Biomedical Technologies) and 10 μg/mL heparin (Sigma-Aldrich). Twenty-four hours posttransfection this solution was aspirated off and normal flow media was applied. Validation of transfection was performed on HUVEC plates (54 hours posttransfection) via DNMT1 Western blotting.

Western Blot Analysis

HUVECs were lysed in radioimmunoprecipitation assay buffer (Sigma-Aldrich, #R0278) with protease inhibitor (Sigma, 1:50, #P8340). Samples were then cleared for 30 minutes at 4°C under constant agitation. Samples were centrifuged for 1 minute at 10 000*g*, the supernatant was collected, and a Pierce BCA assay (ThermoFisher Scientific, #23225) was used to determine total protein concentration. Samples were diluted 1:1 in 2× Laemmli sample buffer (Bio-Rad, #1610737) with β-mercaptoethanol (1:200) and boiled for 10 minutes. Equal protein was loaded onto a 10% SDS-PAGE gel and blotted on a nitrocellulose membrane. After transfer, membranes were blocked for 1 hour at room temperature with Odyssey Blocking Buffer (LICOR, #927-40000) and then incubated with primary antibodies overnight at 4°C. Western blots were performed by using primary antibodies directed against DNMT1 (Abcam, 1:1000, ab92314) and GAPDH (EMD Millipore, 0.0625 μg/mL, #AB2302). Secondary antibodies were purchased from LICOR and used at a 1:10 000 dilution. A LICOR Odyssey imager was used for blot image acquisition and densitometry analysis.

Monocyte Adhesion Functional Assay

Human-derived monocytes (THP-1 cell line) were purchased from the ATCC. Monocytes were unthawed and maintained in RPMI 1640 (Life Technologies, #11875-093) + 10% fetal bovine serum (Life Technologies Inc) + 0.05 mmol/L β-mercaptoethanol per ATCC culture instructions. Monocytes subcultured once cell density approached 800 000 cells/mL. Cells were used between passages 2 to 6.

Before the adhesion assay, cells were counted to obtain 3 000 000 cells per plate of HUVECs. Cells were pelleted, washed with PBS, pelleted, and then resuspended in serum-free RPMI media at 1 000 000 cells/mL. Thawed calcein AM was added at 1 μg/mL and incubated with cells for 15 minutes at 37°C. After 15 minutes, the reaction was stopped by adding excess serum-free RPMI to the cell solution then pelleted. Cells were washed once with serum-free M199 media, pelleted, and then resuspended in serum-free M199 at 500 000 cells/mL. Immediately following completion of flow exposure to HUVECs, flow media was removed by aspiration. HUVECs were quickly washed with serum-free M199 media. This media was then aspirated off and 6 mL of serum-free M199+monocytes (3 000 000 cells per plate) were added to and incubated with HUVECs for 30 minutes at 37°C. Following the 30 minutes, cells were washed twice with PBS to remove unbound monocytes. Adhered monocytes and HUVECs were fixed with 4% PFA for 10 minutes followed by 2 washes with PBS. Coverslips were mounted with Prolong Gold (Life Technologies). Plates were then imaged using a Nikon TE2000 C1 laser scanning confocal microscope. Randomly selected fields of view (8-9) per condition for 3 independent experiments were obtained. Images were then deidentified and randomized in MATLAB. Images were converted to 8-bit images, set to an equivalent threshold, and bound monocytes were quantified using Fiji's Analyze Particles tool (20 μm^2 minimum particle size). Results were centered on the mean of all conditions within each independent experiment.

Immunofluorescence Labeling of Pericollateral Mac3$^+$ Cells

Sections (5-μm thickness) of paraffin-embedded muscle from the muscular and saphenous regions were rehydrated and subjected to heat-mediated antigen retrieval for 10 minutes in a citrate-based antigen retrieval buffer (Vector Laboratories; H-3300). Slides were then quenched of endogenous peroxidase activity with a 30-minute incubation in 3% H_2O_2, blocked, and labeled with rat-anti-Mac3 (1:100, M3/4 clone, 550292; BD Biosciences) overnight at 4°C. Slides were washed and incubated with a biotinylated sheep-anti-rat secondary antibody (Abcam, ab6851, 1:500) for 1 hour at room temperature. Slides were washed and incubated with an avidin-biotin complex (Vectastain ABC solution, Vector Laboratories) for 30 minutes at room temperature. Slides were washed and incubated with a Tyramide Signal Amplification reagent (Perkin Elmer; 1:50) for 10 minutes at room temperature. Slides were washed and incubated with streptavidin-488 (Life Technologies Inc; 1:500), Cy3-anti-SMA (1A4 clone, Sigma; 1:1000) and DRAQ5 (Thermo Scientific Inc; 1:1000). Slides were then mounted with Prolong Gold (Life Technologies Inc) to minimize photobleaching, allowed to cure overnight, and imaged using a Nikon TE2000 C1 laser scanning confocal microscope with a 20× oil objective. Cropped fields of view (512×512 pixels) encompassing the collaterals in each region were randomized and deidentified. The pericollateral region was outlined (25 microns around the vessel) and pericollateral Mac3$^+$ nuclei were counted in Fiji.[30]

Statistical Analyses

All results are reported as mean±SEM, unless otherwise noted. All data for group comparisons were first tested for normality and equal variance; no significant deviations from these assumptions were found. Statistical significance was then assessed by Student *t* test or a 2-way ANOVA followed by a Holm-Sidak multiple comparisons test, unless otherwise noted (SigmaStat 3.5, Systat Inc). Significance was assessed at $P<0.05$.

Results

Collateral Artery Segments Exposed to an Increase in Shear Stress, Without a Change in Flow Direction, Exhibit DNA Hypermethylation, and Constrained Arteriogenic Capacity

Using an FAL model identical to that employed previously by our group to demonstrate differential arteriogenesis at either end of gracilis collateral arteries (Figure 1A), we first sought to determine whether these two collateral artery regions displayed differential EC DNA methylation. To this end, we immunolabeled collateral artery cross-sections for 5-mC, a marker of DNA methylation, along with EC (CD31) and nuclear (DRAQ5) counterlabels (Figure 1B). These cross-sections confirmed our previous findings[6] that muscular region (nonreversed flow) collateral artery segments grow to a smaller diameter when compared with collateral segments in the saphenous (reversed flow) region at 12 weeks post FAL (Figure 1C). Nuclear 5-mC staining intensity (Figure 1D) and total 5-mC+ staining area per nuclear area (Figure 1E) were significantly increased in muscular (nonreversed flow) segments compared with both saphenous (reversed flow) segments and unligated controls.

ECs Exposed to a Nonreversed Increase in Shear Stress Magnitude Exhibit Augmented DNMT1 Expression

To further investigate the influence of these FAL-elicited hemodynamic changes on EC DNA methylation, HUVECs were exposed to flow waveforms biomimetic of those experienced by collateral arteries following FAL in vivo[42] (Figure 2A). Briefly, ECs were preconditioned for 24 hours at 15 dynes/cm^2 to establish basal EC alignment and planar cell polarity, thereby mimicking the in vivo baseline state. An FAL was then simulated by a step-wise 100% increase in shear stress, in either the same direction or in the opposite direction, to mimic shear stress changes occurring in the muscular branch (nonreversed flow) and saphenous artery (reversed flow) entrance regions, respectively (Figure 2A). We examined DNMT1 mRNA expression by quantitative reverse transcriptase PCR 1 hour and 6 hours after our simulated FAL, determining it was transiently increased by ≈25% after 1 hour in HUVECs exposed to nonreversed flow, but was unchanged in reversed flow conditions (Figure 2B). DNMT1 mRNA expression returned to basal level by 6-hours after simulated FAL (Figure 2B).

Genome-Wide DNA Methylation Patterns Are Altered in ECs Exposed to Biomimetic Arteriogenic Flow Waveforms In Vitro

To then determine how these biomimetic waveforms affect global DNA methylation patterns, we exposed HUVECs to these same flow waveforms. Six hours after simulated FAL, we isolated both gDNA and total RNA and performed both RRBS and mRNA-Seq on these samples, respectively. Both data sets were mapped to the hg19 human genome assembly (GRCh37/hg19, NCBI, Feb. 2009) and showed a similar degree of coverage between our nonreversed and reversed data sets (Tables S1 and S2). In addition, there was a similar

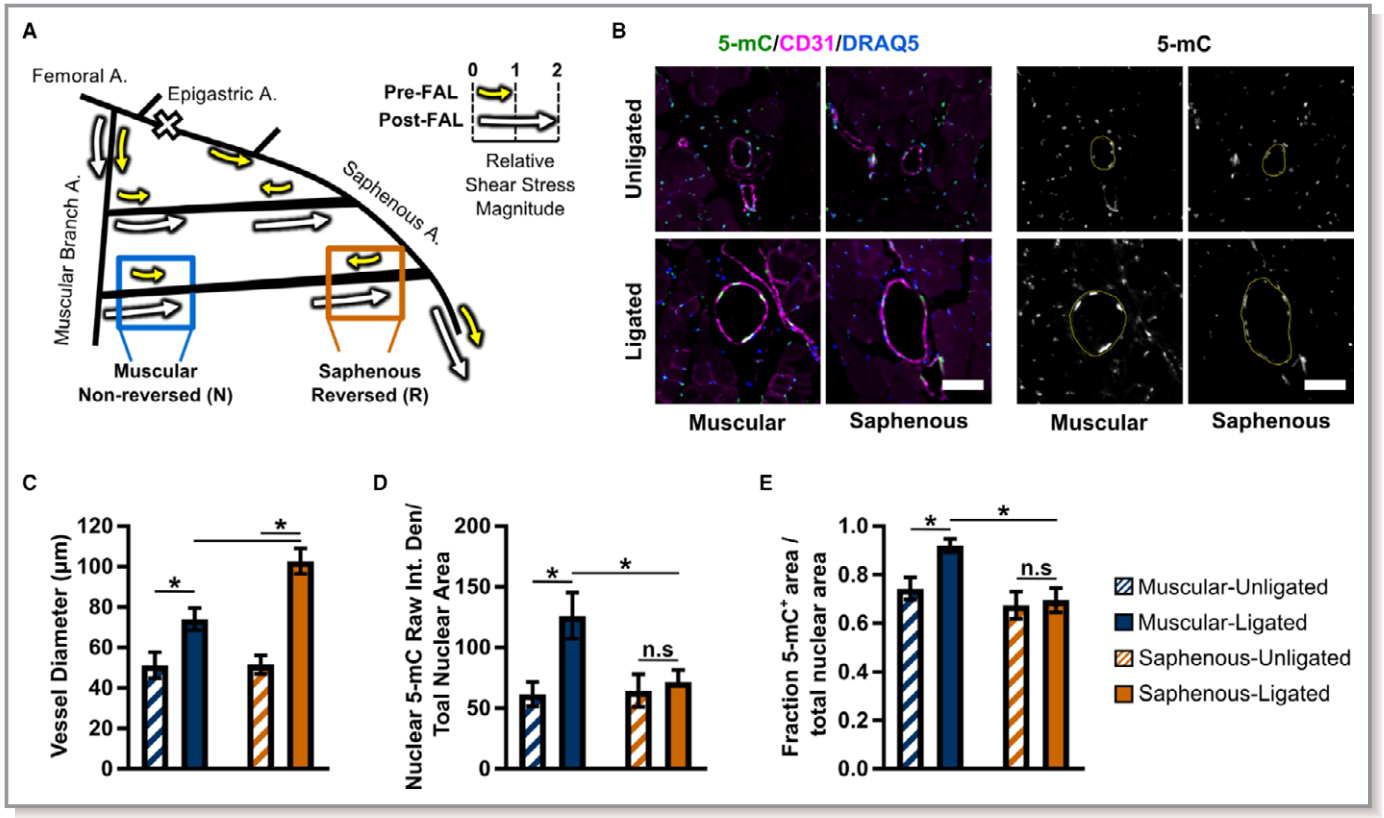

Figure 1. Gracilis collateral arteries exposed to a nonreversed increase in shear stress magnitude exhibit limited arteriogenic capacity and hypermethylated DNA. A, Schematic of the primary gracilis adductor collateral flow pathways after femoral artery ligation (FAL). Arrows indicate the direction and magnitude of blood flow pre (yellow) and post (white) FAL. The femoral artery is ligated just distal to the epigastric artery such that some collateral segments ("muscular") experience a 2-fold increase in shear stress magnitude ("nonreversed" flow), while other segments ("saphenous") are exposed to both a 2-fold increase in shear stress magnitude and reversed flow direction ("reversed" flow). B, Representative cross-sections of gracilis collateral regions in C57BL/6 mice 12 weeks post FAL immunolabeled with 5-methylcytodine (5-mC, green), CD31 (endothelial cells, magenta), and DRAQ5 (nuclei, blue) (scale bar=50 μm). Yellow line indicates vessel wall. C–E, Bar graphs of luminal diameter, nuclear 5-mC raw integrated density per total nuclear area, and fraction of 5-mC+ area per total nuclear area for both muscular and saphenous regions 12 weeks post FAL (n=6–7). **P*<0.05, 2-way ANOVA followed by a Holm-Sidak multiple comparisons test. Data are mean±SEM. n.s. indicates not significant.

degree of total CpG and promoter CpG coverage in both nonreversed and reversed data sets (Figure S1).

To characterize global DNA methylation changes between nonreversed (N) and reversed (R) data sets in genomic regions, we analyzed the CpG methylation in promoter (transcription start site ±1 kb), exon, and intron regions. From our RRBS analysis, only read regions with at least 10x CpG read coverage (henceforth termed DMRs) and mRNA expression in both nonreversed and reversed data sets were selected for further analysis. Intron regions displayed a higher degree of CpG methylation compared with exon or promoter regions; however, exon regions displayed the highest mean methylation density within a DMR, consistent with a previous study[19] (Figure S2A and S2B). Average methylation across gene regions was similar for both nonreversed and reversed data sets. However, when we considered only significantly different (false discovery rate <0.1) DMRs, we observed global hypermethylation in nonreversed conditions compared with reversed conditions, across all gene regions (Figure S2C and S2D). Expectedly, we observed that the degree of promoter methylation inversely correlated with raw gene expression levels on a global scale (Figure S3).

As numerous studies have shown that DNA methylation in the promoter region regulates transcription[44], we focused on DNA methylation differences within gene promoters. We found that 4.74% (816/17 227) of DMRs in promoter regions have a ≥|10%|difference in CpG methylation and a false discovery rate <0.1 between nonreversed and reversed conditions (Table S3). Of these 816 genes, 73.9% (603/816) were hypermethylated in nonreversed compared with reversed conditions (Figure 2C and 2D, red). To determine which mechanosensitive genes demonstrate a correlation between relative gene expression and promoter DNA methylation status, we further filtered this list of 816 genes to contain only genes with expression changes in the expected

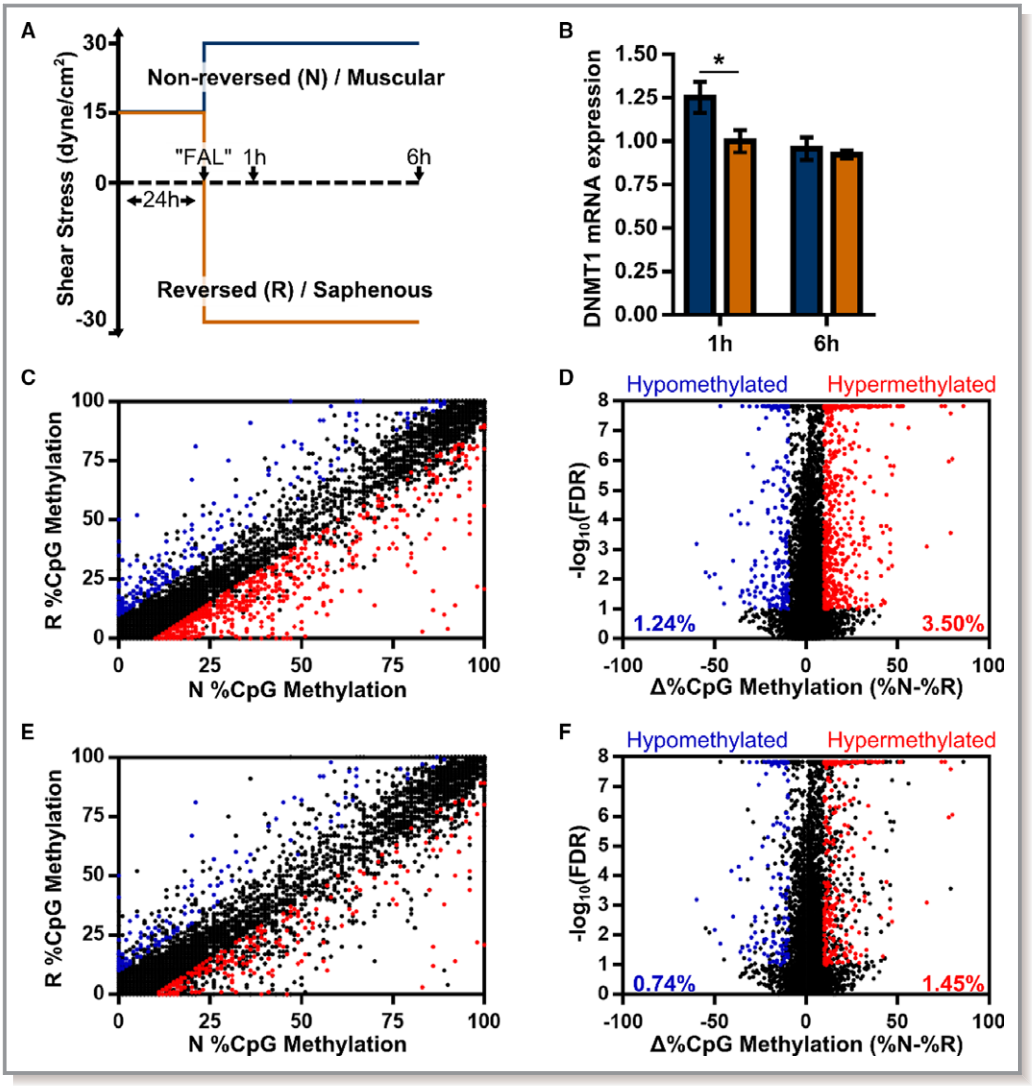

Figure 2. Endothelial cells exposed to a nonreversed increase in shear stress magnitude exhibit augmented DNA methyltransferase 1 (DNMT1) expression and altered genome-wide DNA methylation patterns in vitro. A, Schematic depicting biomimetic shear stress conditions applied to human umbilical vein endothelial cells to simulate nonreversed/muscular (N, blue) and reversed/saphenous (R, orange) regions. B, Bar graph of DNMT1 mRNA expression in each flow condition 1 hour or 6 hours after simulated femoral artery ligation (FAL) (n=8 for 1 hour and n=6 for 6 hours). **P*<0.05 between reversed and nonreversed within a time point, Student *t* test. Data are mean±SEM. C through D, Scatter plot and Volcano plot of all differentially methylated regions in a gene promoter region (17 227 total). Significant differentially methylated regions were designated as hypomethylated (blue, 213 total) or hypermethylated (red, 603 total) with respect to the nonreversed condition (Table S3). E through F, Using our mRNA-sequencing data set, we further filtered this list of significantly hypermethylated and hypomethylated genes (816 total genes) to contain only those with gene expression changes between nonreversed and reversed conditions in the expected direction based on their change in promoter methylation, ie, genes that were downregulated and had a hypermethylated promoter (red, 250 genes) or were upregulated and had a hypomethylated promoter (blue, 127 genes) in nonreversed vs reversed conditions (Tables S4 and S5). FDR indicates false discovery rate.

direction based on their change in promoter methylation (ie, genes that were downregulated and had a hypermethylated promoter in nonreversed versus reversed conditions and vice versa; Figure S4 and Table S4). We found that 66.3% of these genes (250/377) were hypermethylated and downregulated compared with 33.7% (127/377) that were upregulated and hypomethylated in nonreversed versus reversed conditions (Figure 2E and 2F, Tables S4 and S5). We then performed gene ontology analysis on these 377 genes to identify overrepresented pathways (Figure S5 and Table S6). Cellular

metabolism, nucleic acid metabolism, and transcription processes were among the most significantly regulated pathways. However, a number of additional pathways were overrepresented, including protein metabolism, MAPK signaling, apoptosis, cellular localization and transport, and signal transduction.

DNMT1 Regulates the Adhesion of Monocytes to Endothelial Cells Exposed to a Nonreversed Increase in Shear Stress Magnitude

We next sought to determine whether DNMT1 regulates monocyte adhesion to ECs, which is a required step in the arteriogenesis cascade.[45–50] HUVECs were transfected with DNMT1 small interfering RNA or nontargeting control (siC) and subjected to the biomimetic flow waveforms. Western blot analysis showed a dominant band at the expected full length molecular weight ≈183 kDa for DNMT1 as well as a weaker, lower molecular weight band. This weaker band is approximately the same molecular weight (≈144 kDa) as the spliced isoform of DNMT1, which is missing amino acids 1-336. DNMT1 expression was increased >40% in HUVECs exposed to the nonreversed flow waveform when compared with HUVECs exposed to the reversed flow waveform in siC-treated conditions (Figure 3A). This corresponded to a 60% reduction in monocyte adhesion (P=0.023) to HUVECs exposed to the nonreversed flow waveform (Figure 3B and 3C). Knockdown of DNMT1 significantly (P=0.002) increased monocyte adhesion to HUVECs exposed to the nonreversed waveform compared with siC, while there was no significant effect on HUVECs exposed to the reversed waveform (Figure 3B and 3C).

DNMT1 Inhibition Restores the Arteriogenic Capacity of Nonreversed Flow Collateral Artery Segments and Improves Perfusion Recovery in Aged Mice

Our observations led us to test the hypothesis that arteriogenic capacity can be rescued in nonreversed collateral artery segments by reversing DNA hypermethylation through DNMT1 inhibition. As outlined in Figure 4A, we performed FALs on C57BL/6 mice and allowed them to recover for 2 weeks, which is sufficient time for collaterals to achieve steady-state diameters in this model.[6] We then treated mice with daily IP injections of 0.1 mg/kg 5AZA or 0.1% DMSO vehicle control for an additional 2 weeks (Figure 4A). 5AZA is a nucleoside analog that preferentially targets DNMT1 via ubiquitin-dependent proteasomal degradation.[51] 5AZA treatment was shown to be effective in reducing global DNA methylation after only 1 week by HRM (Figure 4B).

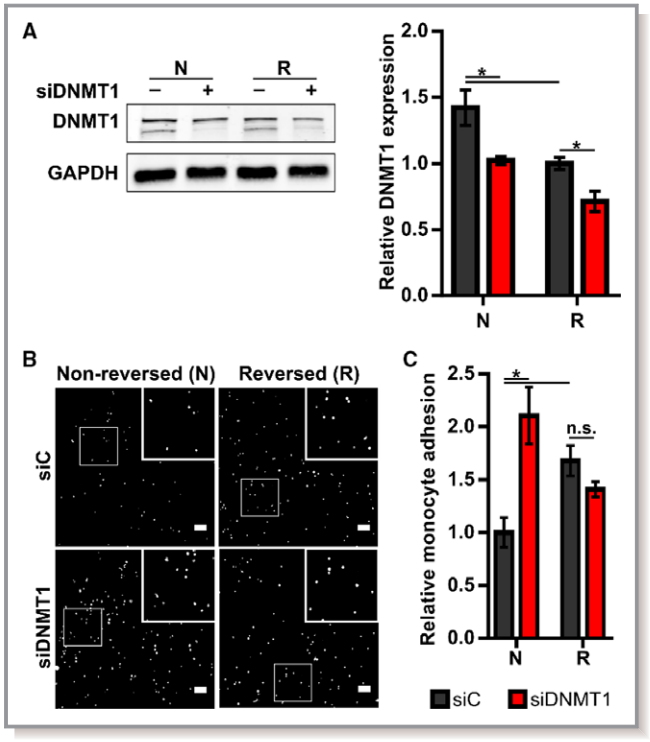

Figure 3. DNA methyltransferase 1 (DNMT1) regulates the adhesion of monocytes to endothelial cells exposed to a nonreversed increase in shear stress magnitude in vitro. A, Relative DNMT1 protein expression, normalized to GAPDH, in human umbilical vein endothelial cells transfected with either DNMT1 small interfering RNA (siDNMT1) or nontargeting control (siC) and exposed to the nonreversed (N) or reversed (R) biomimetic shear stress waveforms in Figure 2, 6 hours after simulated femoral artery ligation (n=4). *P<0.05, 2-way ANOVA followed by a Holm-Sidak multiple comparisons test. B, Representative confocal microscopy images of fluorescently labeled THP-1 monocytes (white) adhered to flow-exposed human umbilical vein endothelial cells (scale bar=100 μm). Insets are the magnified 300 μm×300 μm regions outlined by white boxes. C, Bar graph of the relative number of adhered monocytes in each condition (n=3). *P<0.05, 2-way ANOVA followed by a Holm-Sidak multiple comparisons test. Data are mean±SEM. n.s. indicates not significant.

Vascular casting was used to determine collateral artery diameter in both muscular (nonreversed flow) and saphenous (reversed flow) regions 28 days post FAL. Consistent with previous results (Figure 1C and Heuslein et al[6]), we observed limited arteriogenesis in muscular (nonreversed flow) compared with saphenous (reversed flow) collateral artery segments in DMSO-treated vehicle control mice. However, DNMT1 inhibition increased the arteriogenic capacity of nonreversed flow collateral segments by >40%, while there was no significant (P=0.33) effect on reversed flow segments (Figure 4C and 4D). Cross-sections were used to determine collateral wall area, a metric that further indicated that the differential arteriogenic capacity along the collateral length in

DMSO-treated mice was normalized by DNMT1 inhibition (Figure 4E and 4F). Of note, we observed similar results in FAL-treated Balb/c mice (Figure S6). Here, DNMT1 inhibition increased arteriogenic capacity by ≈44% in nonreversed segments, while there was no effect on reversed flow segments (P=0.163), indicating that this response is not limited to the C57BL/6 strain. We also sought to determine whether this increased arteriogenic capacity in nonreversed flow segments following DNMT1 inhibition corresponded to altered macrophage recruitment, a necessary component of collateral artery growth[45–50,52] in vivo. Nonreversed flow collateral segments exhibited a trend (P=0.057) toward increased pericollateral Mac3$^+$ macrophages in 5AZA-treated mice (day 17 post FAL, 3 days of 5AZA treatment), corresponding to our previous in vitro results (Figure S7). There was no difference in macrophage recruitment in reversed segments between 5AZA- and DMSO-treated mice (Figure S7).

We next sought to determine whether DNMT1 inhibition could improve perfusion recovery. As young C57BL/6 mice do not exhibit a significant long-term perfusion deficit (ie, they fully recover in ≈7 days following FAL),[6] we chose to used aged (10 to 11 months old) Balb/c mice instead. We hypothesized that these mice would have a poorer baseline perfusion recovery, thus enabling the necessary dynamic range to test whether DNMT1 inhibition altered perfusion recovery. Mice were subjected to FAL, allowed to recover for 2 weeks and then treated daily with either 5AZA or DMSO vehicle control for an additional 2 weeks, according to Figure 4A. As expected, FAL-operated limbs of DMSO-treated mice exhibited impaired perfusion recovery, only reaching ≈73% of unligated limb blood flow (Figure S8). There was no difference in perfusion between day 14 and day 28 post FAL in control-treated mice (P=0.441), indicating that perfusion had reached steady state by day 14. Despite beginning at a similar degree of foot perfusion at day 14 (ie, start of 5AZA treatment), DNMT1 inhibition via 5AZA significantly (P=0.04) improved perfusion recovery (≈90% of unligated limb) compared with DMSO-treated mice (Figure S8).

Shear Stress Set Point is Reestablished in Nonreversed Flow Collateral Artery Segments by DNMT1 Inhibition

Finally, we sought to determine whether DNMT1-dependent DNA hypermethylation alters nonreversed collateral artery shear stress set point. Mice were treated with 5AZA or DMSO according to Figure 4A. Relative changes in collateral artery shear rates were then determined by transillumination laser speckle flowmetry[42] 28 days post FAL. Interestingly, in DMSO-treated vehicle control mice, shear stress remained elevated (≈2.5-fold) in muscular (nonreversed flow) collateral segments 28 days after FAL, while it was restored to pre-FAL levels in saphenous (reversed flow) segments (Figure 5). DNMT1 inhibition restored shear stress in nonreversed flow segments to pre-FAL levels, whereas there was no significant effect on reversed flow segments (Figure 5).

Discussion

In this study, we tested the hypothesis that DNMT1-dependent EC DNA methylation regulates arteriogenic capacity via adjustments to shear stress set point. Previously, we demonstrated that collateral artery segments exposed to an increase in shear stress magnitude, without a change in flow direction, display limited arteriogenic capacity when compared with segments exposed to both increased shear stress magnitude and reversed flow direction. Here, we first determined that these nonreversed flow collateral segments exhibit global DNA hypermethylation in vivo. We then applied flow waveforms, biomimetic of those leading to either amplified arteriogenic capacity (ie, reversed flow) or constrained arteriogenic capacity (ie, nonreversed flow) in vivo, to ECs in vitro, and performed both RRBS and mRNA-Seq. ECs exposed to the nonreversed waveform exhibited increased DNMT1 expression, genome-wide hypermethylation of significantly regulated gene promoters, and a DNMT1-dependent reduction in proarteriogenic monocyte adhesion. Together, this led us to next test whether DNMT1 regulates arteriogenic capacity in vivo. We ascertained that, in nonreversed flow collateral artery segments, DNMT1 inhibition rescued arteriogenic capacity and returned the elevated shear stress back to its original set point. Collectively, these results demonstrate that DNMT1-dependent DNA hypermethylation constrains arteriogenesis by dampening EC mechanosensing, which effectively augments shear stress set point. The epigenetic regulation of shear stress set point may therefore have critical impact on both endogenous and therapeutic arteriogenesis in patients with arterial occlusive disease.

Mapping EC Mechanosensitive DNA Methylation to Differential Arteriogenic Capacity

The significance of epigenetics in vascular biology, with roles as regulators of molecular signaling known to drive physiology and as potential therapeutic targets to treat disease, is now well recognized.[9,15,53] Both histone modifications and microRNAs regulate flow-mediated EC gene expression[54–60] and arteriogenesis[61–65]; however, DNA methylation has only recently been shown to regulate flow-mediated EC gene expression in any context.[16–19] Moreover, to our knowledge, the role of DNMT1-mediated DNA methylation in arteriogenesis has not been previously studied.

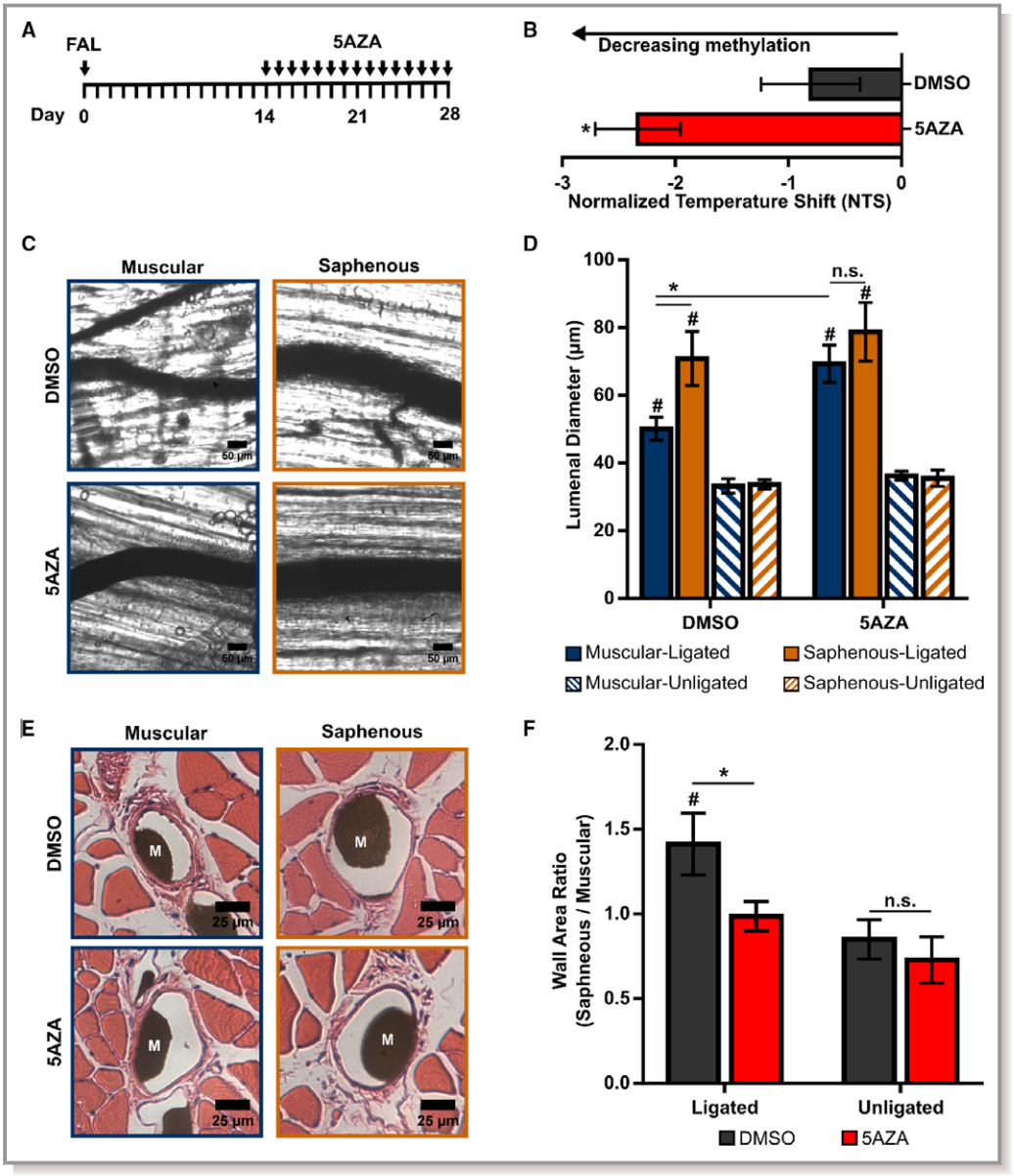

Figure 4. The arteriogenic capacity of nonreversed collateral artery segments is restored by DNA methyltransferase 1 inhibition. A, Experimental treatment time course. Femoral artery ligation (FAL) is performed on day 0. On day 14, mice begin receiving daily intraperitoneal injections of dimethyl sulfoxide (DMSO) or 5-aza-2′-deoxycytidine (5AZA) until day 28. B, Bar graph of normalized temperature shift (NTS) determined by high-resolution melting (HRM) of LINE1 repeat elements after 7 days of treatment (n=6). **P*<0.05 between DMSO and 5AZA, Student *t* test. C, Representative vascular cast images from muscular (nonreversed) and saphenous (reversed) collateral artery regions 28 days post FAL from C57BL/6 mice treated according to (B) (scale bar=50 µm). D, Bar graph of regional luminal diameter in DMSO- or 5AZA-treated mice. **P*<0.05; #*P*<0.01 between ligated and unligated within the given region. Two-way ANOVA followed by a Holm-Sidak multiple comparisons test. E, Representative hematoxylin-eosin–stained cross-sections of gracilis collateral artery regions in DMSO- and 5AZA-treated mice at day 28 post FAL (scale bar=25 µm). Microfil casting material (M) is evident in the artery lumen. F, Bar graph of wall area ratio of saphenous:muscular collateral regions. #*P*<0.01 between ligated and unligated for a given treatment; **P*<0.05 between DMSO- and 5AZA-treated mice; 2-way ANOVA followed by a Holm-Sidak multiple comparisons test. Data are mean±SEM. n.s. indicates not significant.

Our study directly maps EC mechanosensitive DNA methylation to differential, sustained arteriogenesis responses. In addition, by using both RRBS and mRNA-Seq, we discovered a set of mechanosensitive genes whose expression correlates to gene promoter DNA methylation status. Gene ontology analysis of these genes identified a

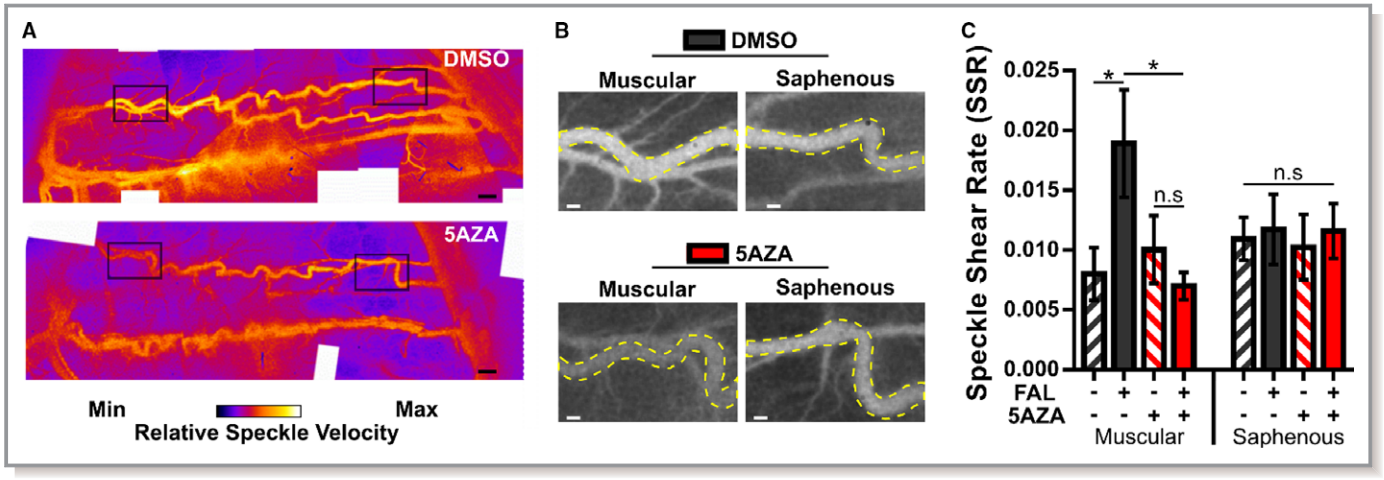

Figure 5. Shear stress set point in nonreversed flow collateral artery segments is restored by DNA methyltransferase 1 inhibition. A, Representative relative speckle velocity maps across the primary gracilis muscle collateral pathways 28 days post femoral artery ligation (FAL) in C57BL/6 mice treated with dimethyl sulfoxide (DMSO) and 5-aza-2′-deoxycytidine (5AZA) according to Figure 4A. (Scale bar=500 μm). B, Greyscale images of the 300×200 pixel boxed regions shown in (A) for both the muscular (nonreversed, left) and saphenous (reversed, right) collateral regions. (Scale bar=100 μm). Dotted line indicates collateral artery region of interest used for analysis. C, Bar graph of regional speckle shear rate in DMSO- and 5AZA-treated mice (n=6 for DMSO, n=5 for 5AZA). **P*<0.05, n.s. (not significant). Student *t* test. Data are mean±SEM.

number of pathways crucial for EC mechanotransduction and arteriogenesis, including several metabolism, transcription, MAPK signaling, and cell transport pathways.[31,66] Of note, SIRT4 was involved in a number of these significantly overrepresented pathways (Figure S5). SIRT4 has been shown to disrupt the nuclear factor κB pathway, whereby overexpression of SIRT4 in ECs abrogates nuclear factor κB nuclear translocation and decreases expression of proinflammatory cytokines (interleukin 1β, interleukin 6, and interleukin 8), matrix metallopeptidase 9, and intercellular adhesion molecule 1.[67] As we have previously reported, ECs exposed to nonreversed flow waveforms exhibit decreased nuclear factor κB–intercellular adhesion molecule-1 activity.[6] Thus, because the nuclear factor κB–intercellular adhesion molecule-1 pathway is crucial for arteriogenesis,[6,45,68] the flow-dependent regulation of SIRT4 could be of particular interest.

In addition, studies examining flow-mediated EC DNA methylation have identified Homeobox transcription factors (eg, HOXA5) as being differentially regulated in atheroprone conditions.[17,19] HOX transcription factors are considered "master regulators" as they regulate EC proliferation, migration, differentiation, morphogenesis, and permeability during

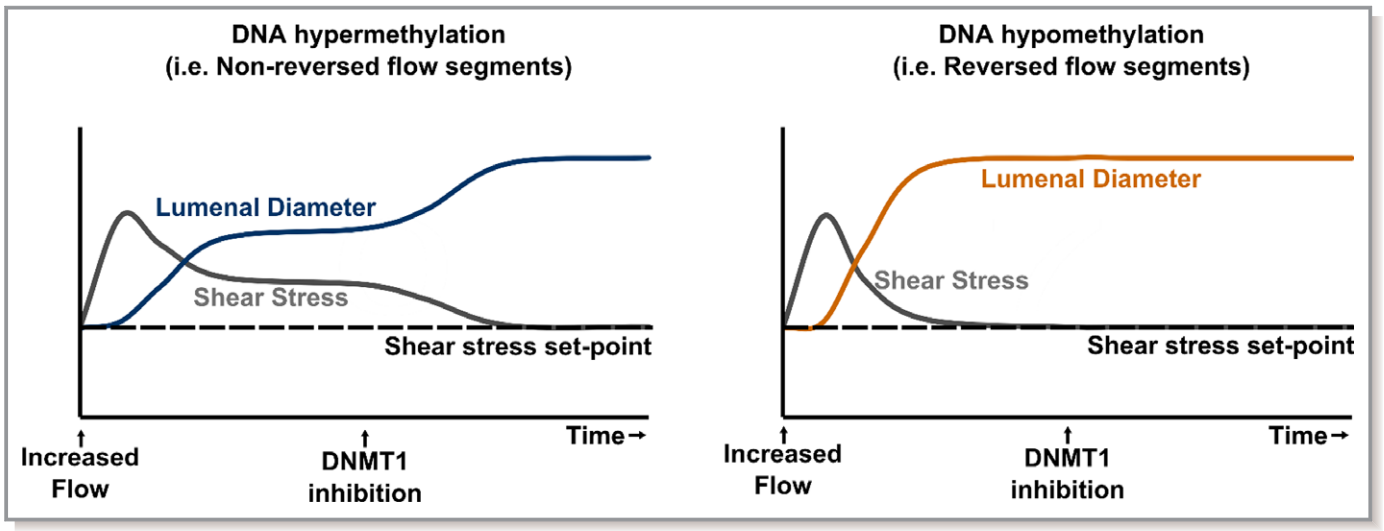

Figure 6. Summary of DNA methyltransferase 1 (DNMT1)–dependent regulation of arteriogenic capacity and shear stress set point in gracilis adductor collateral arteries following femoral artery ligation.

development and vascular remodeling.[69] Interestingly, we found HOXB3 to be among the genes downregulated (decreased 25%) and hypermethylated (20% versus 0.1% methylation) in nonreversed compared with reversed flow conditions (Table S4). As HOXB3 regulates EC activation and promotes angiogenesis,[70] our results are consistent with the hypothesis that hypermethylation of the HOXB3 promoter decreases its expression, thereby limiting EC activation and arteriogenic potential of collateral artery segments.

The Role of DNMT1 in Flow-Mediated Endothelial Inflammation is Dependent on Hemodynamic Context

Monocyte adhesion to an activated endothelium is required for collateral artery growth.[45–50,52] Here, we employed a monocyte adhesion assay, which has been previously used to examine flow-mediated EC function,[6,17,40,71] to determine the role of endothelial DNMT1 expression in regulating this essential step in arteriogenesis. Our results showed increased DNMT1 expression and limited monocyte adhesion to ECs exposed to the nonreversed flow waveform. Upon DNMT-1 inhibition, monocyte adhesion was increased >2-fold to ECs exposed to the nonreversed flow waveform. Corresponding to these in vitro results, DNMT1 inhibition in vivo via 5-AZA increased pericollateral $Mac3^+$ macrophages in nonreversed flow collateral segments (Figure S7). We observed no changes in monocyte adhesion or pericollateral macrophage accumulation in reversed flow conditions, indicating an anti-inflammatory role for DNMT1 that is dependent on hemodynamic context. In contrast, DNMT1 has been shown to promote EC inflammation in HUVECs exposed to atheroprone flow conditions, as demonstrated by a DNMT1-dependent increase in monocyte adhesion.[17] However, our proarteriogenic flow conditions, which include a laminar flow preconditioning phase, are different from the oscillatory, atheroprone conditions of previous studies,[17] further supporting the idea that DNMT1's role in endothelial inflammation is dependent on hemodynamic context. Furthermore, exposure to atheroprone conditions led to a chronic increase in DNMT1 expression,[17] whereas our results suggest a transient increase in DNMT1 expression. This adaptive, instead of chronic, response may contribute to a context-dependent role of DNMT1 on monocyte adhesion to ECs.

Molecular Regulation of Collateral Artery Shear Stress Set Point

Finally, we have determined that DNMT1-dependent DNA methylation regulates, at least in part, long-term arteriogenic capacity and shear stress set point. The concept of an arterial homeostatic wall shear stress magnitude (ie, shear stress set point) at which vessels maintain a steady-state luminal diameter[72] arises from Murray's principle of minimum work.[73] Outward collateral artery growth is therefore hypothesized to stop once normalization to the shear stress set point has been achieved.[2–5] Premature normalization to the shear stress set point has been a predominant rationalization for the failure of collateral arteries to realize full arteriogenic capacity, frequently reaching only 30% to 40% of the maximal conductance.[74] However, our results indicate that shear stress actually remains elevated in collateral artery segments exhibiting limited arteriogenic capacity. In essence, EC DNA hypermethylation prevents these collaterals from continuing to increase in diameter; therefore, shear stress remains chronically elevated. Yet, when DNMT1-dependent DNA methylation is inhibited, these collaterals become resensitized to their elevated shear stress and are able to resume the arteriogenic process until the original set point is achieved (Figure 6). This response appears to require a basal level of DNA methylation, as there was no effect of DNMT1 inhibition on collateral artery segments that were not hypermethylated.

There are several other studies that have reported an altered set point following arterial adaptation. To this end, a left-right carotid anastomosis was used to induce an acute increase in blood flow in the common carotid artery of mature and weanling rabbits. Two months later, shear stress remained augmented in mature rabbits caused by a lack of compensatory arterial enlargement, whereas weanling rabbits exhibited significant diameter enlargement, enabling for shear stress to normalize to the set point.[75] This age-dependent remodeling was also observed in rats in which ligation of the left internal and external carotid arteries increased right carotid blood flow by 46%. After 4 weeks, the right carotid outer diameter increased and shear stress returned to initial values in juvenile but not adult rats.[76] The constrained arterial remodeling and augmented shear stress set point of aged animals is strikingly similar to the phenotype we observed in nonreversed flow collateral segments. Given that age alters DNA methylation,[77] together, these results would be consistent with the hypothesis that acutely increased shear stress yields incomplete arterial remodeling and augmented shear stress set point caused by DNA hypermethylation.

Potential Clinical Implications

Given our results, modulation of the shear stress set point by DNMT1 inhibition could represent a therapeutic strategy for treating arterial occlusive diseases. By focusing on the molecular mechanisms regulating the maturation stage of arteriogenesis, as opposed to initiation and growth stages, such an approach could better account for the chronic nature of arterial occlusive diseases in humans. To this end, we did not begin DNMT1 inhibition until 2 weeks after FAL. We

observed an increase in nonreversed collateral artery diameter in both C57BL/6 mice and Balb/c mice. Moreover, DNMT1 inhibition trended toward improved perfusion recovery in aged (10 to 11 months old) Balb/c mice (Figure S8). Although a few previous studies have demonstrated increased arteriogenic capacity after such a delayed treatment,[46,78,79] ours is the first to demonstrate an epigenetic mechanism. DNMT1 inhibition may also be clinically advantageous because it appears to avoid the so-called Janus phenomenon, which refers to the conundrum created by the fact that proarteriogenic therapies also tend to promote atherosclerosis.[80] To this point, DNMT1 inhibition with 5AZA reverses DNA hypermethylation induced by atheroprone shear stress[17,18] and reduces atherosclerotic plaque size.[17]

Conclusions

Ultimately, because shear stress–induced changes in DNMT1 expression markedly affect both atherosclerosis and arteriogenic capacity, DNMT1 may represent an interesting target for peripheral arterial disease therapy.

Acknowledgments

The authors would like to thank the University of Virginia Research Histology Core (under the direction of Sheri VanHoose) for histological tissue processing.

Sources of Funding

This work was supported by National Institutes of Health R03 EB017927 and R01 EB020147. JLH was supported by a National Science Foundation Graduate Research Fellowship Program grant No. NSF DGE-1315231.

Disclosures

None.

References

1. Schaper W. Collateral circulation: past and present. *Basic Res Cardiol*. 2009;104:5–21.
2. Meisner JK, Price RJ. Spatial and temporal coordination of bone marrow-derived cell activity during arteriogenesis: regulation of the endogenous response and therapeutic implications. *Microcirculation*. 2010;17:583–599.
3. Heil M, Schaper W. Pathophysiology of collateral development. *Coron Artery Dis*. 2004;15:373–378.
4. Unthank JL, Fath SW, Burkhart HM, Miller SC, Dalsing MC. Wall remodeling during luminal expansion of mesenteric arterial collaterals in the rat. *Circ Res*. 1996;79:1015–1023.
5. Langille BL, O'Donnell F. Reductions in arterial diameter produced by chronic decreases in blood flow are endothelium-dependent. *Science*. 1986;231:405–407.
6. Heuslein JL, Meisner JK, Li X, Song J, Vincentelli H, Leiphart RJ, Ames EG, Blackman BR, Price RJ. Mechanisms of amplified arteriogenesis in collateral artery segments exposed to reversed flow direction. *Arterioscler Thromb Vasc Biol*. 2015;35:2354–2365.
7. Goldberg AD, Allis CD, Bernstein E. Epigenetics: a landscape takes shape. *Cell*. 2007;128:635–638.
8. Dunn J, Thabet S, Jo H. Flow-dependent epigenetic DNA methylation in endothelial gene expression and atherosclerosis. *Arterioscler Thromb Vasc Biol*. 2015;35:1562–1569.
9. Yan MS, Marsden PA. Epigenetics in the vascular endothelium: looking from a different perspective in the epigenomics era. *Arterioscler Thromb Vasc Biol*. 2015;35:2297–2306.
10. Song F, Smith JF, Kimura MT, Morrow AD, Matsuyama T, Nagase H, Held WA. Association of tissue-specific differentially methylated regions (TDMs) with differential gene expression. *Proc Natl Acad Sci USA*. 2005;102:3336.
11. Grunau C, Hindermann W, Rosenthal A. Large-scale methylation analysis of human genomic DNA reveals tissue-specific differences between the methylation profiles of genes and pseudogenes. *Hum Mol Genet*. 2000;9:2651–2663.
12. Weber M, Davies JJ, Wittig D, Oakeley EJ, Haase M, Lam WL, Schübeler D. Chromosome-wide and promoter-specific analyses identify sites of differential DNA methylation in normal and transformed human cells. *Nat Genet*. 2005;37:853–862.
13. Bestor TH. The DNA methyltransferases of mammals. *Hum Mol Genet*. 2000;9:2395–2402.
14. Handy DE, Castro R, Loscalzo J. Epigenetic modifications: basic mechanisms and role in cardiovascular disease. *Circulation*. 2011;123:2145–2156.
15. Matouk CC, Marsden PA. Epigenetic regulation of vascular endothelial gene expression. *Circ Res*. 2008;102:873–887.
16. Jiang YZ, Jiménez JM, Ou K, McCormick ME, Zhang LD, Davies PF. Hemodynamic disturbed flow induces differential DNA methylation of endothelial Kruppel-Like Factor 4 promoter in vitro and in vivo. *Circ Res*. 2014;115:32–43.
17. Dunn J, Qiu H, Kim S, Jjingo D, Hoffman R, Kim CW, Jang I, Son DJ, Kim D, Pan C, Fan Y, Jordan IK, Jo H. Flow-dependent epigenetic DNA methylation regulates endothelial gene expression and atherosclerosis. *J Clin Invest*. 2014;124:3187–3199.
18. Zhou J, Li YS, Chien S. Epigenetic mechanism in regulation of endothelial function by disturbed flow: induction of DNA hypermethylation by DNMT1. *Cell Mol Bioeng*. 2014;7:218–224.
19. Jiang YZ, Manduchi E, Stoeckert CJ, Davies PF. Arterial endothelial methylome: differential DNA methylation in athero-susceptible disturbed flow regions in vivo. *BMC Genom*. 2015;16:506.
20. Meisner JK, Sumer S, Murrell KP, Higgins TJ, Price RJ. Laser speckle flowmetry method for measuring spatial and temporal hemodynamic alterations throughout large microvascular networks. *Microcirculation*. 2012;19:619–631.
21. Heuslein JL, Murrell KP, Leiphart RJ, Llewellyn RA, Meisner JK, Price RJ. Vascular growth responses to chronic arterial occlusion are unaffected by myeloid specific focal adhesion kinase (FAK) deletion. *Sci Rep*. 2016;6:27029.
22. Chappell JC, Song J, Burke CW, Klibanov AL, Price RJ. Targeted delivery of nanopartides bearing fibroblast growth factor-2 by ultrasonic microbubble destruction for therapeutic arteriogenesis. *Small*. 2008;4:1769–1777.
23. Nickerson MM, Burke CW, Meisner JK, Shuptrine CW, Song J, Price RJ. Capillary arterialization requires the bone marrow-derived cell (BMC)-specific expression of chemokine (C-C motif) receptor-2, but BMCs do not transdifferentiate into microvascular smooth muscle. *Angiogenesis*. 2009;12:355–363.
24. Distasi MR, Case J, Ziegler MA, Dinauer MC, Yoder MC, Haneline LS, Dalsing MC, Miller SJ, Labarrere CA, Murphy MP, Ingram DA, Unthank JL. Suppressed hindlimb perfusion in Rac2-/- and Nox2-/- mice does not result from impaired collateral growth. *Am J Physiol Heart Circ Physiol*. 2009;296:H877–H886.
25. Dai X, Faber JE. Endothelial nitric oxide synthase deficiency causes collateral vessel rarefaction and impairs activation of a cell cycle gene network during arteriogenesis. *Circ Res*. 2010;106:1870–1881.
26. Meisner JK, Annex BH, Price RJ. Despite normal arteriogenic and angiogenic responses, hind limb perfusion recovery and necrotic and fibroadipose tissue clearance are impaired in matrix metalloproteinase 9-deficient mice. *J Vasc Surg*. 2015;61:1583–1594. e1–10
27. Meisner JK, Song J, Annex BH, Price RJ. Myoglobin overexpression inhibits reperfusion in the ischemic mouse hindlimb through impaired angiogenesis but not arteriogenesis. *Am J Pathol*. 2013;183:1710–1718.
28. Newman MR, Blyth BJ, Hussey DJ, Jardine D, Sykes PJ, Ormsby RJ. Sensitive quantitative analysis of murine LINE1 DNA methylation using high resolution melt analysis. *Epigenetics*. 2012;7:92–105.
29. Tse MY, Ashbury JE, Zwingerman N, King WD, Taylor SA, Pang SC. A refined, rapid and reproducible high resolution melt (HRM)-based method suitable for

quantification of global LINE-1 repetitive element methylation. *BMC Res Notes*. 2011;4:565.

30. Schindelin J, Arganda-Carreras I, Frise E, Kaynig V, Longair M, Pietzsch T, Preibisch S, Rueden C, Saalfeld S, Schmid B, Tinevez J-Y, White DJ, Hartenstein V, Eliceiri K, Tomancak P, Cardona A. Fiji: an open-source platform for biological-image analysis. *Nat Methods*. 2012;9:676–682.
31. Davies PF. Flow-mediated endothelial mechanotransduction. *Physiol Rev*. 1995;75:519–560.
32. Hergenreider E, Heydt S, Tréguer K, Boettger T, Horrevoets AJG, Zeiher AM, Scheffer MP, Frangakis AS, Yin X, Mayr M, Braun T, Urbich C, Boon RA, Dimmeler S. Atheroprotective communication between endothelial cells and smooth muscle cells through miRNAs. *Nat Cell Biol*. 2012;14:249–256.
33. Fledderus JO, Van Thienen JV, Boon RA, Dekker RJ, Rohlena J, Volger OL, Bijnens APJJ, Daemen MJAP, Kuiper J, Van Berkel TJC, Pannekoek H, Horrevoets AJG. Prolonged shear stress and KLF2 suppress constitutive proinflammatory transcription through inhibition of ATF2. *Blood*. 2007;109:4249–4257.
34. Dekker RJ, Boon RA, Rondaij MG, Kragt A, Volger OL, Elderkamp YW, Meijers JCM, Voorberg J, Pannekoek H, Horrevoets AJG. KLF2 provokes a gene expression pattern that establishes functional quiescent differentiation of the endothelium. *Blood*. 2006;107:4354–4363.
35. Dekker RJ, van Thienen JV, Rohlena J, de Jager SC, Elderkamp YW, Seppen J, de Vries CJM, Biessen EAL, van Berkel TJC, Pannekoek H, Horrevoets AJG. Endothelial KLF2 links local arterial shear stress levels to the expression of vascular tone-regulating genes. *Am J Pathol*. 2005;167:609–618.
36. Garcia-Cardeña G, Comander J, Anderson KR, Blackman BR, Gimbrone MA. Biomechanical activation of vascular endothelium as a determinant of its functional phenotype. *Proc Natl Acad Sci USA*. 2001;98:4478–4485.
37. Li J, Hou B, Tumova S, Muraki K, Bruns A, Ludlow MJ, Sedo A, Hyman AJ, McKeown L, Young RS, Yuldasheva NY, Majeed Y, Wilson LA, Rode B, Bailey MA, Kim HR, Fu Z, Carter DA, Bilton J, Imrie H, Ajuh P, Dear TN, Cubbon RM, Kearney MT, Prasad RK, Evans PC, Ainscough JFX, Beech DJ. Piezo1 integration of vascular architecture with physiological force. *Nature*. 2014;515:279–282.
38. Simmers MB, Pryor AW, Blackman BR. Arterial shear stress regulates endothelial cell-directed migration, polarity, and morphology in confluent monolayers. *Am J Physiol Heart Circ Physiol*. 2007;293:1937–1946.
39. Blackman BR, García-Cardeña G, Gimbrone MAJ. A new in vitro model to evaluate differential responses of endothelial cells to simulated arterial shear stress waveforms. *J Biomech Eng*. 2002;124:397–407.
40. Hastings NE, Feaver RE, Lee MY, Wamhoff BR, Blackman BR. Human IL-8 regulates smooth muscle cell VCAM-1 expression in response to endothelial cells exposed to atheroprone flow. *Arterioscler Thromb Vasc Biol*. 2009;29:725–731.
41. Wu W, Xiao H, Laguna-Fernandez A, Villarreal G, Wang KC, Geary GG, Zhang Y, Wang WC, Huang HD, Zhou J, Li YS, Chien S, Garcia-Cardena G, Shyy JY. Flow-Dependent Regulation of Kruppel-Like Factor 2 Is Mediated by MicroRNA-92a. *Circulation*. 2011;124:633–641.
42. Meisner JK, Niu J, Sumer S, Price RJ. Trans-illuminated laser speckle imaging of collateral artery blood flow in ischemic mouse hindlimb. *J Biomed Opt*. 2013;18:96011.
43. Subramanian A, Tamayo P, Mootha VK, Mukherjee S, Ebert BL. Gene set enrichment analysis: a knowledge-based approach for interpreting genome-wide. *Proc Natl Acad Sci USA*. 2005;102:15545–15550.
44. Jones PA. Functions of DNA methylation: islands, start sites, gene bodies and beyond. *Nat Rev Genet*. 2012;13:484–492.
45. Hoefer IE, van Royen N, Rectenwald JE, Deindl E, Hua J, Jost M, Grundmann S, Voskuil M, Ozaki CK, Piek JJ, Buschmann IR. Arteriogenesis proceeds via ICAM-1/Mac-1- mediated mechanisms. *Circ Res*. 2004;94:1179–1185.
46. Buschmann IR, Hoefer IE, van Royen N, Katzer E, Braun-Dulleaus R, Heil M, Kostin S, Bode C, Schaper W. GM-CSF: a strong arteriogenic factor acting by amplification of monocyte function. *Atherosclerosis*. 2001;159:343–356.
47. Hoefer IE, Grundmann S, Van Royen N, Voskuil M, Schirmer SH, Ulusans S, Bode C, Buschmann IR, Piek JJ. Leukocyte subpopulations and arteriogenesis: specific role of monocytes, lymphocytes and granulocytes. *Atherosclerosis*. 2005;181:285–293.
48. Bergmann CE, Hoefer IE, Meder B, Roth H, van Royen N, Breit SM, Jost MM, Aharinejad S, Hartmann S, Buschmann IR. Arteriogenesis depends on circulating monocytes and macrophage accumulation and is severely depressed in op/op mice. *J Leukoc Biol*. 2006;80:59–65.
49. Arras M, Ito WD, Scholz D, Winkler B, Schaper J, Schaper W. Monocyte activation in angiogenesis and collateral growth in the rabbit hindlimb. *J Clin Invest*. 1998;101:40–50.
50. Scholz D, Ito W, Fleming I, Deindl E, Sauer A, Wiesnet M, Busse R, Schaper J, Schaper W. Ultrastructure and molecular histology of rabbit hind-limb collateral artery growth (arteriogenesis). *Virchows Arch*. 2000;436:257–270.
51. Ghoshal K, Datta J, Majumder S, Bai S, Kutay H, Motiwala T, Jacob ST. 5-Aza-deoxycytidine induces selective degradation of DNA methyltransferase 1 by a proteasomal pathway that requires the KEN box, bromo-adjacent homology domain, and nuclear localization signal. *Mol Cell Biol*. 2005;25:4727–4741.
52. Bruce AC, Kelly-Goss MR, Heuslein JL, Meisner JK, Price RJ, Peirce SM. Monocytes are recruited from venules during arteriogenesis in the murine spinotrapezius ligation model. *Arterioscler Thromb Vasc Biol*. 2014;34:2012–2022.
53. Chen LJ, Wei SY, Chiu JJ. Mechanical regulation of epigenetics in vascular biology and pathobiology. *J Cell Mol Med*. 2013;17:437–448.
54. Illi B, Nanni S, Scopece A, Farsetti A, Biglioli P, Capogrossi MC, Gaetano C. Shear stress-mediated chromatin remodeling provides molecular basis for flow-dependent regulation of gene expression. *Circ Res*. 2003;93:155–161.
55. Chen W, Bacanamwo M, Harrison DG. Activation of p300 histone acetyltransferase activity is an early endothelial response to laminar shear stress and is essential for stimulation of endothelial nitric-oxide synthase mRNA transcription. *J Biol Chem*. 2008;283:16293–16298.
56. Lee DY, Lee CI, Lin TE, Lim SH, Zhou J, Tseng YC, Chien S, Chiu JJ. Role of histone deacetylases in transcription factor regulation and cell cycle modulation in endothelial cells in response to disturbed flow. *Proc Natl Acad Sci USA*. 2012;109:1967–1972.
57. Chen LJ, Chuang L, Huang YH, Zhou J, Lim SH, Lee CI, Lin WW, Lin TE, Wang WL, Chen L, Chien S, Chiu JJ. MicroRNA mediation of endothelial inflammatory response to smooth muscle cells and its inhibition by atheroprotective shear stress. *Circ Res*. 2015;116:1157–1169.
58. Fang Y, Shi C, Manduchi E, Civelek M, Davies PF. MicroRNA-10a regulation of proinflammatory phenotype in athero-susceptible endothelium in vivo and in vitro. *Proc Natl Acad Sci USA*. 2010;107:13450–13455.
59. Ni CW, Qiu H, Jo H. MicroRNA-663 upregulated by oscillatory shear stress plays a role in inflammatory response of endothelial cells. *Am J Physiol Heart Circ Physiol*. 2011;300:H1762–H1769.
60. Qin X, Wang X, Wang Y, Tang Z, Cui Q, Xi J, Li YS, Chien S, Wang N. MicroRNA-19a mediates the suppressive effect of laminar flow on cyclin D1 expression in human umbilical vein endothelial cells. *Proc Natl Acad Sci USA*. 2010;107:3240–3244.
61. Lei Z, van Mil A, Brandt MM, Grundmann S, Hoefer I, Smits M, El Azzouzi H, Fukao T, Cheng C, Doevendans PA, Sluijter JPG. MicroRNA-132/212 family enhances arteriogenesis after hindlimb ischaemia through modulation of the Ras-MAPK pathway. *J Cell Mol Med*. 2015;20:1–12.
62. Welten SM, Bastiaansen AJ, de Jong RC, de Vries MR, Peters EA, Boonstra MC, Sheikh SP, La Monica N, Kandimalla ER, Quax PH, Nossent AY. Inhibition of 14q32 MicroRNAs miR-329, miR-487b, miR-494, and miR-495 increases neovascularization and blood flow recovery after ischemia. *Circ Res*. 2014;115:696–708.
63. Landskroner-Eiger S, Qiu C, Perrotta P, Siragusa M, Lee MY, Ulrich V, Luciano AK, Zhuang ZW, Corti F, Simons M, Montgomery RL, Wu D, Yu J, Sessa WC. Endothelial miR-17 ~ 92 cluster negatively regulates arteriogenesis via miRNA-19 repression of WNT signaling. *Proc Natl Acad Sci USA*. 2015;112:12812–12817.
64. Pankratz F, Bemtgen X, Zeiser R, Leonhardt F, Kreuzaler S, Hilgendorf I, Smolka C, Helbing T, Hoefer I, Esser JS, Kustermann M, Moser M, Bode C, Grundmann S. MicroRNA-155 exerts cell-specific antiangiogenic but proarteriogenic effects during adaptive neovascularization. *Circulation*. 2015;131:1575–1589.
65. Bastiaansen AJ, Ewing MM, de Boer HC, van der Pouw Kraan TC, de Vries MR, Peters EA, Welten SM, Arens R, Moore SM, Faber JE, Jukema JW, Hamming JF, Nossent AY, Quax PH. Lysine acetyltransferase PCAF is a key regulator of arteriogenesis. *Arterioscler Thromb Vasc Biol*. 2013;33:1902–1910.
66. Heil M, Schaper W. Influence of mechanical, cellular, and molecular factors on collateral artery growth (Arteriogenesis). *Circ Res*. 2004;95:449–458.
67. Tao Y, Huang C, Huang Y, Hong L, Wang H, Zhou Z, Qiu Y. SIRT4 suppresses inflammatory responses in human umbilical vein endothelial cells. *Cardiovasc Toxicol*. 2015;15:217–223.
68. Tirziu D, Jaba IM, Yu P, Larrivée B, Coon BG, Cristofaro B, Zhuang ZW, Lanahan AA, Schwartz MA, Eichmann A, Simons M. Endothelial nuclear factor-κB-dependent regulation of arteriogenesis and branching. *Circulation*. 2012;126:2589–2600.
69. Gorski DH, Walsh K. The role of homeobox genes in vascular remodeling and angiogenesis. *Circ Res*. 2000;87:865–872.
70. Myers C, Charboneau A, Boudreau N. Homeobox B3 promotes capillary morphogenesis and angiogenesis. *J Cell Biol*. 2000;148:343–351.
71. Chiu JJ, Wung BS, Shyy JYJ, Hsieh HJ, Wang DL. Reactive oxygen species are involved in shear stress-induced intercellular adhesion molecule-1 expression in endothelial cells. *Arterioscler Thromb Vasc Biol*. 1997;17:3570–3577.

72. Kassab GS, Fung YC. The pattern of coronary arteriolar bifurcations and the uniform shear hypothesis. *Ann Biomed Eng*. 1995;23:13–20.
73. Murray CD. The physiological principle of minimum work: I. The vascular system and the cost of blood volume. *Proc Natl Acad Sci USA*. 1926;12:207–214.
74. Eitenmüller I, Volger O, Kluge A, Troidl K, Barancik M, Cai WJ, Heil M, Pipp F, Fischer S, Horrevoets AJG, Schmitz-Rixen T, Schaper W. The range of adaptation by collateral vessels after femoral artery occlusion. *Circ Res*. 2006;99:656–662.
75. Brownlee RD, Langille BL. Arterial adaptations to altered blood flow. *Can J Physiol Pharmacol*. 1991;69:978–983.
76. Miyashiro JK, Poppa V, Berk BC. Flow-induced vascular remodeling in the rat carotid artery diminishes with age. *Circ Res*. 1997;81:311–319.
77. Pal S, Tyler JK. Epigenetics and aging. *Sci Adv*. 2016;2:e1600584.
78. Awojoodu AO, Ogle ME, Sefcik LS, Bowers DT, Martin K, Brayman KL, Lynch KR, Peirce-Cottler SM, Botchwey E. Sphingosine 1-phosphate receptor 3 regulates recruitment of anti-inflammatory monocytes to microvessels during implant arteriogenesis. *Proc Natl Acad Sci USA*. 2013;110:13785–13790.
79. Herold J, Pipp F, Fernandez B, Xing Z, Heil M, Tillmanns H, Braun-Dullaeus RC. Transplantation of monocytes: a novel strategy for in vivo augmentation of collateral vessel growth. *Hum Gene Ther*. 2004;15:1–12.
80. Epstein SE, Stabile E, Kinnaird T, Lee CW, Clavijo L, Burnett MS. Janus phenomenon: the interrelated tradeoffs inherent in therapies designed to enhance collateral formation and those designed to inhibit atherogenesis. *Circulation*. 2004;109:2826–2831.

Supplemental Material

Table S1. Summary of total number of reads, mapping ratio, and CpG coverage in RRBS datasets

Label	Species	Seq Type	Total Read #	Mapped Read #	Mapping Ratio	Unique CpG	CpG Coverage (X)	Bisulfite Conversion Rate
N	human (hg19)	MiniSeq	34,206,095	15,411,220	45.05%	7,126,531	7	98.24%
R	human (hg19)	MiniSeq	23,777,663	13,438,821	56.52%	7,269,847	7	99.21%

Table S2. Summary of total number of reads, mapped reads, and mapping ratio for mRNA-seq datasets

Label	Species	Seq Type	Total Read Count	Total Read Count After QC	Mapped Read Count	Mapping Ratio
N	human (hg19)	mRNASeq	93,600,141	91,395,543	86,700,087	94.90%
R	human (hg19)	mRNASeq	85,738,933	83,771,202	79,624,282	95.00%

Table S3. *All DMRs corresponding to the promoter regions of genes with a methylation ratio difference ≥ |0.10| and FDR<0.1 between non-reversed and reversed conditions*

gene name	R methylation %	N methylation %	methylation % difference (N-R)	methylation adjusted Pvalue	mRNASeq Nvalue	mRNASeq Rvalue	mRNASeq Log2FC
EPS8L3	81	21	-60	6.33E-04	0.03	0.01	1.90
DSCR8	91	36	-55	5.92E-03	0.22	0.28	-0.36
MAB21L2	100	47	-53	8.13E-03	0.01	0.07	-2.72
EGFLAM	50	0	-50	6.61E-03	0.77	0.39	0.98
C8orf74	52	5	-47	1.44E-08	0.01	0.03	-1.55
MICB	67	20	-47	1.94E-02	8.63	5.20	0.73
AQP4-AS1	75	30	-45	6.69E-02	0.13	0.16	-0.38
BPNT1	41	0	-41	6.95E-05	27.27	24.52	0.15
POM121L9P	98	58	-40	2.38E-03	0.02	0.01	1.59
ITGBL1	92	55	-37	4.98E-05	0.89	0.65	0.47
PLCH2	81	45	-36	1.33E-04	0.04	0.02	1.30
SYNPO2L	92	56	-36	3.69E-02	0.16	0.13	0.36
PMEPA1	35	0	-35	1.44E-08	14.44	17.10	-0.24
BTBD16	100	65	-35	2.46E-02	0.11	0.41	-1.90
CSAD	83	48	-35	2.73E-02	9.61	7.18	0.42
NRG1	100	66	-34	5.92E-02	29.29	34.46	-0.23
SLC22A15	33	1	-32	5.96E-07	0.01	0.01	-1.18
POTEF	95	63	-32	1.38E-04	0.02	0.02	-0.51
ACOT2	82	50	-32	2.29E-02	0.87	0.46	0.91
ACP5	57	26	-31	1.48E-08	46.28	30.30	0.61
CCDC74B-AS1	94	63	-31	3.27E-02	0.12	0.11	0.11
C9orf153	74	43	-31	6.69E-02	0.09	0.07	0.39
CD79B	71	41	-30	2.58E-05	0.38	0.34	0.16
KIAA1549L	80	50	-30	4.65E-03	4.04	4.36	-0.11
LAMB3	95	65	-30	1.18E-02	10.22	8.45	0.27
LAMB3	95	65	-30	1.18E-02	10.22	8.45	0.27
PAPOLB	52	23	-29	1.60E-06	0.00	0.02	-2.59
METTL5	48	20	-28	2.43E-03	66.99	63.77	0.07
ZNF503-AS1	33	5	-28	3.35E-03	0.38	0.20	0.93
RGS12	31	3	-28	8.09E-03	29.65	28.00	0.08
PLEKHB1	60	32	-28	2.61E-02	2.43	2.29	0.09
KCNK2	69	41	-28	3.75E-02	0.09	0.13	-0.49
PDGFB	41	13	-28	9.14E-02	3.77	4.11	-0.13
EZH1	45	18	-27	1.47E-08	13.01	10.64	0.29
ZNF423	92	65	-27	1.89E-02	2.56	2.41	0.08
CCDC152	46	20	-26	8.49E-08	1.33	1.11	0.26
GGT1	34	9	-25	2.79E-02	74.25	78.80	-0.09
SLC13A3	25	1	-24	1.44E-08	0.07	0.09	-0.34
MPDU1	52	28	-24	1.02E-05	44.96	44.47	0.02
PRKACA	54	30	-24	1.18E-03	67.05	61.07	0.13
FGL2	35	11	-24	7.45E-03	0.04	0.05	-0.21
TOMM22	23	0	-23	1.44E-08	75.48	58.83	0.36
PLA2G4C	36	13	-23	5.39E-06	18.51	39.81	-1.11
LINC00672	88	65	-23	1.42E-02	0.32	0.25	0.34
KLK10	26	3	-23	1.61E-02	0.37	0.32	0.22
GGT1	30	7	-23	1.85E-02	74.25	78.80	-0.09
DAND5	59	36	-23	4.23E-02	0.31	0.20	0.67
ZNF597	49	27	-22	1.48E-08	1.27	1.51	-0.25
DRG2	33	11	-22	3.61E-08	10.53	10.52	0.00
ERAL1	22	0	-22	1.97E-03	41.46	49.11	-0.24
CPVL	33	11	-22	3.62E-03	0.07	0.11	-0.76
SPIN3	42	20	-22	1.37E-02	1.37	1.01	0.44

CSTF2T	23	2	-21	1.44E-08	9.50	8.92	0.09
INPP5D	23	2	-21	1.44E-08	60.83	48.65	0.32
HELB	46	25	-21	5.02E-06	1.03	0.93	0.14
RAX2	83	62	-21	4.50E-05	0.03	0.03	0.01
MSL3	40	19	-21	5.74E-05	86.41	96.78	-0.16
PKN1	56	35	-21	5.04E-02	59.22	41.39	0.52
RNF166	28	8	-20	1.44E-08	16.37	15.28	0.10
CLASRP	26	6	-20	1.44E-08	27.58	25.50	0.11
ITGAM	74	54	-20	6.76E-02	0.03	0.09	-1.51
BPIFB1	80	60	-20	8.40E-02	0.11	0.11	0.03
NAA60	46	27	-19	1.87E-08	105.11	95.31	0.14
SIRT4	47	28	-19	2.69E-04	0.79	0.68	0.21
RBMX2	37	18	-19	2.48E-02	22.84	22.56	0.02
NLRP11	68	49	-19	4.81E-02	0.00	0.00	-0.23
ZC3H4	18	0	-18	1.44E-08	15.21	10.06	0.60
ATHL1	31	13	-18	1.65E-08	3.98	3.19	0.32
S1PR4	24	6	-18	1.94E-06	0.23	0.12	0.90
HPRT1	38	20	-18	6.50E-06	31.01	35.05	-0.18
RGN	65	47	-18	1.12E-04	0.18	0.06	1.51
COMMD6	29	11	-18	7.77E-03	98.08	105.99	-0.11
RCN3	95	77	-18	8.90E-03	82.51	39.28	1.07
SLC7A8	28	10	-18	1.12E-02	2.60	2.49	0.06
SPC24	31	13	-18	1.67E-02	6.08	5.49	0.15
SLC6A10P	95	77	-18	4.42E-02	0.00	0.02	-2.87
SERPINA4	82	64	-18	7.75E-02	0.10	0.06	0.58
STYX	17	0	-17	1.44E-08	26.56	25.30	0.07
MED1	22	5	-17	3.94E-05	19.87	20.22	-0.03
SPON2	38	21	-17	1.30E-03	0.19	0.28	-0.60
MAP4K1	26	9	-17	2.84E-03	0.93	0.54	0.79
PCDHB3	48	31	-17	1.91E-02	0.04	0.02	1.26
C8orf44	17	1	-16	1.44E-08	14.52	12.54	0.21
PHF14	20	4	-16	1.45E-08	20.98	21.22	-0.02
HEXB	17	1	-16	1.47E-08	410.11	529.01	-0.37
TTC38	19	3	-16	1.52E-08	12.85	12.93	-0.01
PLEKHG6	30	14	-16	1.55E-08	0.34	0.12	1.47
PLEKHG6	30	14	-16	1.55E-08	0.34	0.12	1.47
SPAG4	24	8	-16	1.67E-08	1.89	1.20	0.66
RGMA	28	12	-16	1.12E-06	0.01	0.01	-0.28
APOE	17	1	-16	1.63E-06	4.60	4.09	0.17
TMEM209	52	36	-16	1.07E-03	1.92	1.17	0.71
TCF3	34	18	-16	3.92E-03	71.64	55.68	0.36
DBNDD2	95	79	-16	4.39E-03	14.96	17.62	-0.24
C1orf86	27	11	-16	3.81E-02	4.82	4.10	0.24
PKD1L1	76	60	-16	7.03E-02	1.48	1.20	0.30
AMPD2	70	54	-16	7.53E-02	41.20	35.57	0.21
CALD1	42	26	-16	8.38E-02	571.85	513.31	0.16
PPID	16	1	-15	1.52E-08	47.81	64.65	-0.44
ZNF493	15	0	-15	2.03E-08	5.54	5.51	0.01
BAK1	21	6	-15	8.76E-05	3.54	2.95	0.27
BDKRB2	25	10	-15	2.31E-03	0.03	0.13	-2.21
RPL38	24	9	-15	2.94E-03	2612.63	3092.61	-0.24
ANKRD33	35	20	-15	3.71E-03	0.09	0.07	0.42
SLCO1A2	100	85	-15	7.77E-03	0.10	0.24	-1.30
ASGR1	73	58	-15	4.08E-02	3.04	2.98	0.03
LPIN2	15	1	-14	1.44E-08	2.38	8.63	-1.86
TAB1	14	0	-14	1.44E-08	5.50	8.00	-0.54
DKKL1	19	5	-14	1.47E-08	0.17	0.12	0.46
DKKL1	19	5	-14	1.47E-08	0.17	0.12	0.46
BRCA1	18	4	-14	1.74E-06	5.17	5.14	0.01

ZNF207	27	13	-14	9.74E-06	168.27	171.22	-0.03
PHF17	14	0	-14	9.24E-05	13.84	12.17	0.19
MBNL3	26	12	-14	1.25E-04	0.67	0.73	-0.12
MED24	14	0	-14	2.69E-04	52.08	47.89	0.12
OCRL	20	6	-14	4.18E-04	16.60	13.84	0.26
SYCE1L	97	83	-14	2.29E-02	16.68	14.18	0.23
C12orf36	93	79	-14	9.90E-02	0.14	0.04	1.94
AGPAT6	13	0	-13	1.44E-08	68.63	66.13	0.05
DGCR14	15	2	-13	1.44E-08	4.17	4.07	0.04
IDUA	13	0	-13	1.52E-08	8.72	5.44	0.68
SNX29	17	4	-13	1.07E-05	5.30	5.94	-0.17
USP16	28	15	-13	2.24E-05	15.29	15.39	-0.01
ADAM32	30	17	-13	3.37E-05	1.50	1.52	-0.02
DMPK	23	10	-13	4.92E-04	39.58	37.02	0.10
TCEB3B	97	84	-13	2.64E-03	0.01	0.01	-0.06
PCYT1B	19	6	-13	6.38E-03	0.07	0.10	-0.46
SLC5A4	100	87	-13	1.42E-02	0.10	0.08	0.33
DMKN	14	1	-13	2.24E-02	0.09	0.05	0.78
C1QTNF1	35	22	-13	3.09E-02	0.46	0.22	1.06
MUTYH	13	0	-13	4.32E-02	4.19	4.03	0.06
TOE1	13	0	-13	4.32E-02	3.62	3.14	0.21
NRN1L	68	55	-13	5.14E-02	34.26	35.66	-0.06
FTLP10	94	81	-13	6.78E-02	0.04	0.11	-1.50
LINC00574	13	0	-13	8.23E-02	0.13	0.12	0.10
RFESD	12	0	-12	1.44E-08	0.57	0.22	1.35
RFESD	12	0	-12	1.44E-08	0.57	0.22	1.35
PI4KB	13	1	-12	1.47E-08	31.10	26.02	0.26
PI4KB	13	1	-12	1.47E-08	31.10	26.02	0.26
TSSK3	20	8	-12	1.67E-08	0.53	0.48	0.16
EDARADD	12	0	-12	3.66E-08	0.20	0.16	0.29
SUMO2	28	16	-12	2.15E-06	441.13	338.71	0.38
RHBDL1	27	15	-12	4.01E-06	0.13	0.10	0.50
SUGT1P3	25	13	-12	5.12E-06	1.39	2.47	-0.83
MARS	47	35	-12	4.05E-05	90.69	97.27	-0.10
SNAPC5	21	9	-12	4.51E-04	30.90	31.57	-0.03
MRPL28	20	8	-12	2.57E-03	39.19	34.56	0.18
KBTBD7	39	27	-12	3.96E-03	2.99	2.59	0.21
FXYD2	88	76	-12	1.89E-02	15.81	24.14	-0.61
MORN3	91	79	-12	6.08E-02	0.67	0.45	0.58
APOBEC3D	12	0	-12	7.81E-02	11.13	9.90	0.17
C19orf33	47	35	-12	8.20E-02	39.79	40.11	-0.01
CKS1B	12	0	-12	8.87E-02	5.51	5.85	-0.09
SHC1	12	0	-12	8.87E-02	202.71	208.14	-0.04
ASL	14	3	-11	1.44E-08	70.34	67.45	0.06
ERICH1	13	2	-11	1.51E-08	37.35	23.08	0.69
TUBGCP2	22	11	-11	1.55E-08	15.68	12.74	0.30
GP1BB	16	5	-11	1.57E-08	8.91	9.43	-0.08
ARC	21	10	-11	1.64E-08	0.02	0.06	-2.00
CRISPLD2	11	0	-11	2.32E-08	2.74	2.11	0.38
RASSF1	12	1	-11	7.16E-07	5.10	5.37	-0.07
P2RY2	16	5	-11	7.63E-07	1.54	1.44	0.10
P2RY2	16	5	-11	7.63E-07	1.54	1.44	0.10
RGPD2	100	89	-11	1.51E-05	0.08	0.09	-0.24
PMVK	13	2	-11	3.89E-05	7.59	6.70	0.18
MSL3	38	27	-11	3.12E-04	86.41	96.78	-0.16
RBP5	23	12	-11	4.10E-04	0.87	0.87	0.00
FLT3LG	22	11	-11	5.74E-04	782.26	935.32	-0.26
ZC4H2	26	15	-11	5.96E-04	8.73	8.31	0.07
C20orf196	15	4	-11	7.96E-04	2.89	2.91	-0.01

MSL3	39	28	-11	8.02E-04	86.41	96.78	-0.16
MGAT5B	21	10	-11	1.27E-03	0.15	0.08	0.91
SPON2	24	13	-11	1.34E-03	0.19	0.28	-0.60
KCNH2	34	23	-11	8.19E-03	0.02	0.03	-0.34
ZNF177	21	10	-11	1.51E-02	10.72	9.81	0.13
MYADM	22	11	-11	1.86E-02	32.83	34.40	-0.07
ZNF682	37	26	-11	2.03E-02	1.07	0.90	0.26
HYPK	19	8	-11	2.37E-02	304.92	347.00	-0.19
AR	24	13	-11	2.86E-02	2.56	2.19	0.23
MYO1H	99	88	-11	3.22E-02	0.09	0.30	-1.79
DNAJC8	51	40	-11	3.70E-02	113.66	116.81	-0.04
NUP160	27	16	-11	4.44E-02	37.20	35.05	0.09
BDNF	13	2	-11	4.61E-02	2.82	3.05	-0.11
LYNX1	67	56	-11	9.05E-02	4.97	5.21	-0.07
EIF4G1	12	2	-10	1.44E-08	193.74	209.84	-0.12
GRM4	13	3	-10	1.51E-08	0.00	0.00	0.08
HMBS	12	2	-10	2.40E-08	5.93	6.03	-0.02
IRF7	20	10	-10	2.64E-08	1.87	2.87	-0.62
LGALS1	10	0	-10	6.26E-08	1405.19	820.91	0.78
LZTS2	11	1	-10	1.93E-07	10.24	10.10	0.02
USP39	16	6	-10	2.29E-07	55.11	72.89	-0.40
C2orf68	16	6	-10	2.29E-07	7.45	6.91	0.11
CREB3L1	12	2	-10	1.10E-06	1.10	1.01	0.12
ASL	18	8	-10	2.56E-06	70.34	67.45	0.06
FAM57B	11	1	-10	2.91E-06	0.11	0.14	-0.42
TNK1	14	4	-10	7.13E-06	0.16	0.56	-1.84
RGMA	18	8	-10	1.33E-05	0.01	0.01	-0.28
NOP2	12	2	-10	1.17E-04	24.14	22.62	0.09
CCDC78	21	11	-10	2.50E-04	0.10	0.07	0.57
THUMPD1	20	10	-10	2.81E-04	29.93	34.48	-0.20
NFRKB	18	8	-10	2.62E-03	5.75	6.45	-0.17
POC5	24	14	-10	2.71E-03	6.05	4.78	0.34
TTC25	30	20	-10	6.50E-03	0.13	0.07	0.78
NUP210L	41	31	-10	7.33E-03	0.04	0.04	-0.03
WDR38	29	19	-10	1.48E-02	0.05	0.05	0.10
DDX43	96	86	-10	1.49E-02	0.26	0.17	0.63
JDP2	98	88	-10	2.33E-02	3.98	5.75	-0.53
POM121L10P	89	79	-10	3.81E-02	0.06	0.06	-0.15
SEMA4D	99	89	-10	4.39E-02	4.05	3.11	0.38
TRIM72	41	31	-10	4.91E-02	0.04	0.04	-0.23
CD320	71	61	-10	5.49E-02	25.89	23.20	0.16
PKP3	59	49	-10	5.49E-02	0.18	0.09	1.04
WBSCR27	38	28	-10	9.71E-02	0.13	0.19	-0.50
ADPGK-AS1	4	14	10	1.44E-08	1.01	1.25	-0.31
PDLIM5	3	13	10	1.44E-08	46.85	54.30	-0.21
KIAA1598	1	11	10	1.44E-08	1.42	1.52	-0.10
KLC4	1	11	10	1.44E-08	11.20	11.40	-0.03
KLC4	1	11	10	1.44E-08	11.20	11.40	-0.03
POLR3H	1	11	10	1.44E-08	10.20	9.57	0.09
POLR3H	1	11	10	1.44E-08	10.20	9.57	0.09
MRPL2	1	11	10	1.44E-08	30.42	27.23	0.16
DEGS1	6	16	10	1.44E-08	147.47	120.36	0.29
SLC12A6	4	14	10	1.44E-08	20.84	23.38	-0.17
TRNT1	6	16	10	1.46E-08	26.46	31.82	-0.27
PITPNA	5	15	10	1.47E-08	106.60	108.69	-0.03
WDR85	7	17	10	1.48E-08	8.45	6.47	0.39
VKORC1	9	19	10	1.52E-08	55.52	42.57	0.38
ZNF707	8	18	10	1.57E-08	5.34	4.73	0.17
SSB	2	12	10	1.57E-08	654.63	681.75	-0.06

NLK	7	17	10	1.60E-08	18.02	18.78	-0.06
B3GALNT1	9	19	10	1.67E-08	7.45	8.31	-0.16
CXXC1	6	16	10	1.76E-08	28.92	22.11	0.39
TSPAN15	3	13	10	8.05E-08	34.23	30.63	0.16
C12orf29	2	12	10	9.87E-08	10.01	9.63	0.06
UBA52	9	19	10	2.17E-07	365.84	531.97	-0.54
SDHC	12	22	10	2.99E-07	42.94	46.05	-0.10
C11orf92	6	16	10	1.63E-06	0.08	0.09	-0.29
SNRNP35	15	25	10	2.32E-06	10.38	5.57	0.90
HCG11	8	18	10	7.14E-06	2.54	2.32	0.13
ZFR	7	17	10	8.39E-06	42.36	47.72	-0.17
C9orf3	10	20	10	1.28E-05	44.26	43.18	0.04
CCDC103	3	13	10	6.69E-05	6.99	5.36	0.38
PTGDS	8	18	10	6.81E-05	18.31	13.32	0.46
CORO1B	18	28	10	1.19E-04	51.78	37.39	0.47
STIL	9	19	10	1.24E-04	2.96	2.74	0.11
PPP1R14A	13	23	10	1.75E-04	6.36	7.54	-0.25
ZFYVE26	8	18	10	2.62E-04	18.97	15.73	0.27
KCNJ11	12	22	10	3.43E-04	0.11	0.06	0.84
STX6	10	20	10	5.54E-04	28.34	26.31	0.11
ZNF552	18	28	10	5.73E-04	0.24	0.46	-0.95
PAIP2	10	20	10	6.26E-04	200.32	160.85	0.32
GYPC	12	22	10	9.27E-04	1.17	1.08	0.11
MAPK15	11	21	10	1.08E-03	0.05	0.02	1.49
RPL11	15	25	10	1.36E-03	917.46	985.09	-0.10
TRAPPC12	12	22	10	1.50E-03	17.57	18.98	-0.11
KLHL12	37	47	10	1.74E-03	11.53	11.68	-0.02
ZNF391	13	23	10	1.95E-03	1.04	0.44	1.25
MAP3K13	11	21	10	2.04E-03	9.80	10.21	-0.06
FAM215A	18	28	10	2.74E-03	0.07	0.14	-0.98
LHB	20	30	10	2.89E-03	0.03	0.03	0.16
KCNJ11	23	33	10	3.04E-03	0.11	0.06	0.84
BTBD2	29	39	10	3.62E-03	23.13	35.63	-0.62
SYNE4	19	29	10	4.06E-03	4.57	3.64	0.33
DHX8	23	33	10	4.26E-03	15.44	15.56	-0.01
FBXW4P1	77	87	10	5.56E-03	0.23	0.28	-0.26
PDHA1	22	32	10	5.85E-03	155.70	162.93	-0.07
CWF19L1	18	28	10	6.65E-03	11.89	11.96	-0.01
ELAC1	11	21	10	7.78E-03	79.22	69.68	0.19
OIP5-AS1	12	22	10	7.78E-03	28.34	17.94	0.66
AIPL1	70	80	10	1.02E-02	0.11	0.12	-0.03
RIBC2	41	51	10	1.48E-02	0.34	0.47	-0.48
SMC1B	41	51	10	1.48E-02	0.02	0.02	-0.03
FGFBP3	0	10	10	1.67E-02	0.18	0.07	1.30
LAPTM5	3	13	10	1.75E-02	59.38	53.75	0.14
PAFAH2	2	12	10	2.73E-02	6.94	3.98	0.80
CPLX3	14	24	10	2.79E-02	0.02	0.04	-0.93
PCDHGC4	38	48	10	2.80E-02	44.63	44.34	0.01
EXOC7	50	60	10	2.85E-02	44.66	54.64	-0.29
KIF20B	6	16	10	3.22E-02	4.68	3.57	0.39
ZNF165	18	28	10	3.33E-02	0.22	0.29	-0.35
GHITM	22	32	10	4.18E-02	117.28	115.52	0.02
PTP4A3	89	99	10	4.48E-02	2.51	2.57	-0.03
SPESP1	75	85	10	4.92E-02	3.15	2.05	0.62
NOX5	75	85	10	4.92E-02	3.15	2.05	0.62
TBPL2	43	53	10	5.75E-02	0.76	0.48	0.67
ISLR	78	88	10	6.20E-02	0.03	0.03	-0.05
ZDHHC9	28	38	10	7.65E-02	14.97	18.54	-0.31
LIMS2	9	19	10	8.73E-02	18.41	16.73	0.14

MED11	7	17	10	9.21E-02	4.32	5.14	-0.25
RP1L1	90	100	10	9.46E-02	0.44	0.26	0.78
ZNF808	2	13	11	1.44E-08	16.48	25.19	-0.61
MIS18BP1	0	11	11	1.44E-08	14.50	20.73	-0.52
IQGAP1	3	14	11	1.44E-08	248.25	307.74	-0.31
FLT3LG	0	11	11	1.44E-08	782.26	935.32	-0.26
GMNN	0	11	11	1.44E-08	22.50	17.67	0.35
MCU	2	13	11	1.47E-08	18.85	19.38	-0.04
AUH	4	15	11	1.47E-08	6.69	6.75	-0.01
VPS11	8	19	11	1.55E-08	27.65	24.21	0.19
LAMP1	9	20	11	1.90E-08	258.24	234.38	0.14
XPO4	5	16	11	1.95E-08	6.71	6.76	-0.01
CHST7	26	37	11	2.07E-08	4.57	4.10	0.15
ANKRD30BL	27	38	11	2.34E-08	0.04	0.07	-0.91
FGFRL1	13	24	11	2.41E-08	4.36	3.94	0.15
IKBKE	0	11	11	5.88E-08	10.37	7.64	0.44
CDC42	4	15	11	2.51E-07	185.16	192.43	-0.06
ZSWIM3	2	13	11	1.09E-06	1.08	1.18	-0.12
C3orf55	9	20	11	1.47E-06	9.52	9.75	-0.03
EMR2	2	13	11	2.21E-06	0.18	0.22	-0.34
USP51	19	30	11	4.29E-06	1.23	0.92	0.41
PIH1D3	24	35	11	6.35E-06	0.08	0.09	-0.23
ZNF560	18	29	11	1.77E-05	0.00	0.00	-0.22
GGACT	6	17	11	2.08E-05	1.56	1.20	0.38
NLRX1	8	19	11	6.05E-05	1.27	0.97	0.39
PSMB4	14	25	11	1.23E-04	89.62	80.22	0.16
CEND1	10	21	11	1.33E-04	0.28	0.19	0.60
TMEM218	10	21	11	1.63E-04	18.41	13.72	0.42
TMEM218	10	21	11	1.63E-04	18.41	13.72	0.42
RNF8	7	18	11	2.32E-04	29.41	30.97	-0.07
TGDS	13	24	11	2.55E-04	4.97	4.86	0.03
RGAG4	23	34	11	2.72E-04	0.52	0.43	0.28
FOXO4	8	19	11	3.07E-04	4.45	3.31	0.42
CDK20	7	18	11	3.99E-04	0.41	0.44	-0.09
CCM2	4	15	11	4.77E-04	41.58	30.78	0.43
AMMECR1	16	27	11	5.11E-04	5.61	5.56	0.02
MSN	24	35	11	8.21E-04	283.85	304.74	-0.10
AGA	6	17	11	9.90E-04	12.45	15.11	-0.28
PTPLAD2	27	38	11	1.10E-03	4.87	5.90	-0.28
ZMYND10	19	30	11	1.47E-03	0.07	0.06	0.33
SNRPF	11	22	11	2.89E-03	91.74	114.33	-0.32
TLE2	12	23	11	3.43E-03	22.37	19.69	0.18
RAD51D	27	38	11	5.73E-03	8.49	9.87	-0.22
RAD9A	40	51	11	1.25E-02	3.72	2.38	0.64
PIWIL1	60	71	11	1.33E-02	0.06	0.04	0.74
ZNF551	30	41	11	1.38E-02	8.81	7.22	0.29
LPIN3	11	22	11	1.66E-02	0.14	0.17	-0.25
PPAPDC3	56	67	11	1.74E-02	0.36	0.31	0.19
FAM9C	81	92	11	2.02E-02	0.14	0.16	-0.19
GLUD2	18	29	11	2.42E-02	0.09	0.12	-0.38
TCTEX1D4	77	88	11	2.79E-02	0.20	0.16	0.32
ASIC2	46	57	11	5.88E-02	0.00	0.04	-3.22
ZNF492	45	56	11	6.60E-02	0.08	0.07	0.18
DNAH6	16	27	11	7.47E-02	0.01	0.05	-2.92
GON4L	34	45	11	8.31E-02	14.46	17.91	-0.31
PIGA	25	36	11	8.45E-02	3.85	2.88	0.42
MS4A10	82	93	11	8.49E-02	0.18	0.15	0.29
ADTRP	89	100	11	9.37E-02	14.26	14.84	-0.06
BCL2L14	81	92	11	9.88E-02	0.32	0.63	-0.96

PIWIL2	46	57	11	9.96E-02	0.13	0.13	-0.05
RNASEH1	7	19	12	1.44E-08	18.38	17.32	0.09
SNX33	4	16	12	1.44E-08	4.38	3.92	0.16
SRP14	1	13	12	1.44E-08	1089.93	942.41	0.21
ZNF771	1	13	12	1.44E-08	1.15	0.90	0.35
METTL13	6	18	12	1.44E-08	15.91	11.91	0.42
C6orf57	5	17	12	1.44E-08	5.46	3.87	0.50
ZNHIT6	2	14	12	1.44E-08	15.33	12.92	0.25
POLR3F	5	17	12	1.47E-08	11.01	12.78	-0.22
SNAPC1	10	22	12	1.57E-08	406.34	404.96	0.00
MAP7D3	17	29	12	1.60E-08	22.27	16.64	0.42
ACOT4	10	22	12	1.73E-08	0.03	0.03	-0.16
GNAS	31	43	12	2.51E-08	458.16	442.50	0.05
MCM5	27	39	12	3.67E-08	12.56	9.31	0.43
TMEM62	8	20	12	4.94E-08	30.43	35.77	-0.23
RHPN2	11	23	12	6.11E-08	1.55	1.56	-0.01
TCTN3	12	24	12	1.67E-06	56.15	52.02	0.11
EIF1AX	24	36	12	2.43E-06	56.38	47.36	0.25
RUFY1	5	17	12	2.95E-06	109.75	111.85	-0.03
MRPS25	7	19	12	7.02E-06	33.83	29.94	0.18
BLVRB	11	23	12	7.04E-06	12.40	14.19	-0.20
NHLRC1	18	30	12	7.90E-06	0.41	0.29	0.49
PHF16	16	28	12	1.42E-05	5.93	8.25	-0.48
PHF16	16	28	12	1.42E-05	5.93	8.25	-0.48
C16orf80	35	47	12	1.69E-04	68.93	72.29	-0.07
SMARCAL1	8	20	12	2.02E-04	13.36	13.73	-0.04
SMARCAL1	8	20	12	2.02E-04	13.36	13.73	-0.04
C1GALT1C1	36	48	12	2.36E-04	33.64	38.22	-0.18
MMADHC	0	12	12	3.32E-04	65.47	73.95	-0.18
CSTF2	36	48	12	6.15E-04	6.05	7.68	-0.35
KCNN3	9	21	12	8.37E-04	6.89	6.08	0.18
C14orf2	17	29	12	9.41E-04	283.38	220.43	0.36
SYCE2	43	55	12	1.10E-03	0.25	0.12	1.04
MAOA	30	42	12	1.15E-03	3.31	2.91	0.19
C2orf74	82	94	12	1.63E-03	40.17	44.10	-0.13
MDM4	27	39	12	3.48E-03	11.11	11.93	-0.10
BCL6	4	16	12	3.71E-03	6.69	6.92	-0.05
LY6K	67	79	12	9.63E-03	0.83	0.71	0.23
MED16	16	28	12	1.73E-02	10.24	7.71	0.41
DNAJC19	38	50	12	1.73E-02	30.36	23.15	0.39
DNAJC19	34	46	12	1.87E-02	30.36	23.15	0.39
CDHR5	72	84	12	2.84E-02	0.02	0.02	0.20
C1D	12	24	12	2.88E-02	16.36	13.16	0.31
TNFRSF25	45	57	12	3.60E-02	29.69	24.12	0.30
RHBDL2	9	21	12	6.21E-02	1.74	2.10	-0.27
PEX19	31	43	12	8.24E-02	96.70	79.61	0.28
DIO1	82	94	12	8.31E-02	0.06	0.07	-0.11
ALDH3B1	80	92	12	8.56E-02	0.29	0.18	0.71
EVI5L	79	91	12	9.86E-02	23.04	21.63	0.09
UBE2L6	0	13	13	1.44E-08	19.57	22.84	-0.22
MLH3	1	14	13	1.44E-08	5.17	5.83	-0.17
ING4	1	14	13	1.44E-08	33.56	35.69	-0.09
COA6	3	16	13	1.44E-08	28.20	29.70	-0.07
TBCCD1	1	14	13	1.44E-08	9.27	9.72	-0.07
C11orf48	2	15	13	1.44E-08	306.26	300.07	0.03
MKS1	0	13	13	1.44E-08	7.54	6.41	0.24
FOXRED2	29	42	13	1.91E-08	3.21	3.15	0.03
FOXRED2	30	43	13	2.30E-08	3.21	3.15	0.03
AMZ2P1	9	22	13	5.41E-08	6.21	5.71	0.12

CHST6	12	25	13	6.54E-08	0.06	0.11	-0.93
WIF1	23	36	13	2.36E-07	0.01	0.01	0.03
DNAJC15	8	21	13	2.46E-07	5.56	5.21	0.09
SERF2	15	28	13	4.74E-07	304.92	347.00	-0.19
IFFO1	14	27	13	6.39E-07	11.83	10.79	0.13
UBQLN2	16	29	13	1.13E-06	11.33	10.28	0.14
ANGEL2	9	22	13	2.44E-06	16.92	17.08	-0.01
TNFSF11	3	16	13	3.65E-06	0.01	0.01	-0.41
GANC	3	16	13	7.39E-06	13.30	13.94	-0.07
ZNF695	7	20	13	8.06E-06	2.38	2.13	0.16
ABCC10	9	22	13	8.90E-06	12.79	11.98	0.09
CCND3	9	22	13	1.16E-05	32.18	30.73	0.07
RINT1	10	23	13	2.48E-05	30.19	29.98	0.01
SSTR5	9	22	13	2.91E-05	0.10	0.01	2.97
TGFB1I1	5	18	13	4.61E-05	10.45	10.33	0.02
TGFB1I1	5	18	13	4.61E-05	10.45	10.33	0.02
TGFB1I1	5	18	13	6.50E-05	10.45	10.33	0.02
TAF1A	23	36	13	1.02E-04	2.19	3.27	-0.58
CYP11A1	8	21	13	1.40E-04	0.05	0.03	0.53
ZNF331	38	51	13	1.93E-04	3.57	2.98	0.26
USP18	9	22	13	2.21E-04	5.00	5.69	-0.19
C15orf26	5	18	13	2.59E-04	1.50	0.93	0.69
MAP2K3	1	14	13	4.89E-04	12.12	10.05	0.27
SFR1	0	13	13	5.81E-04	22.46	23.37	-0.06
SFR1	0	13	13	5.81E-04	22.46	23.37	-0.06
PEX14	18	31	13	9.82E-04	12.49	11.03	0.18
IZUMO1	27	40	13	1.22E-03	0.29	0.41	-0.52
DNALI1	18	31	13	2.12E-03	4.45	5.35	-0.27
RSPH10B	14	27	13	2.87E-03	0.18	0.38	-1.10
RSPH10B2	14	27	13	2.87E-03	0.04	0.06	-0.58
MIR202	63	76	13	3.90E-03	0.37	0.42	-0.20
NGFRAP1	26	39	13	4.76E-03	151.93	159.11	-0.07
PCDHGA2	24	37	13	8.40E-03	44.63	44.34	0.01
CAMKK2	58	71	13	9.04E-03	12.21	11.78	0.05
DDIT3	11	24	13	1.23E-02	5.17	5.66	-0.13
MFAP2	9	22	13	3.66E-02	114.38	150.38	-0.39
KLK6	59	72	13	5.26E-02	1.88	2.03	-0.11
CT45A6	81	94	13	6.60E-02	0.06	0.04	0.81
DAB2IP	24	37	13	7.52E-02	17.74	19.02	-0.10
LRRC36	3	17	14	1.44E-08	0.23	0.32	-0.47
CIR1	0	14	14	1.44E-08	32.00	38.12	-0.25
SCRN3	0	14	14	1.44E-08	23.96	27.89	-0.22
FRS2	1	15	14	1.44E-08	10.88	12.61	-0.21
PNPO	1	15	14	1.44E-08	47.87	55.37	-0.21
CARS	1	15	14	1.44E-08	15.79	17.60	-0.16
SNW1	5	19	14	1.44E-08	80.71	86.15	-0.09
SCAP	6	20	14	1.44E-08	11.47	11.46	0.00
MRP63	1	15	14	1.44E-08	7.54	7.52	0.00
RUFY2	1	15	14	1.44E-08	32.12	31.90	0.01
RUFY2	1	15	14	1.44E-08	32.12	31.90	0.01
HN1L	1	15	14	1.44E-08	171.21	156.30	0.13
PPT1	0	14	14	1.44E-08	99.58	80.88	0.30
PSMC1	1	15	14	1.44E-08	83.29	65.49	0.35
XKR9	0	14	14	1.44E-08	0.43	0.34	0.35
COPS3	4	18	14	1.44E-08	136.84	100.11	0.45
KCTD19	3	17	14	1.44E-08	1.31	0.88	0.59
LACTB2	0	14	14	1.44E-08	1.95	0.71	1.46
NDUFA6	5	19	14	1.52E-08	56.97	73.19	-0.36
COX8A	14	28	14	1.52E-08	49.36	45.00	0.13

PLK4	11	25	14	1.55E-08	4.44	2.41	0.88
CDC25B	8	22	14	1.63E-08	241.43	191.42	0.33
FAM71E1	10	24	14	1.79E-08	0.12	0.15	-0.30
EMC10	10	24	14	1.79E-08	48.33	17.51	1.46
LONRF3	24	38	14	2.21E-08	4.25	4.17	0.03
LRFN4	26	40	14	3.12E-08	2.48	2.21	0.17
FAM83D	13	27	14	3.90E-08	8.08	5.55	0.54
GATA2	33	47	14	4.12E-08	13.84	13.07	0.08
RNF113A	31	45	14	6.46E-08	6.27	5.73	0.13
NDUFA1	31	45	14	1.33E-07	70.69	78.72	-0.16
TCOF1	9	23	14	2.19E-07	19.21	18.95	0.02
KIAA1919	13	27	14	8.61E-07	2.65	2.60	0.03
GNAS	33	47	14	4.93E-06	458.16	442.50	0.05
TRIP4	13	27	14	5.73E-06	36.61	27.87	0.39
OXGR1	8	22	14	1.22E-05	0.05	0.02	1.11
RPSAP58	9	23	14	3.78E-05	0.75	0.74	0.00
NCMAP	8	22	14	4.37E-05	0.05	0.08	-0.65
SUMF1	25	39	14	3.60E-04	22.44	20.47	0.13
ALDH1L2	25	39	14	4.11E-04	0.34	0.29	0.22
EPHA1	33	47	14	1.06E-03	1.04	1.67	-0.68
MTIF2	4	18	14	1.23E-03	16.40	16.32	0.01
ZMAT1	32	46	14	1.85E-03	2.42	3.10	-0.36
ZCCHC4	22	36	14	3.13E-03	4.57	5.04	-0.14
PFDN5	52	66	14	7.59E-03	165.38	213.81	-0.37
GABRB3	45	59	14	7.66E-03	1.19	1.16	0.04
NEURL3	41	55	14	8.07E-03	0.03	0.01	2.08
PCDHA9	13	27	14	1.31E-02	0.88	0.67	0.39
PYCRL	36	50	14	2.15E-02	0.48	0.48	0.00
ANO4	17	31	14	4.60E-02	0.56	1.79	-1.69
PRND	35	49	14	8.78E-02	0.06	0.09	-0.54
PIGB	1	16	15	1.44E-08	9.07	10.53	-0.22
ZNF497	5	20	15	1.44E-08	1.91	1.49	0.36
FAM127B	13	28	15	5.65E-07	33.00	30.29	0.12
TOP1MT	24	39	15	5.95E-07	9.47	8.28	0.19
DGKA	10	25	15	7.82E-07	198.25	199.67	-0.01
GPR19	0	15	15	6.35E-06	0.13	0.32	-1.25
C9orf129	20	35	15	8.63E-06	0.05	0.14	-1.43
CALHM2	2	17	15	3.33E-05	35.25	30.30	0.22
MGARP	34	49	15	7.52E-05	62.54	63.24	-0.02
MTL5	27	42	15	1.86E-04	0.72	0.70	0.05
RUSC1	20	35	15	1.07E-03	7.78	7.27	0.10
KLC4	14	29	15	1.08E-03	11.20	11.40	-0.03
EID3	24	39	15	1.33E-03	1.30	1.95	-0.58
ZMAT4	9	24	15	4.69E-03	0.17	0.27	-0.64
C2orf50	56	71	15	4.90E-03	0.07	0.10	-0.54
MRVI1	70	85	15	1.14E-02	0.52	0.48	0.12
C1orf64	81	96	15	1.32E-02	0.08	0.10	-0.34
ZNF235	3	18	15	1.54E-02	5.76	5.89	-0.03
CARD14	56	71	15	2.64E-02	0.51	0.41	0.30
C19orf38	57	72	15	3.30E-02	0.17	0.14	0.22
LIG1	2	17	15	3.50E-02	0.97	2.31	-1.25
AQP7	53	68	15	6.55E-02	0.14	0.09	0.70
C11orf83	0	16	16	1.44E-08	2.48	3.10	-0.32
UFSP2	0	16	16	1.44E-08	71.39	84.81	-0.25
TMEM219	13	29	16	1.44E-08	28.20	28.97	-0.04
GINS1	1	17	16	1.44E-08	4.54	3.91	0.21
WDR66	5	21	16	1.44E-08	23.62	19.81	0.25
KPNA6	9	25	16	1.52E-08	28.25	21.96	0.36
C11orf70	7	23	16	1.52E-08	0.33	0.17	0.93

SET	2	18	16	1.60E-08	275.42	222.70	0.31
ZNF414	11	27	16	1.63E-08	3.94	3.86	0.03
ZNF726	21	37	16	1.84E-08	0.95	0.99	-0.07
SEPSECS	9	25	16	9.29E-08	3.84	3.66	0.07
RBMXL2	51	67	16	9.89E-08	0.17	0.16	0.07
PKD2L2	11	27	16	4.90E-07	0.65	0.82	-0.34
ZNF350	14	30	16	7.06E-07	6.13	11.48	-0.90
SMUG1	18	34	16	3.41E-06	6.35	5.63	0.17
UFC1	15	31	16	3.90E-06	120.85	88.13	0.46
HSDL2	3	19	16	5.77E-06	19.85	18.99	0.06
DYNLT3	16	32	16	7.12E-06	33.88	32.82	0.05
DUS3L	15	31	16	1.09E-05	6.30	4.87	0.37
MFSD5	5	21	16	1.09E-05	21.51	18.82	0.19
SYCE1	56	72	16	2.25E-05	0.57	0.25	1.20
HOXB8	12	28	16	2.28E-05	4.92	5.01	-0.02
ANO7	76	92	16	2.59E-04	0.70	0.57	0.30
KIAA1598	60	76	16	2.71E-04	1.42	1.52	-0.10
HEMK1	15	31	16	2.73E-04	1.37	1.44	-0.07
KCNE3	33	49	16	9.06E-04	0.06	0.10	-0.83
TOR1AIP2	10	26	16	1.28E-03	51.44	46.67	0.14
QPRT	69	85	16	2.23E-03	0.50	0.50	0.00
IGF2	77	93	16	3.13E-03	8.78	7.78	0.17
ISG15	51	67	16	4.76E-03	10.67	13.13	-0.30
RASAL3	52	68	16	1.64E-02	0.34	0.24	0.49
NEK8	29	45	16	1.84E-02	0.68	0.48	0.52
PAK6	22	38	16	2.05E-02	17.78	9.87	0.85
CAPN12	74	90	16	2.26E-02	13.78	12.26	0.17
SNAPC4	76	92	16	2.53E-02	2.77	1.86	0.57
SLC23A1	78	94	16	3.23E-02	0.15	0.11	0.34
IDI2-AS1	80	96	16	3.32E-02	0.04	0.04	-0.04
SLC38A7	13	29	16	4.59E-02	17.72	18.57	-0.07
MTO1	11	28	17	1.44E-08	21.26	26.76	-0.33
ATL3	0	17	17	1.44E-08	42.26	39.60	0.09
ZNF440	1	18	17	1.44E-08	4.24	3.89	0.12
NINL	2	19	17	1.44E-08	12.26	9.74	0.33
AKR1E2	17	34	17	1.46E-08	1.94	1.50	0.37
DLG3	19	36	17	1.52E-08	1.70	1.94	-0.19
SMUG1	17	34	17	5.07E-07	6.35	5.63	0.17
SYTL4	20	37	17	3.32E-06	356.86	227.69	0.65
SYTL4	20	37	17	3.32E-06	356.86	227.69	0.65
SOX30	27	44	17	6.21E-06	0.04	0.03	0.29
TGIF1	8	25	17	6.61E-06	30.13	24.18	0.32
BBS2	26	43	17	1.31E-04	90.58	81.61	0.15
POLR2G	41	58	17	3.21E-04	36.69	40.07	-0.13
EXOC7	23	40	17	5.72E-04	44.66	54.64	-0.29
CCDC58	14	31	17	8.36E-04	24.64	25.73	-0.06
JAK3	19	36	17	2.89E-03	0.20	0.15	0.47
IVD	4	21	17	3.17E-03	17.42	16.32	0.09
KCNE1L	47	64	17	4.83E-03	35.93	35.28	0.03
POGZ	81	98	17	2.27E-02	43.20	30.12	0.52
MORF4L2	3	20	17	2.55E-02	301.86	347.28	-0.20
C1orf168	69	86	17	5.04E-02	0.17	0.13	0.42
CNN1	26	43	17	6.16E-02	0.39	0.25	0.68
CCDC73	74	91	17	8.45E-02	3.61	4.21	-0.22
LCT	80	97	17	8.59E-02	0.00	0.00	0.87
SERF2	16	34	18	1.57E-08	304.92	347.00	-0.19
LARS	15	33	18	5.69E-08	122.66	129.09	-0.07
DNM1P46	12	30	18	1.52E-07	0.16	0.06	1.43
ZNF331	34	52	18	2.15E-07	3.57	2.98	0.26

EBPL	21	39	18	2.49E-07	18.18	17.40	0.06
POLR2D	20	38	18	4.74E-07	17.62	24.88	-0.50
C5orf63	9	27	18	1.48E-05	0.48	0.24	1.01
NHLRC4	40	58	18	2.85E-05	7.35	6.73	0.13
COX7A1	20	38	18	4.67E-05	5.18	10.00	-0.95
CECR1	11	29	18	4.67E-04	5.87	4.76	0.30
CLNS1A	15	33	18	6.44E-04	198.48	174.26	0.19
MKLN1	3	21	18	1.39E-02	18.39	17.39	0.08
MCTS1	18	36	18	1.55E-02	30.71	26.45	0.22
ZNF439	77	95	18	5.01E-02	0.40	0.35	0.17
NAP1L5	36	54	18	7.74E-02	4.00	4.13	-0.05
SATL1	63	81	18	8.61E-02	2.29	2.10	0.13
STARD8	13	32	19	1.44E-08	11.86	12.08	-0.03
ECSIT	21	40	19	1.47E-08	26.08	12.80	1.03
TCP11	30	49	19	1.52E-08	0.02	0.01	0.74
MAFG	68	87	19	1.57E-08	17.53	12.47	0.49
SSR4P1	31	50	19	1.62E-08	0.14	0.21	-0.58
RBM5	14	33	19	1.64E-08	312.40	296.50	0.08
FAM217B	27	46	19	1.87E-08	4.34	4.88	-0.17
CCDC19	15	34	19	3.38E-06	0.62	0.47	0.40
LRRC37A6P	19	38	19	4.49E-06	0.17	0.24	-0.48
REEP2	4	23	19	1.10E-05	2.15	1.32	0.70
ACBD4	0	19	19	1.97E-04	1.18	0.84	0.49
PLA2G6	22	41	19	1.37E-03	4.90	2.67	0.87
PLA2G6	22	41	19	1.37E-03	4.90	2.67	0.87
ZNF331	51	70	19	1.41E-03	3.57	2.98	0.26
ZNF331	51	70	19	1.41E-03	3.57	2.98	0.26
HOXB3	1	20	19	4.90E-03	5.12	6.78	-0.41
ZNF711	16	35	19	5.80E-03	7.58	6.58	0.20
SH3BGR	44	63	19	1.59E-02	2.03	2.06	-0.02
CHM	18	37	19	2.19E-02	17.05	16.25	0.07
CACNA2D4	56	75	19	3.02E-02	0.08	0.02	1.82
CEP85	13	33	20	1.44E-08	4.58	4.28	0.10
MYSM1	2	22	20	1.44E-08	15.49	13.92	0.15
TBL2	6	26	20	1.44E-08	12.16	10.49	0.21
RPS24	11	31	20	1.50E-08	2446.97	2193.85	0.16
ECSIT	24	44	20	1.51E-08	26.08	12.80	1.03
ZRSR2	9	29	20	1.52E-08	10.87	10.98	-0.01
COL4A3BP	1	21	20	1.52E-08	15.96	16.99	-0.09
ZXDB	23	43	20	1.55E-08	2.26	1.85	0.29
TTLL10	34	54	20	1.67E-08	0.30	0.12	1.33
CABYR	16	36	20	2.00E-07	2.47	1.91	0.37
HOXB5	39	59	20	7.20E-06	63.50	50.37	0.33
GPR35	64	84	20	4.56E-04	2.99	3.07	-0.04
INPP5F	45	65	20	7.75E-04	13.34	14.35	-0.11
RDH13	27	47	20	1.41E-03	0.77	0.43	0.85
CREBL2	0	20	20	2.22E-03	18.61	15.84	0.23
ZNF749	0	20	20	3.15E-03	13.20	12.87	0.04
COMT	67	87	20	2.84E-02	98.34	72.18	0.45
TSSC4	75	95	20	4.71E-02	6.96	4.30	0.70
SIPA1L1	80	100	20	8.53E-02	9.01	9.36	-0.06
TOMM20	5	26	21	1.44E-08	56.21	49.11	0.19
VILL	12	33	21	1.44E-08	1.75	1.43	0.29
GCAT	1	22	21	1.44E-08	1.93	1.16	0.74
MRPS22	16	37	21	1.52E-08	70.84	99.59	-0.49
STPG1	22	43	21	1.55E-08	8.50	12.38	-0.54
PSTK	1	22	21	1.55E-08	1.88	1.82	0.05
CCDC8	23	44	21	1.60E-08	0.03	0.03	0.00
FAM96A	13	34	21	7.54E-08	82.61	87.34	-0.08

CUEDC2	1	22	21	3.96E-07	27.78	31.40	-0.18
CABYR	22	43	21	6.00E-07	2.47	1.91	0.37
CBWD2	2	23	21	1.97E-06	5.73	6.26	-0.13
UBE2L3	14	35	21	9.09E-05	101.13	76.80	0.40
PAK6	13	34	21	3.10E-04	17.78	9.87	0.85
CLK2	31	52	21	2.53E-03	25.67	22.67	0.18
GHRL	49	70	21	3.94E-02	97.76	108.06	-0.14
SUSD2	66	87	21	5.03E-02	0.03	0.06	-1.03
C1orf198	7	29	22	1.44E-08	7.65	5.78	0.40
PUM1	7	29	22	1.44E-08	110.62	80.78	0.45
IL10RA	13	35	22	1.47E-08	2.31	3.39	-0.55
STOM	8	30	22	1.60E-08	301.47	266.40	0.18
PIGU	20	42	22	9.81E-08	27.67	26.12	0.08
LDLRAD4	26	48	22	2.78E-05	1.20	1.04	0.21
LDLRAD4	26	48	22	2.78E-05	1.20	1.04	0.21
ELN	12	34	22	3.41E-04	9.47	6.93	0.45
RGPD2	44	66	22	2.13E-03	0.08	0.09	-0.24
RGS4	4	26	22	6.93E-03	55.64	51.60	0.11
RGS4	4	26	22	6.93E-03	55.64	51.60	0.11
RGS4	4	26	22	6.93E-03	55.64	51.60	0.11
ZSCAN23	76	98	22	9.68E-03	0.23	0.43	-0.88
HMSD	14	36	22	1.79E-02	32.21	33.50	-0.06
KRT8	73	95	22	2.79E-02	84.31	101.27	-0.26
ABAT	8	30	22	4.97E-02	0.32	0.37	-0.18
TMPRSS6	67	89	22	5.98E-02	0.02	0.01	1.78
NSA2	8	31	23	1.47E-08	176.72	195.11	-0.14
ZMAT3	3	26	23	1.52E-08	62.84	52.54	0.26
VMA21	20	43	23	1.68E-08	24.56	22.91	0.10
GEMIN5	28	51	23	2.13E-06	6.55	7.35	-0.17
SPARC	21	44	23	3.67E-06	2342.55	2385.35	-0.03
UBE2L3	12	35	23	3.87E-06	101.13	76.80	0.40
ETV4	30	53	23	1.47E-05	3.25	4.36	-0.42
MGAT1	25	48	23	1.36E-04	36.02	28.16	0.36
MCTS1	18	41	23	1.81E-03	30.71	26.45	0.22
OC90	54	77	23	7.60E-02	0.80	1.13	-0.50
LINC00320	59	82	23	9.29E-02	0.07	0.03	1.36
PLEC	15	39	24	1.56E-08	35.07	27.76	0.34
ATP5J2	25	49	24	2.99E-07	389.08	433.24	-0.16
AARS	15	39	24	2.33E-06	52.17	48.55	0.10
HSD3B7	41	65	24	1.98E-04	0.78	0.66	0.24
RAPGEF1	72	96	24	3.49E-04	56.37	51.44	0.13
SCG5	42	66	24	2.10E-02	0.68	0.51	0.40
INS-IGF2	54	78	24	3.47E-02	8.78	7.78	0.17
INS	54	78	24	3.47E-02	8.78	7.78	0.17
P2RX3	67	91	24	3.57E-02	0.02	0.19	-3.44
MR1	40	64	24	3.64E-02	2.24	2.22	0.01
IFITM10	17	41	24	7.83E-02	61.13	46.32	0.40
ATF5	3	28	25	1.44E-08	12.77	8.74	0.55
ATF5	3	28	25	1.44E-08	12.77	8.74	0.55
TASP1	9	34	25	1.47E-08	2.91	3.38	-0.22
STPG1	32	57	25	2.08E-08	8.50	12.38	-0.54
MIR503	23	48	25	4.06E-07	3.89	3.39	0.20
MIR424	23	48	25	4.06E-07	3.89	3.39	0.20
XKRX	38	63	25	2.58E-06	0.03	0.01	1.56
RPL24	20	45	25	1.21E-05	913.12	1152.83	-0.34
LSG1	17	42	25	5.52E-05	51.45	50.61	0.02
FAM74A3	50	75	25	8.40E-05	0.35	0.04	3.10
SV2A	6	31	25	6.56E-04	0.16	0.20	-0.29
GPATCH2	28	53	25	5.50E-03	6.47	10.20	-0.66

SPATA17	28	53	25	5.50E-03	0.34	0.49	-0.51
RPAP1	61	86	25	2.52E-02	8.67	9.04	-0.06
SEC61A2	10	36	26	1.44E-08	7.47	10.53	-0.50
MRPS17	29	55	26	1.44E-08	63.91	55.15	0.21
ALKBH7	5	31	26	2.49E-07	3.86	3.92	-0.02
ZNF468	15	41	26	2.16E-05	5.89	6.96	-0.24
FAM101A	50	76	26	5.65E-04	55.48	48.24	0.20
C19orf21	47	73	26	1.40E-03	0.00	0.01	-0.88
HSPA9	22	49	27	1.44E-08	318.67	415.42	-0.38
DCAF8	3	30	27	1.44E-08	96.70	79.61	0.28
CAPS2	1	28	27	1.47E-08	0.49	0.54	-0.14
COIL	18	45	27	1.57E-08	11.05	9.17	0.27
PALM2	11	38	27	1.01E-07	284.69	216.88	0.39
NDN	23	50	27	1.12E-06	15.12	13.74	0.14
CFD	58	85	27	3.84E-06	0.10	0.10	0.00
LAS1L	52	79	27	1.01E-03	4.84	5.32	-0.14
RBBP9	13	40	27	3.45E-03	7.35	5.78	0.35
PPP1R2P3	36	63	27	4.26E-02	0.06	0.09	-0.68
MYT1L	61	88	27	5.91E-02	0.12	0.17	-0.55
CCDC106	16	44	28	1.44E-08	30.48	27.18	0.17
SMU1	9	37	28	1.55E-08	54.58	55.96	-0.04
GBAP1	8	36	28	5.85E-08	11.40	10.46	0.12
IFITM1	29	57	28	9.88E-02	96.29	88.64	0.12
BMPR1B	18	46	28	9.97E-02	0.68	0.64	0.10
GRAMD1C	2	31	29	1.44E-08	6.13	6.35	-0.05
CDKL3	27	56	29	3.39E-07	771.93	681.71	0.18
AMBRA1	16	45	29	6.63E-04	8.10	6.58	0.30
GFI1B	19	48	29	1.54E-03	0.10	0.07	0.64
TNFRSF8	47	76	29	8.20E-03	0.01	0.03	-1.63
ATP6V0A4	17	46	29	8.70E-02	0.02	0.09	-1.93
C1orf141	34	64	30	1.44E-08	0.02	0.04	-1.10
CKLF-CMTM1	35	65	30	1.28E-04	30.75	34.38	-0.16
CKLF	35	65	30	1.28E-04	30.75	34.38	-0.16
HHIPL2	66	96	30	4.79E-02	0.02	0.06	-1.25
GCFC2	1	32	31	1.44E-08	1.10	1.19	-0.12
APC2	4	35	31	8.53E-05	0.41	0.32	0.36
TMPRSS12	33	64	31	2.08E-04	0.05	0.03	0.71
DCAF8	3	35	32	1.44E-08	96.70	79.61	0.28
DCAF8	3	35	32	1.44E-08	96.70	79.61	0.28
DVL3	7	39	32	1.48E-08	24.04	21.47	0.16
C10orf11	9	41	32	5.61E-06	10.04	11.32	-0.17
TNFRSF1A	31	63	32	3.68E-04	210.02	172.32	0.29
MFSD4	10	42	32	4.90E-04	0.60	0.70	-0.22
FBXL22	29	61	32	7.10E-04	0.08	0.09	-0.07
PSMF1	63	96	33	5.96E-03	49.90	47.08	0.08
GBA	0	33	33	8.91E-03	103.23	93.11	0.15
GBA	0	33	33	8.91E-03	103.23	93.11	0.15
C12orf71	60	93	33	3.16E-02	0.01	0.08	-2.45
PC	38	71	33	5.08E-02	14.53	11.54	0.33
MYL4	23	56	33	8.42E-02	1.55	1.22	0.35
ANKRD20A5P	17	51	34	1.44E-08	0.14	0.19	-0.47
EXOSC5	8	42	34	1.44E-08	1.92	2.63	-0.46
FMO5	31	65	34	1.44E-08	1.33	1.32	0.01
ZNF878	21	55	34	1.44E-08	1.65	1.38	0.26
HOOK2	8	42	34	1.44E-08	9.77	7.90	0.31
MEG3	30	64	34	1.60E-08	40.71	33.61	0.28
MEG3	30	64	34	1.60E-08	40.71	33.61	0.28
DDX19B	22	56	34	4.40E-07	44.14	44.31	-0.01
HIF3A	5	39	34	4.00E-04	1.25	0.71	0.82

SETDB1	17	52	35	1.44E-08	21.03	20.94	0.01
DND1	35	70	35	1.57E-08	45.60	37.72	0.27
LYPD3	40	75	35	3.52E-06	0.01	0.11	-3.00
LIMK1	22	57	35	8.77E-04	11.62	9.79	0.25
KPTN	14	50	36	1.44E-08	0.47	0.58	-0.31
NAPA-AS1	14	50	36	1.44E-08	0.30	0.32	-0.08
ZNF70	13	49	36	1.44E-08	1.78	1.86	-0.06
ZNF615	0	36	36	1.44E-08	4.13	3.05	0.44
BSG	38	74	36	1.47E-08	256.20	194.09	0.40
CFP	43	79	36	7.96E-02	1.11	0.88	0.34
GMFG	50	87	37	1.12E-05	12.75	10.41	0.29
SLC22A17	38	76	38	1.44E-08	1.15	1.16	-0.01
TJP2	4	42	38	1.44E-08	46.09	42.79	0.11
RBM34	0	39	39	1.51E-08	123.18	128.23	-0.06
DDX1	1	41	40	1.44E-08	124.08	159.39	-0.36
KIAA1755	2	42	40	2.16E-03	0.04	0.03	0.62
RAB17	15	56	41	1.62E-04	0.77	0.39	1.00
ALG1L2	44	85	41	2.59E-03	0.18	0.35	-0.98
SNORA69	44	85	41	7.76E-03	7.84	3.33	1.24
GPR141	20	61	41	7.22E-02	0.18	0.10	0.87
HCCS	14	56	42	1.44E-08	30.54	34.21	-0.16
AIMP1	16	58	42	1.47E-08	38.94	35.05	0.15
AIMP1	16	58	42	1.47E-08	38.94	35.05	0.15
SLC1A5	42	84	42	2.64E-04	22.59	21.97	0.04
CLK3	50	92	42	5.19E-02	63.88	63.92	0.00
MSTO1	5	48	43	1.44E-08	5.02	4.72	0.09
GABPB2	11	54	43	1.44E-08	2.67	2.16	0.30
SELPLG	7	50	43	5.92E-02	0.78	0.74	0.08
ARHGAP6	0	43	43	6.18E-02	0.74	0.68	0.11
SLC19A3	36	80	44	1.44E-08	0.13	0.08	0.62
MAT2B	2	46	44	7.75E-07	112.95	110.35	0.03
CECR1	56	100	44	1.43E-05	5.87	4.76	0.30
ZFYVE27	52	96	44	1.62E-04	6.01	6.34	-0.08
GZF1	0	45	45	4.43E-03	5.19	5.05	0.04
RNASEH2A	20	66	46	1.44E-08	8.73	8.43	0.05
IFT172	34	80	46	1.50E-06	12.97	12.61	0.04
NR1H3	0	46	46	2.05E-04	2.64	2.35	0.17
WNT2B	4	50	46	6.40E-04	2.47	2.42	0.03
LYVE1	0	46	46	1.23E-03	107.15	114.96	-0.10
NCR1	49	96	47	6.15E-08	0.07	0.07	0.10
TRIM5	0	47	47	2.92E-06	72.47	66.35	0.13
CCM2L	10	57	47	3.50E-03	11.59	12.04	-0.05
PARP6	31	79	48	1.53E-06	58.49	55.67	0.07
TMEM177	1	51	50	1.44E-08	1.44	1.27	0.18
INTS2	38	89	51	1.47E-08	9.14	12.60	-0.46
PTX3	44	96	52	1.44E-08	107.71	114.02	-0.08
RNF125	28	81	53	1.44E-08	47.96	47.68	0.01
ABCB9	14	70	56	7.88E-08	2.64	1.98	0.42
C9orf117	20	86	66	8.11E-04	0.64	0.69	-0.11
SLC9A1	12	86	74	1.44E-08	25.16	29.17	-0.21
IQCD	22	98	76	1.44E-08	0.19	0.21	-0.17
SLC25A22	14	92	78	1.08E-06	3.14	3.31	-0.08
NUAK2	21	100	79	2.54E-08	0.29	0.42	-0.54
BTC	10	89	79	2.76E-04	0.22	0.17	0.39
EMP3	3	83	80	8.78E-07	848.00	949.45	-0.16
FOLH1	4	90	86	1.44E-08	1.06	0.96	0.15

Table S4. All significantly hypermethylated promoter regions corresponding to genes that are down- regulated in non-reversed conditions compared to reversed conditions

gene name	R methylation %	N methylation %	methylation % difference (N-R)	methylation adjusted Pvalue	mRNASeq Nvalue	mRNASeq Rvalue	mRNASeq Log2FC
EMP3	3	83	80	8.78E-07	848.00	949.45	-0.16
NUAK2	21	100	79	2.54E-08	0.29	0.42	-0.54
SLC25A22	14	92	78	1.08E-06	3.14	3.31	-0.08
IQCD	22	98	76	1.44E-08	0.19	0.21	-0.17
SLC9A1	12	86	74	1.44E-08	25.16	29.17	-0.21
C9orf117	20	86	66	8.11E-04	0.64	0.69	-0.11
PTX3	44	96	52	1.44E-08	107.71	114.02	-0.08
INTS2	38	89	51	1.47E-08	9.14	12.60	-0.46
CCM2L	10	57	47	3.50E-03	11.59	12.04	-0.05
LYVE1	0	46	46	1.23E-03	107.15	114.96	-0.10
ZFYVE27	52	96	44	1.62E-04	6.01	6.34	-0.08
HCCS	14	56	42	1.44E-08	30.54	34.21	-0.16
CLK3	50	92	42	5.19E-02	63.88	63.92	0.00
ALG1L2	44	85	41	2.59E-03	0.18	0.35	-0.98
DDX1	1	41	40	1.44E-08	124.08	159.39	-0.36
RBM34	0	39	39	1.51E-08	123.18	128.23	-0.06
SLC22A17	38	76	38	1.44E-08	1.15	1.16	-0.01
KPTN	14	50	36	1.44E-08	0.47	0.58	-0.31
NAPA-AS1	14	50	36	1.44E-08	0.30	0.32	-0.08
ZNF70	13	49	36	1.44E-08	1.78	1.86	-0.06
LYPD3	40	75	35	3.52E-06	0.01	0.11	-3.00
ANKRD20A5P	17	51	34	1.44E-08	0.14	0.19	-0.47
EXOSC5	8	42	34	1.44E-08	1.92	2.63	-0.46
DDX19B	22	56	34	4.40E-07	44.14	44.31	-0.01
C12orf71	60	93	33	3.16E-02	0.01	0.08	-2.45
MFSD4	10	42	32	4.90E-04	0.60	0.70	-0.22
C10orf11	9	41	32	5.61E-06	10.04	11.32	-0.17
FBXL22	29	61	32	7.10E-04	0.08	0.09	-0.07
GCFC2	1	32	31	1.44E-08	1.10	1.19	-0.12
HHIPL2	66	96	30	4.79E-02	0.02	0.06	-1.25
C1orf141	34	64	30	1.44E-08	0.02	0.04	-1.10
CKLF-CMTM1	35	65	30	1.28E-04	30.75	34.38	-0.16
CKLF	35	65	30	1.28E-04	30.75	34.38	-0.16
ATP6V0A4	17	46	29	8.70E-02	0.02	0.09	-1.93
TNFRSF8	47	76	29	8.20E-03	0.01	0.03	-1.63
GRAMD1C	2	31	29	1.44E-08	6.13	6.35	-0.05
SMU1	9	37	28	1.55E-08	54.58	55.96	-0.04
PPP1R2P3	36	63	27	4.26E-02	0.06	0.09	-0.68
MYT1L	61	88	27	5.91E-02	0.12	0.17	-0.55
HSPA9	22	49	27	1.44E-08	318.67	415.42	-0.38
CAPS2	1	28	27	1.47E-08	0.49	0.54	-0.14
LAS1L	52	79	27	1.01E-03	4.84	5.32	-0.14
C19orf21	47	73	26	1.40E-03	0.00	0.01	-0.88
SEC61A2	10	36	26	1.44E-08	7.47	10.53	-0.50
ZNF468	15	41	26	2.16E-05	5.89	6.96	-0.24
ALKBH7	5	31	26	2.49E-07	3.86	3.92	-0.02
GPATCH2	28	53	25	5.50E-03	6.47	10.20	-0.66
STPG1	32	57	25	2.08E-08	8.50	12.38	-0.54
SPATA17	28	53	25	5.50E-03	0.34	0.49	-0.51
RPL24	20	45	25	1.21E-05	913.12	1152.83	-0.34
SV2A	6	31	25	6.56E-04	0.16	0.20	-0.29
TASP1	9	34	25	1.47E-08	2.91	3.38	-0.22

RPAP1	61	86	25	2.52E-02	8.67	9.04	-0.06
P2RX3	67	91	24	3.57E-02	0.02	0.19	-3.44
ATP5J2	25	49	24	2.99E-07	389.08	433.24	-0.16
OC90	54	77	23	7.60E-02	0.80	1.13	-0.50
ETV4	30	53	23	1.47E-05	3.25	4.36	-0.42
GEMIN5	28	51	23	2.13E-06	6.55	7.35	-0.17
NSA2	8	31	23	1.47E-08	176.72	195.11	-0.14
SPARC	21	44	23	3.67E-06	2342.55	2385.35	-0.03
ZSCAN23	76	98	22	9.68E-03	0.23	0.43	-0.88
IL10RA	13	35	22	1.47E-08	2.31	3.39	-0.55
KRT8	73	95	22	2.79E-02	84.31	101.27	-0.26
RGPD2	44	66	22	2.13E-03	0.08	0.09	-0.24
ABAT	8	30	22	4.97E-02	0.32	0.37	-0.18
HMSD	14	36	22	1.79E-02	32.21	33.50	-0.06
SUSD2	66	87	21	5.03E-02	0.03	0.06	-1.03
STPG1	22	43	21	1.55E-08	8.50	12.38	-0.54
MRPS22	16	37	21	1.52E-08	70.84	99.59	-0.49
CUEDC2	1	22	21	3.96E-07	27.78	31.40	-0.18
GHRL	49	70	21	3.94E-02	97.76	108.06	-0.14
CBWD2	2	23	21	1.97E-06	5.73	6.26	-0.13
FAM96A	13	34	21	7.54E-08	82.61	87.34	-0.08
CCDC8	23	44	21	1.60E-08	0.03	0.03	0.00
INPP5F	45	65	20	7.75E-04	13.34	14.35	-0.11
COL4A3BP	1	21	20	1.52E-08	15.96	16.99	-0.09
SIPA1L1	80	100	20	8.53E-02	9.01	9.36	-0.06
GPR35	64	84	20	4.56E-04	2.99	3.07	-0.04
ZRSR2	9	29	20	1.52E-08	10.87	10.98	-0.01
SSR4P1	31	50	19	1.62E-08	0.14	0.21	-0.58
LRRC37A6P	19	38	19	4.49E-06	0.17	0.24	-0.48
HOXB3	1	20	19	4.90E-03	5.12	6.78	-0.41
FAM217B	27	46	19	1.87E-08	4.34	4.88	-0.17
STARD8	13	32	19	1.44E-08	11.86	12.08	-0.03
SH3BGR	44	63	19	1.59E-02	2.03	2.06	-0.02
COX7A1	20	38	18	4.67E-05	5.18	10.00	-0.95
POLR2D	20	38	18	4.74E-07	17.62	24.88	-0.50
SERF2	16	34	18	1.57E-08	304.92	347.00	-0.19
LARS	15	33	18	5.69E-08	122.66	129.09	-0.07
NAP1L5	36	54	18	7.74E-02	4.00	4.13	-0.05
MTO1	11	28	17	1.44E-08	21.26	26.76	-0.33
EXOC7	23	40	17	5.72E-04	44.66	54.64	-0.29
CCDC73	74	91	17	8.45E-02	3.61	4.21	-0.22
MORF4L2	3	20	17	2.55E-02	301.86	347.28	-0.20
DLG3	19	36	17	1.52E-08	1.70	1.94	-0.19
POLR2G	41	58	17	3.21E-04	36.69	40.07	-0.13
CCDC58	14	31	17	8.36E-04	24.64	25.73	-0.06
ZNF350	14	30	16	7.06E-07	6.13	11.48	-0.90
KCNE3	33	49	16	9.06E-04	0.06	0.10	-0.83
PKD2L2	11	27	16	4.90E-07	0.65	0.82	-0.34
C11orf83	0	16	16	1.44E-08	2.48	3.10	-0.32
ISG15	51	67	16	4.76E-03	10.67	13.13	-0.30
UFSP2	0	16	16	1.44E-08	71.39	84.81	-0.25
KIAA1598	60	76	16	2.71E-04	1.42	1.52	-0.10
ZNF726	21	37	16	1.84E-08	0.95	0.99	-0.07
HEMK1	15	31	16	2.73E-04	1.37	1.44	-0.07
SLC38A7	13	29	16	4.59E-02	17.72	18.57	-0.07
IDI2-AS1	80	96	16	3.32E-02	0.04	0.04	-0.04
TMEM219	13	29	16	1.44E-08	28.20	28.97	-0.04
HOXB8	12	28	16	2.28E-05	4.92	5.01	-0.02
QPRT	69	85	16	2.23E-03	0.50	0.50	0.00

C9orf129	20	35	15	8.63E-06	0.05	0.14	-1.43
GPR19	0	15	15	6.35E-06	0.13	0.32	-1.25
LIG1	2	17	15	3.50E-02	0.97	2.31	-1.25
ZMAT4	9	24	15	4.69E-03	0.17	0.27	-0.64
EID3	24	39	15	1.33E-03	1.30	1.95	-0.58
C2orf50	56	71	15	4.90E-03	0.07	0.10	-0.54
C1orf64	81	96	15	1.32E-02	0.08	0.10	-0.34
PIGB	1	16	15	1.44E-08	9.07	10.53	-0.22
ZNF235	3	18	15	1.54E-02	5.76	5.89	-0.03
KLC4	14	29	15	1.08E-03	11.20	11.40	-0.03
MGARP	34	49	15	7.52E-05	62.54	63.24	-0.02
DGKA	10	25	15	7.82E-07	198.25	199.67	-0.01
ANO4	17	31	14	4.60E-02	0.56	1.79	-1.69
EPHA1	33	47	14	1.06E-03	1.04	1.67	-0.68
NCMAP	8	22	14	4.37E-05	0.05	0.08	-0.65
PRND	35	49	14	8.78E-02	0.06	0.09	-0.54
LRRC36	3	17	14	1.44E-08	0.23	0.32	-0.47
PFDN5	52	66	14	7.59E-03	165.38	213.81	-0.37
NDUFA6	5	19	14	1.52E-08	56.97	73.19	-0.36
ZMAT1	32	46	14	1.85E-03	2.42	3.10	-0.36
FAM71E1	10	24	14	1.79E-08	0.12	0.15	-0.30
CIR1	0	14	14	1.44E-08	32.00	38.12	-0.25
SCRN3	0	14	14	1.44E-08	23.96	27.89	-0.22
FRS2	1	15	14	1.44E-08	10.88	12.61	-0.21
PNPO	1	15	14	1.44E-08	47.87	55.37	-0.21
CARS	1	15	14	1.44E-08	15.79	17.60	-0.16
NDUFA1	31	45	14	1.33E-07	70.69	78.72	-0.16
ZCCHC4	22	36	14	3.13E-03	4.57	5.04	-0.14
SNW1	5	19	14	1.44E-08	80.71	86.15	-0.09
RSPH10B	14	27	13	2.87E-03	0.18	0.38	-1.10
CHST6	12	25	13	6.54E-08	0.06	0.11	-0.93
RSPH10B2	14	27	13	2.87E-03	0.04	0.06	-0.58
TAF1A	23	36	13	1.02E-04	2.19	3.27	-0.58
IZUMO1	27	40	13	1.22E-03	0.29	0.41	-0.52
TNFSF11	3	16	13	3.65E-06	0.01	0.01	-0.41
MFAP2	9	22	13	3.66E-02	114.38	150.38	-0.39
DNALI1	18	31	13	2.12E-03	4.45	5.35	-0.27
UBE2L6	0	13	13	1.44E-08	19.57	22.84	-0.22
MIR202	63	76	13	3.90E-03	0.37	0.42	-0.20
USP18	9	22	13	2.21E-04	5.00	5.69	-0.19
SERF2	15	28	13	4.74E-07	304.92	347.00	-0.19
MLH3	1	14	13	1.44E-08	5.17	5.83	-0.17
DDIT3	11	24	13	1.23E-02	5.17	5.66	-0.13
KLK6	59	72	13	5.26E-02	1.88	2.03	-0.11
DAB2IP	24	37	13	7.52E-02	17.74	19.02	-0.10
ING4	1	14	13	1.44E-08	33.56	35.69	-0.09
COA6	3	16	13	1.44E-08	28.20	29.70	-0.07
TBCCD1	1	14	13	1.44E-08	9.27	9.72	-0.07
GANC	3	16	13	7.39E-06	13.30	13.94	-0.07
NGFRAP1	26	39	13	4.76E-03	151.93	159.11	-0.07
SFR1	0	13	13	5.81E-04	22.46	23.37	-0.06
SFR1	0	13	13	5.81E-04	22.46	23.37	-0.06
ANGEL2	9	22	13	2.44E-06	16.92	17.08	-0.01
PHF16	16	28	12	1.42E-05	5.93	8.25	-0.48
PHF16	16	28	12	1.42E-05	5.93	8.25	-0.48
CSTF2	36	48	12	6.15E-04	6.05	7.68	-0.35
RHBDL2	9	21	12	6.21E-02	1.74	2.10	-0.27
TMEM62	8	20	12	4.94E-08	30.43	35.77	-0.23
POLR3F	5	17	12	1.47E-08	11.01	12.78	-0.22

BLVRB	11	23	12	7.04E-06	12.40	14.19	-0.20
C1GALT1C1	36	48	12	2.36E-04	33.64	38.22	-0.18
MMADHC	0	12	12	3.32E-04	65.47	73.95	-0.18
ACOT4	10	22	12	1.73E-08	0.03	0.03	-0.16
C2orf74	82	94	12	1.63E-03	40.17	44.10	-0.13
DIO1	82	94	12	8.31E-02	0.06	0.07	-0.11
MDM4	27	39	12	3.48E-03	11.11	11.93	-0.10
C16orf80	35	47	12	1.69E-04	68.93	72.29	-0.07
BCL6	4	16	12	3.71E-03	6.69	6.92	-0.05
SMARCAL1	8	20	12	2.02E-04	13.36	13.73	-0.04
SMARCAL1	8	20	12	2.02E-04	13.36	13.73	-0.04
RUFY1	5	17	12	2.95E-06	109.75	111.85	-0.03
RHPN2	11	23	12	6.11E-08	1.55	1.56	-0.01
ASIC2	46	57	11	5.88E-02	0.00	0.04	-3.22
DNAH6	16	27	11	7.47E-02	0.01	0.05	-2.92
BCL2L14	81	92	11	9.88E-02	0.32	0.63	-0.96
ANKRD30BL	27	38	11	2.34E-08	0.04	0.07	-0.91
ZNF808	2	13	11	1.44E-08	16.48	25.19	-0.61
MIS18BP1	0	11	11	1.44E-08	14.50	20.73	-0.52
GLUD2	18	29	11	2.42E-02	0.09	0.12	-0.38
EMR2	2	13	11	2.21E-06	0.18	0.22	-0.34
SNRPF	11	22	11	2.89E-03	91.74	114.33	-0.32
IQGAP1	3	14	11	1.44E-08	248.25	307.74	-0.31
GON4L	34	45	11	8.31E-02	14.46	17.91	-0.31
AGA	6	17	11	9.90E-04	12.45	15.11	-0.28
PTPLAD2	27	38	11	1.10E-03	4.87	5.90	-0.28
FLT3LG	0	11	11	1.44E-08	782.26	935.32	-0.26
LPIN3	11	22	11	1.66E-02	0.14	0.17	-0.25
PIH1D3	24	35	11	6.35E-06	0.08	0.09	-0.23
RAD51D	27	38	11	5.73E-03	8.49	9.87	-0.22
ZNF560	18	29	11	1.77E-05	0.00	0.00	-0.22
FAM9C	81	92	11	2.02E-02	0.14	0.16	-0.19
ZSWIM3	2	13	11	1.09E-06	1.08	1.18	-0.12
MSN	24	35	11	8.21E-04	283.85	304.74	-0.10
CDK20	7	18	11	3.99E-04	0.41	0.44	-0.09
RNF8	7	18	11	2.32E-04	29.41	30.97	-0.07
ADTRP	89	100	11	9.37E-02	14.26	14.84	-0.06
CDC42	4	15	11	2.51E-07	185.16	192.43	-0.06
PIWIL2	46	57	11	9.96E-02	0.13	0.13	-0.05
MCU	2	13	11	1.47E-08	18.85	19.38	-0.04
C3orf55	9	20	11	1.47E-06	9.52	9.75	-0.03
AUH	4	15	11	1.47E-08	6.69	6.75	-0.01
XPO4	5	16	11	1.95E-08	6.71	6.76	-0.01
FAM215A	18	28	10	2.74E-03	0.07	0.14	-0.98
ZNF552	18	28	10	5.73E-04	0.24	0.46	-0.95
CPLX3	14	24	10	2.79E-02	0.02	0.04	-0.93
BTBD2	29	39	10	3.62E-03	23.13	35.63	-0.62
UBA52	9	19	10	2.17E-07	365.84	531.97	-0.54
RIBC2	41	51	10	1.48E-02	0.34	0.47	-0.48
ZNF165	18	28	10	3.33E-02	0.22	0.29	-0.35
ZDHHC9	28	38	10	7.65E-02	14.97	18.54	-0.31
ADPGK-AS1	4	14	10	1.44E-08	1.01	1.25	-0.31
C11orf92	6	16	10	1.63E-06	0.08	0.09	-0.29
EXOC7	50	60	10	2.85E-02	44.66	54.64	-0.29
TRNT1	6	16	10	1.46E-08	26.46	31.82	-0.27
FBXW4P1	77	87	10	5.56E-03	0.23	0.28	-0.26
MED11	7	17	10	9.21E-02	4.32	5.14	-0.25
PPP1R14A	13	23	10	1.75E-04	6.36	7.54	-0.25
PDLIM5	3	13	10	1.44E-08	46.85	54.30	-0.21

ZFR	7	17	10	8.39E-06	42.36	47.72	-0.17
SLC12A6	4	14	10	1.44E-08	20.84	23.38	-0.17
B3GALNT1	9	19	10	1.67E-08	7.45	8.31	-0.16
TRAPPC12	12	22	10	1.50E-03	17.57	18.98	-0.11
RPL11	15	25	10	1.36E-03	917.46	985.09	-0.10
SDHC	12	22	10	2.99E-07	42.94	46.05	-0.10
KIAA1598	1	11	10	1.44E-08	1.42	1.52	-0.10
PDHA1	22	32	10	5.85E-03	155.70	162.93	-0.07
NLK	7	17	10	1.60E-08	18.02	18.78	-0.06
SSB	2	12	10	1.57E-08	654.63	681.75	-0.06
MAP3K13	11	21	10	2.04E-03	9.80	10.21	-0.06
ISLR	78	88	10	6.20E-02	0.03	0.03	-0.05
PTP4A3	89	99	10	4.48E-02	2.51	2.57	-0.03
PITPNA	5	15	10	1.47E-08	106.60	108.69	-0.03
AIPL1	70	80	10	1.02E-02	0.11	0.12	-0.03
SMC1B	41	51	10	1.48E-02	0.02	0.02	-0.03
KLC4	1	11	10	1.44E-08	11.20	11.40	-0.03
KLC4	1	11	10	1.44E-08	11.20	11.40	-0.03
KLHL12	37	47	10	1.74E-03	11.53	11.68	-0.02
DHX8	23	33	10	4.26E-03	15.44	15.56	-0.01
CWF19L1	18	28	10	6.65E-03	11.89	11.96	-0.01
BLVRB	11	23	12	7.04E-06	12.40	14.19	-0.20
DLG3	19	36	17	1.52E-08	1.70	1.94	-0.19
USP18	9	22	13	2.21E-04	5.00	5.69	-0.19
SERF2	15	28	13	4.74E-07	304.92	347.00	-0.19
SERF2	16	34	18	1.57E-08	304.92	347.00	-0.19
FAM9C	81	92	11	2.02E-02	0.14	0.16	-0.19
C1GALT1C1	36	48	12	2.36E-04	33.64	38.22	-0.18
CUEDC2	1	22	21	3.96E-07	27.78	31.40	-0.18
MMADHC	0	12	12	3.32E-04	65.47	73.95	-0.18
ABAT	8	30	22	4.97E-02	0.32	0.37	-0.18
IQCD	22	98	76	1.44E-08	0.19	0.21	-0.17
C10orf11	9	41	32	5.61E-06	10.04	11.32	-0.17
MLH3	1	14	13	1.44E-08	5.17	5.83	-0.17
ZFR	7	17	10	8.39E-06	42.36	47.72	-0.17
FAM217B	27	46	19	1.87E-08	4.34	4.88	-0.17
GEMIN5	28	51	23	2.13E-06	6.55	7.35	-0.17
SLC12A6	4	14	10	1.44E-08	20.84	23.38	-0.17
HCCS	14	56	42	1.44E-08	30.54	34.21	-0.16
EMP3	3	83	80	8.78E-07	848.00	949.45	-0.16
CKLF-CMTM1	35	65	30	1.28E-04	30.75	34.38	-0.16
CKLF	35	65	30	1.28E-04	30.75	34.38	-0.16
B3GALNT1	9	19	10	1.67E-08	7.45	8.31	-0.16
ACOT4	10	22	12	1.73E-08	0.03	0.03	-0.16
CARS	1	15	14	1.44E-08	15.79	17.60	-0.16
NDUFA1	31	45	14	1.33E-07	70.69	78.72	-0.16
ATP5J2	25	49	24	2.99E-07	389.08	433.24	-0.16
GHRL	49	70	21	3.94E-02	97.76	108.06	-0.14
NSA2	8	31	23	1.47E-08	176.72	195.11	-0.14
ZCCHC4	22	36	14	3.13E-03	4.57	5.04	-0.14
CAPS2	1	28	27	1.47E-08	0.49	0.54	-0.14
LAS1L	52	79	27	1.01E-03	4.84	5.32	-0.14
C2orf74	82	94	12	1.63E-03	40.17	44.10	-0.13
DDIT3	11	24	13	1.23E-02	5.17	5.66	-0.13
POLR2G	41	58	17	3.21E-04	36.69	40.07	-0.13
CBWD2	2	23	21	1.97E-06	5.73	6.26	-0.13
ZSWIM3	2	13	11	1.09E-06	1.08	1.18	-0.12
GCFC2	1	32	31	1.44E-08	1.10	1.19	-0.12
KLK6	59	72	13	5.26E-02	1.88	2.03	-0.11

C9orf117	20	86	66	8.11E-04	0.64	0.69	-0.11
TRAPPC12	12	22	10	1.50E-03	17.57	18.98	-0.11
DIO1	82	94	12	8.31E-02	0.06	0.07	-0.11
INPP5F	45	65	20	7.75E-04	13.34	14.35	-0.11
MDM4	27	39	12	3.48E-03	11.11	11.93	-0.10
RPL11	15	25	10	1.36E-03	917.46	985.09	-0.10
MSN	24	35	11	8.21E-04	283.85	304.74	-0.10
LYVE1	0	46	46	1.23E-03	107.15	114.96	-0.10
SDHC	12	22	10	2.99E-07	42.94	46.05	-0.10
DAB2IP	24	37	13	7.52E-02	17.74	19.02	-0.10
KIAA1598	1	11	10	1.44E-08	1.42	1.52	-0.10
KIAA1598	60	76	16	2.71E-04	1.42	1.52	-0.10
CDK20	7	18	11	3.99E-04	0.41	0.44	-0.09
SNW1	5	19	14	1.44E-08	80.71	86.15	-0.09
COL4A3BP	1	21	20	1.52E-08	15.96	16.99	-0.09
ING4	1	14	13	1.44E-08	33.56	35.69	-0.09
PTX3	44	96	52	1.44E-08	107.71	114.02	-0.08
FAM96A	13	34	21	7.54E-08	82.61	87.34	-0.08
ZFYVE27	52	96	44	1.62E-04	6.01	6.34	-0.08
NAPA-AS1	14	50	36	1.44E-08	0.30	0.32	-0.08
SLC25A22	14	92	78	1.08E-06	3.14	3.31	-0.08
COA6	3	16	13	1.44E-08	28.20	29.70	-0.07
RNF8	7	18	11	2.32E-04	29.41	30.97	-0.07
LARS	15	33	18	5.69E-08	122.66	129.09	-0.07
ZNF726	21	37	16	1.84E-08	0.95	0.99	-0.07
TBCCD1	1	14	13	1.44E-08	9.27	9.72	-0.07
C16orf80	35	47	12	1.69E-04	68.93	72.29	-0.07
HEMK1	15	31	16	2.73E-04	1.37	1.44	-0.07
GANC	3	16	13	7.39E-06	13.30	13.94	-0.07
SLC38A7	13	29	16	4.59E-02	17.72	18.57	-0.07
FBXL22	29	61	32	7.10E-04	0.08	0.09	-0.07
NGFRAP1	26	39	13	4.76E-03	151.93	159.11	-0.07
PDHA1	22	32	10	5.85E-03	155.70	162.93	-0.07
ZNF70	13	49	36	1.44E-08	1.78	1.86	-0.06
CCDC58	14	31	17	8.36E-04	24.64	25.73	-0.06
RPAP1	61	86	25	2.52E-02	8.67	9.04	-0.06
NLK	7	17	10	1.60E-08	18.02	18.78	-0.06
SSB	2	12	10	1.57E-08	654.63	681.75	-0.06
MAP3K13	11	21	10	2.04E-03	9.80	10.21	-0.06
ADTRP	89	100	11	9.37E-02	14.26	14.84	-0.06
RBM34	0	39	39	1.51E-08	123.18	128.23	-0.06
SFR1	0	13	13	5.81E-04	22.46	23.37	-0.06
SFR1	0	13	13	5.81E-04	22.46	23.37	-0.06
HMSD	14	36	22	1.79E-02	32.21	33.50	-0.06
SIPA1L1	80	100	20	8.53E-02	9.01	9.36	-0.06
CDC42	4	15	11	2.51E-07	185.16	192.43	-0.06
CCM2L	10	57	47	3.50E-03	11.59	12.04	-0.05
PIWIL2	46	57	11	9.96E-02	0.13	0.13	-0.05
GRAMD1C	2	31	29	1.44E-08	6.13	6.35	-0.05
BCL6	4	16	12	3.71E-03	6.69	6.92	-0.05
ISLR	78	88	10	6.20E-02	0.03	0.03	-0.05
NAP1L5	36	54	18	7.74E-02	4.00	4.13	-0.05
IDI2-AS1	80	96	16	3.32E-02	0.04	0.04	-0.04
MCU	2	13	11	1.47E-08	18.85	19.38	-0.04
SMARCAL1	8	20	12	2.02E-04	13.36	13.73	-0.04
SMARCAL1	8	20	12	2.02E-04	13.36	13.73	-0.04
TMEM219	13	29	16	1.44E-08	28.20	28.97	-0.04
SMU1	9	37	28	1.55E-08	54.58	55.96	-0.04
GPR35	64	84	20	4.56E-04	2.99	3.07	-0.04

C3orf55	9	20	11	1.47E-06	9.52	9.75	-0.03
PTP4A3	89	99	10	4.48E-02	2.51	2.57	-0.03
ZNF235	3	18	15	1.54E-02	5.76	5.89	-0.03
PITPNA	5	15	10	1.47E-08	106.60	108.69	-0.03
RUFY1	5	17	12	2.95E-06	109.75	111.85	-0.03
STARD8	13	32	19	1.44E-08	11.86	12.08	-0.03
AIPL1	70	80	10	1.02E-02	0.11	0.12	-0.03
SPARC	21	44	23	3.67E-06	2342.55	2385.35	-0.03
SMC1B	41	51	10	1.48E-02	0.02	0.02	-0.03
KLC4	1	11	10	1.44E-08	11.20	11.40	-0.03
KLC4	1	11	10	1.44E-08	11.20	11.40	-0.03
KLC4	14	29	15	1.08E-03	11.20	11.40	-0.03
HOXB8	12	28	16	2.28E-05	4.92	5.01	-0.02
ALKBH7	5	31	26	2.49E-07	3.86	3.92	-0.02
SH3BGR	44	63	19	1.59E-02	2.03	2.06	-0.02
KLHL12	37	47	10	1.74E-03	11.53	11.68	-0.02
MGARP	34	49	15	7.52E-05	62.54	63.24	-0.02
ZRSR2	9	29	20	1.52E-08	10.87	10.98	-0.01
ANGEL2	9	22	13	2.44E-06	16.92	17.08	-0.01
AUH	4	15	11	1.47E-08	6.69	6.75	-0.01
SLC22A17	38	76	38	1.44E-08	1.15	1.16	-0.01
DHX8	23	33	10	4.26E-03	15.44	15.56	-0.01
DGKA	10	25	15	7.82E-07	198.25	199.67	-0.01
XPO4	5	16	11	1.95E-08	6.71	6.76	-0.01
RHPN2	11	23	12	6.11E-08	1.55	1.56	-0.01
CWF19L1	18	28	10	6.65E-03	11.89	11.96	-0.01
DDX19B	22	56	34	4.40E-07	44.14	44.31	-0.01
QPRT	69	85	16	2.23E-03	0.50	0.50	0.00
CCDC8	23	44	21	1.60E-08	0.03	0.03	0.00
CLK3	50	92	42	5.19E-02	63.88	63.92	0.00

Table S5. All significantly hypomethylated promoter regions corresponding to genes that are up-regulated in non-reversed conditions compared to reversed conditions

gene name	R methylation %	N methylation %	methylation % difference (N-R)	methylation adjusted Pvalue	mRNASeq Nvalue	mRNASeq Rvalue	mRNASeq Log2FC
EPS8L3	81	21	-60	0.0006334	0.03	0.01	1.90
EGFLAM	50	0	-50	0.0066056	0.77	0.39	0.98
MICB	67	20	-47	0.0194496	8.63	5.20	0.73
BPNT1	41	0	-41	6.95E-05	27.27	24.52	0.15
POM121L9P	98	58	-40	0.0023839	0.02	0.01	1.59
ITGBL1	92	55	-37	4.98E-05	0.89	0.65	0.47
SYNPO2L	92	56	-36	0.0368673	0.16	0.13	0.36
PLCH2	81	45	-36	0.000133	0.04	0.02	1.30
CSAD	83	48	-35	0.0273401	9.61	7.18	0.42
ACOT2	82	50	-32	0.0228887	0.87	0.46	0.91
CCDC74B-AS1	94	63	-31	0.032704	0.12	0.11	0.11
C9orf153	74	43	-31	0.0668777	0.09	0.07	0.39
ACP5	57	26	-31	1.48E-08	46.28	30.30	0.61
CD79B	71	41	-30	2.58E-05	0.38	0.34	0.16
LAMB3	95	65	-30	0.0118139	10.22	8.45	0.27
LAMB3	95	65	-30	0.0118139	10.22	8.45	0.27
METTL5	48	20	-28	0.0024324	66.99	63.77	0.07
RGS12	31	3	-28	0.0080894	29.65	28.00	0.08
PLEKHB1	60	32	-28	0.0261276	2.43	2.29	0.09
ZNF503-AS1	33	5	-28	0.0033454	0.38	0.20	0.93
ZNF423	92	65	-27	0.018858	2.56	2.41	0.08
EZH1	45	18	-27	1.47E-08	13.01	10.64	0.29
CCDC152	46	20	-26	8.49E-08	1.33	1.11	0.26
MPDU1	52	28	-24	1.02E-05	44.96	44.47	0.02
PRKACA	54	30	-24	0.0011804	67.05	61.07	0.13
KLK10	26	3	-23	0.0160831	0.37	0.32	0.22
LINC00672	88	65	-23	0.0141897	0.32	0.25	0.34
TOMM22	23	0	-23	1.44E-08	75.48	58.83	0.36
DAND5	59	36	-23	0.0422705	0.31	0.20	0.67
DRG2	33	11	-22	3.61E-08	10.53	10.52	0.00
SPIN3	42	20	-22	0.0137203	1.37	1.01	0.44
RAX2	83	62	-21	4.50E-05	0.03	0.03	0.01
CSTF2T	23	2	-21	1.44E-08	9.50	8.92	0.09
HELB	46	25	-21	5.02E-06	1.03	0.93	0.14
INPP5D	23	2	-21	1.44E-08	60.83	48.65	0.32
PKN1	56	35	-21	0.05044	59.22	41.39	0.52
BPIFB1	80	60	-20	0.0840179	0.11	0.11	0.03
RNF166	28	8	-20	1.44E-08	16.37	15.28	0.10
CLASRP	26	6	-20	1.44E-08	27.58	25.50	0.11
RBMX2	37	18	-19	0.0247713	22.84	22.56	0.02
NAA60	46	27	-19	1.87E-08	105.11	95.31	0.14
SIRT4	47	28	-19	0.0002685	0.79	0.68	0.21
SLC7A8	28	10	-18	0.0112348	2.60	2.49	0.06
SPC24	31	13	-18	0.016683	6.08	5.49	0.15
ATHL1	31	13	-18	1.65E-08	3.98	3.19	0.32
SERPINA4	82	64	-18	0.0775353	0.10	0.06	0.58
ZC3H4	18	0	-18	1.44E-08	15.21	10.06	0.60
S1PR4	24	6	-18	1.94E-06	0.23	0.12	0.90
RCN3	95	77	-18	0.0088973	82.51	39.28	1.07
RGN	65	47	-18	0.0001121	0.18	0.06	1.51
STYX	17	0	-17	1.44E-08	26.56	25.30	0.07
MAP4K1	26	9	-17	0.0028362	0.93	0.54	0.79

PCDHB3	48	31	-17	0.0190562	0.04	0.02	1.26
CALD1	42	26	-16	0.0838025	571.85	513.31	0.16
APOE	17	1	-16	1.63E-06	4.60	4.09	0.17
C8orf44	17	1	-16	1.44E-08	14.52	12.54	0.21
AMPD2	70	54	-16	0.075339	41.20	35.57	0.21
C1orf86	27	11	-16	0.0381499	4.82	4.10	0.24
PKD1L1	76	60	-16	0.0703096	1.48	1.20	0.30
TCF3	34	18	-16	0.0039221	71.64	55.68	0.36
SPAG4	24	8	-16	1.67E-08	1.89	1.20	0.66
TMEM209	52	36	-16	0.0010652	1.92	1.17	0.71
PLEKHG6	30	14	-16	1.55E-08	0.34	0.12	1.47
PLEKHG6	30	14	-16	1.55E-08	0.34	0.12	1.47
ZNF493	15	0	-15	2.03E-08	5.54	5.51	0.01
ASGR1	73	58	-15	0.0408166	3.04	2.98	0.03
BAK1	21	6	-15	8.76E-05	3.54	2.95	0.27
ANKRD33	35	20	-15	0.0037076	0.09	0.07	0.42
BRCA1	18	4	-14	1.74E-06	5.17	5.14	0.01
MED24	14	0	-14	0.0002685	52.08	47.89	0.12
PHF17	14	0	-14	9.24E-05	13.84	12.17	0.19
SYCE1L	97	83	-14	0.0229148	16.68	14.18	0.23
OCRL	20	6	-14	0.0004179	16.60	13.84	0.26
DKKL1	19	5	-14	1.47E-08	0.17	0.12	0.46
DKKL1	19	5	-14	1.47E-08	0.17	0.12	0.46
C12orf36	93	79	-14	0.0989915	0.14	0.04	1.94
DGCR14	15	2	-13	1.44E-08	4.17	4.07	0.04
AGPAT6	13	0	-13	1.44E-08	68.63	66.13	0.05
MUTYH	13	0	-13	0.043238	4.19	4.03	0.06
DMPK	23	10	-13	0.0004917	39.58	37.02	0.10
LINC00574	13	0	-13	0.0823246	0.13	0.12	0.10
TOE1	13	0	-13	0.043238	3.62	3.14	0.21
SLC5A4	100	87	-13	0.014153	0.10	0.08	0.33
IDUA	13	0	-13	1.52E-08	8.72	5.44	0.68
DMKN	14	1	-13	0.0224113	0.09	0.05	0.78
C1QTNF1	35	22	-13	0.0308779	0.46	0.22	1.06
TSSK3	20	8	-12	1.67E-08	0.53	0.48	0.16
APOBEC3D	12	0	-12	0.0780912	11.13	9.90	0.17
MRPL28	20	8	-12	0.0025746	39.19	34.56	0.18
KBTBD7	39	27	-12	0.0039552	2.99	2.59	0.21
PI4KB	13	1	-12	1.47E-08	31.10	26.02	0.26
PI4KB	13	1	-12	1.47E-08	31.10	26.02	0.26
EDARADD	12	0	-12	3.66E-08	0.20	0.16	0.29
SUMO2	28	16	-12	2.15E-06	441.13	338.71	0.38
RHBDL1	27	15	-12	4.01E-06	0.13	0.10	0.50
MORN3	91	79	-12	0.0607901	0.67	0.45	0.58
RFESD	12	0	-12	1.44E-08	0.57	0.22	1.35
RFESD	12	0	-12	1.44E-08	0.57	0.22	1.35
RBP5	23	12	-11	0.0004105	0.87	0.87	0.00
ASL	14	3	-11	1.44E-08	70.34	67.45	0.06
ZC4H2	26	15	-11	0.0005963	8.73	8.31	0.07
NUP160	27	16	-11	0.0443581	37.20	35.05	0.09
P2RY2	16	5	-11	7.63E-07	1.54	1.44	0.10
P2RY2	16	5	-11	7.63E-07	1.54	1.44	0.10
ZNF177	21	10	-11	0.0151378	10.72	9.81	0.13
PMVK	13	2	-11	3.89E-05	7.59	6.70	0.18
AR	24	13	-11	0.02855	2.56	2.19	0.23
ZNF682	37	26	-11	0.0202531	1.07	0.90	0.26
TUBGCP2	22	11	-11	1.55E-08	15.68	12.74	0.30
CRISPLD2	11	0	-11	2.32E-08	2.74	2.11	0.38
ERICH1	13	2	-11	1.51E-08	37.35	23.08	0.69

MGAT5B	21	10	-11	0.0012686	0.15	0.08	0.91
LZTS2	11	1	-10	1.93E-07	10.24	10.10	0.02
ASL	18	8	-10	2.56E-06	70.34	67.45	0.06
GRM4	13	3	-10	1.51E-08	0.00	0.00	0.08
NOP2	12	2	-10	0.0001167	24.14	22.62	0.09
WDR38	29	19	-10	0.0148011	0.05	0.05	0.10
C2orf68	16	6	-10	2.29E-07	7.45	6.91	0.11
CREB3L1	12	2	-10	1.10E-06	1.10	1.01	0.12
CD320	71	61	-10	0.0548656	25.89	23.20	0.16
POC5	24	14	-10	0.0027068	6.05	4.78	0.34
SEMA4D	99	89	-10	0.0438592	4.05	3.11	0.38
CCDC78	21	11	-10	0.0002496	0.10	0.07	0.57
DDX43	96	86	-10	0.0148694	0.26	0.17	0.63
LGALS1	10	0	-10	6.26E-08	1405.19	820.91	0.78
TTC25	30	20	-10	0.0064954	0.13	0.07	0.78
PKP3	59	49	-10	0.0549248	0.18	0.09	1.04

Table S6. Top 50 significantly overrepresented biological process GO terms for genes with expression patterns corresponding to differential promoter methylation under arteriogenic shear stress waveforms

Gene Set Name	# Genes in Gene Set (K)	# Genes in Overlap (k)	k/K	p-value	FDR
BIOPOLYMER_METABOLIC_PROCESS	1684	98	0.06	2.52E-29	2.08E-26
NUCLEOBASENUCLEOSIDENUCLEOTIDE_AND_ NUCLEIC_ACID_METABOLIC_PROCESS	1244	71	0.06	6.79E-21	2.80E-18
RNA_METABOLIC_PROCESS	841	54	0.06	2.57E-18	7.08E-16
PROTEIN_METABOLIC_PROCESS	1231	65	0.05	1.62E-17	3.35E-15
TRANSCRIPTION	753	45	0.06	2.44E-14	4.02E-12
CELLULAR_PROTEIN_METABOLIC_PROCESS	1117	55	0.05	9.61E-14	1.32E-11
TRANSCRIPTION_DNA_DEPENDENT	636	40	0.06	1.36E-13	1.45E-11
RNA_BIOSYNTHETIC_PROCESS	638	40	0.06	1.51E-13	1.45E-11
CELLULAR_MACROMOLECULE_METABOLIC_PROCESS	1131	55	0.05	1.58E-13	1.45E-11
REGULATION_OF_METABOLIC_PROCESS	799	44	0.06	7.76E-13	6.41E-11
SIGNAL_TRANSDUCTION	1634	66	0.04	2.63E-12	1.97E-10
BIOPOLYMER_MODIFICATION	650	37	0.06	2.07E-11	1.43E-09
BIOSYNTHETIC_PROCESS	470	31	0.07	2.38E-11	1.51E-09
REGULATION_OF_CELLULAR_METABOLIC_PROCESS	787	41	0.05	2.66E-11	1.57E-09
PROTEIN_MODIFICATION_PROCESS	631	36	0.06	3.65E-11	2.01E-09
NEGATIVE_REGULATION_OF_BIOLOGICAL_PROCESS	677	37	0.05	6.58E-11	3.39E-09
NEGATIVE_REGULATION_OF_METABOLIC_PROCESS	262	22	0.08	2.13E-10	9.84E-09

REGULATION_OF_GENE_EXPRESSION	673	36	0.05	2.15E-10	9.84E-09
TRANSCRIPTION_FROM_RNA_POLYMERASE_II_PROMOTER	457	29	0.06	2.59E-10	1.12E-08
NEGATIVE_REGULATION_OF_CELLULAR_PROCESS	646	35	0.05	2.73E-10	1.13E-08
INTRACELLULAR_SIGNALING_CASCADE	667	35	0.05	6.35E-10	2.50E-08
REGULATION_OF_ NUCLEOBASENUCLEOSIDENUCLEOTIDE_AND_NUCLEIC_ACID _METABOLIC_PROCESS	618	33	0.05	1.27E-09	4.78E-08
NEGATIVE_REGULATION_OF_CELLULAR_METABOLIC_PROCESS	259	20	0.08	5.94E-09	2.13E-07
NEGATIVE_REGULATION_OF_ NUCLEOBASENUCLEOSIDENUCLEOTIDE_AND_NUCLEIC_ACID _METABOLIC_PROCESS	211	18	0.09	7.23E-09	2.48E-07
REGULATION_OF_TRANSCRIPTION	566	30	0.05	8.50E-09	2.80E-07
TRANSPORT	795	36	0.05	1.70E-08	5.38E-07
REGULATION_OF_TRANSCRIPTIONDNA_DEPENDENT	461	26	0.06	2.43E-08	7.43E-07
REGULATION_OF_RNA_METABOLIC_PROCESS	471	26	0.06	3.73E-08	1.10E-06
CELLULAR_BIOSYNTHETIC_PROCESS	321	21	0.07	4.50E-08	1.24E-06
MACROMOLECULE_BIOSYNTHETIC_PROCESS	321	21	0.07	4.50E-08	1.24E-06
ESTABLISHMENT_OF_LOCALIZATION	870	37	0.04	5.33E-08	1.42E-06
CELLULAR_COMPONENT_ASSEMBLY	298	20	0.07	6.19E-08	1.60E-06
PROTEIN_AMINO_ACID_PHOSPHORYLATION	279	19	0.07	1.05E-07	2.62E-06
MACROMOLECULAR_COMPLEX_ASSEMBLY	280	19	0.07	1.11E-07	2.68E-06
POSITIVE_REGULATION_OF_BIOLOGICAL_PROCESS	709	32	0.05	1.14E-07	2.68E-06
POST_TRANSLATIONAL_PROTEIN_MODIFICATION	476	25	0.05	1.75E-07	4.00E-06

LIPID_METABOLIC_PROCESS	325	20	0.06	2.51E-07	5.60E-06
NEGATIVE_REGULATION_OF_TRANSCRIPTION	188	15	0.08	3.06E-07	6.64E-06
POSITIVE_REGULATION_OF_CELLULAR_PROCESS	668	30	0.04	3.14E-07	6.64E-06
LIPID_BIOSYNTHETIC_PROCESS	97	11	0.11	3.55E-07	7.32E-06
PHOSPHORYLATION	313	19	0.06	6.12E-07	1.23E-05
CELLULAR_LIPID_METABOLIC_PROCESS	255	17	0.07	6.55E-07	1.29E-05
CARBOXYLIC_ACID_METABOLIC_PROCESS	178	14	0.08	8.97E-07	1.72E-05
ORGANIC_ACID_METABOLIC_PROCESS	180	14	0.08	1.03E-06	1.92E-05
REGULATION_OF_MOLECULAR_FUNCTION	324	18	0.06	4.18E-06	7.67E-05
MAPKKK_CASCADE_GO_0000165	104	10	0.10	5.48E-06	9.83E-05
REGULATION_OF_PROTEIN_KINASE_ACTIVITY	155	12	0.08	6.30E-06	1.11E-04
REGULATION_OF_KINASE_ACTIVITY	157	12	0.08	7.18E-06	1.23E-04
POSITIVE_REGULATION_OF_TRANSFERASE_ACTIVITY	86	9	0.10	8.04E-06	1.35E-04
REGULATION_OF_CATALYTIC_ACTIVITY	276	16	0.06	8.31E-06	1.35E-04

Figure S1. Similar degree of methylation coverage in HUVECs exposed to biomimetic shear stress waveforms.

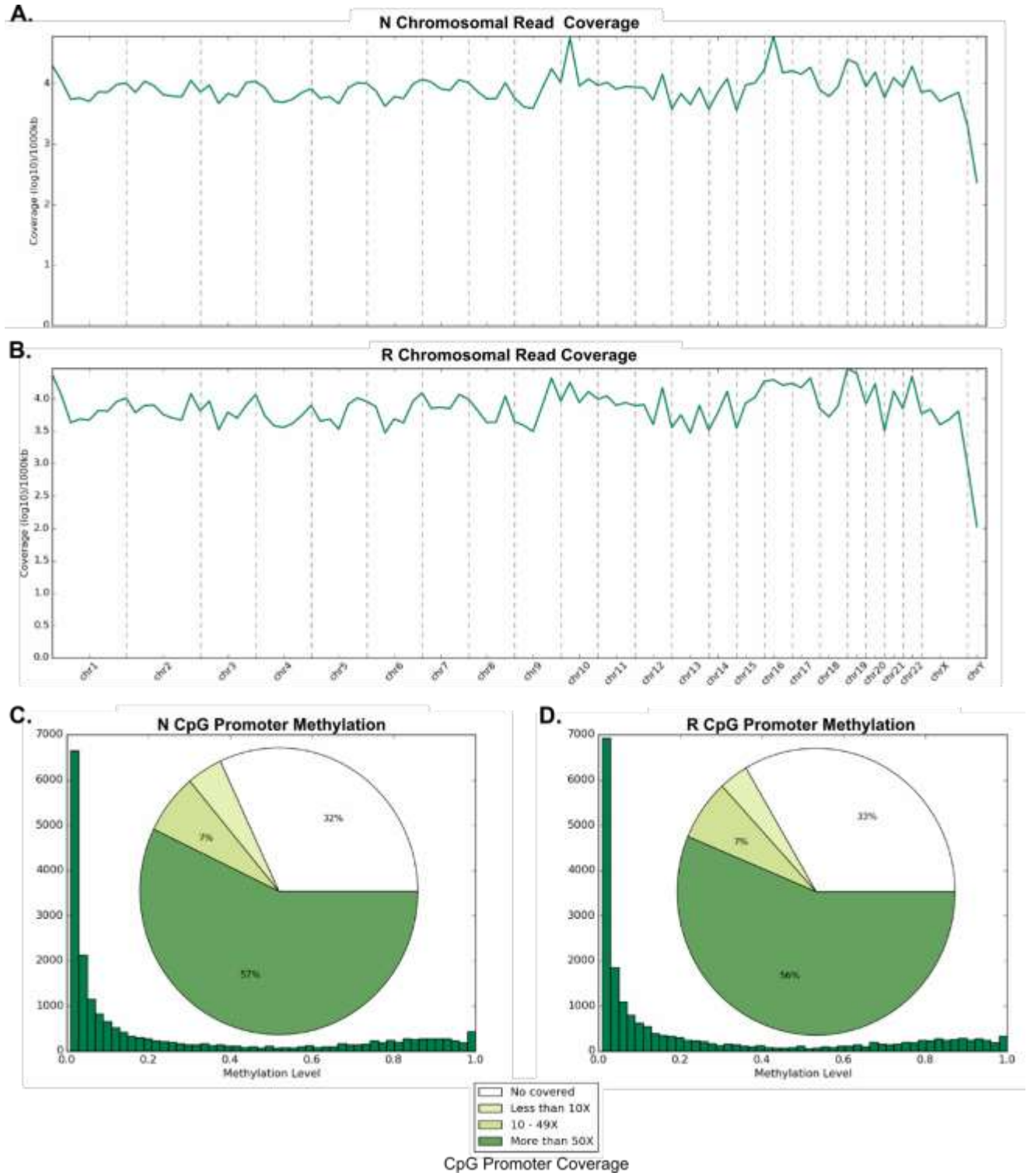

A-B, Representation of methylation read coverage by chromosome across the genome for HUVECs exposed to non-reversed (N) and reversed (R) shear stress waveforms described in Figure 2A. **C-D,** Pie charts of CpG site coverage in gene promoter region in HUVECs exposed to non-reversed (N) and reversed (R) shear stress waveforms.

Figure S2. DNA methylation across different gene regions.

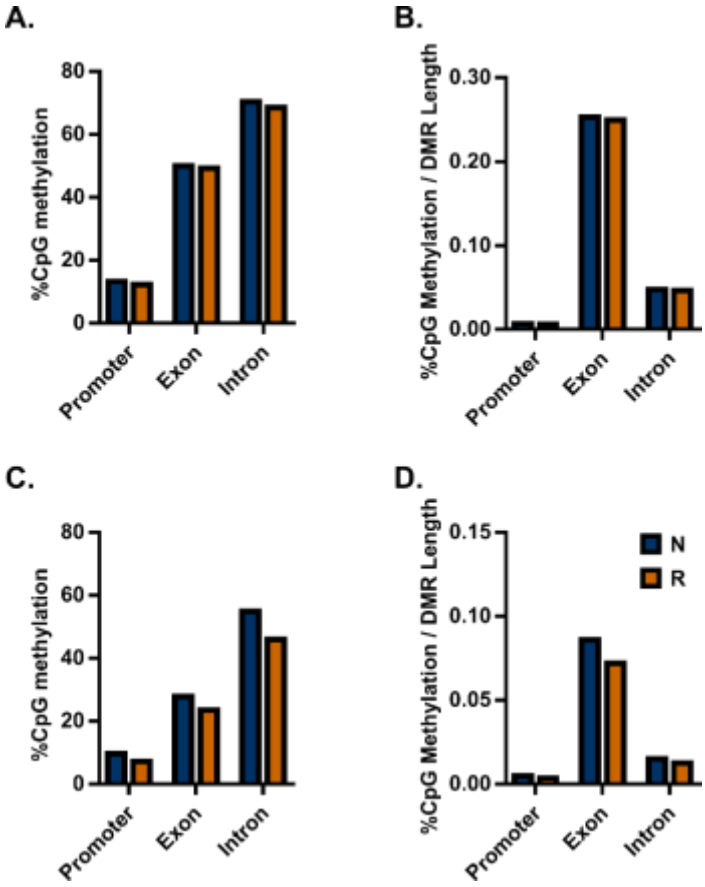

A-B, Mean %CpG methylation (#methylated CpG sites / total CpG sites in given DMR) and mean %CpG methylation normalized by DMR length in promoter, exon, and intron gene regions for all DMRs with ≥10x CpG coverage in a given DMR. **C-D,** Mean %CpG methylation and mean %CpG methylation normalized to DMR length in promoter, exon, and intron gene regions for all DMRs with ≥10x CpG coverage in a given DMR and FDR<0.1 between HUVECs exposed to non-reversed (blue) and reversed (orange) shear stress waveforms.

Figure S3. DNA methylation negatively correlates to mRNA expression in gene promoter regions.

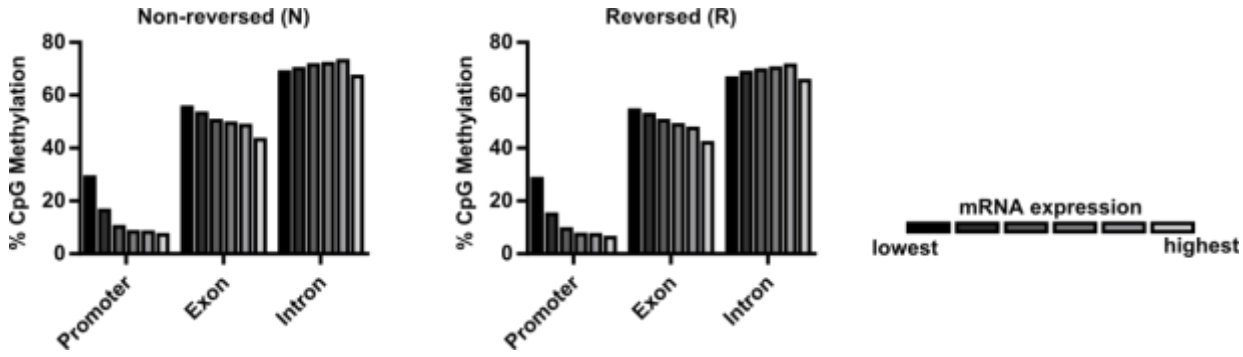

Raw mRNA expression (FPKM) from HUVECs exposed to either non-reversed/N or reversed/R shear stress waveforms was ordered from lowest mRNA expression to highest and divided into six, equal sized bins. Mean %CpG methylation was determined for each bin within the promoter, exon, and intron gene regions. Only DMRs with ≥10x CpG coverage were included in the analysis.

Figure S4. Genome-wide mRNA expression patterns in HUVECs exposed to arteriogenesis biomimetic shear stress waveforms.

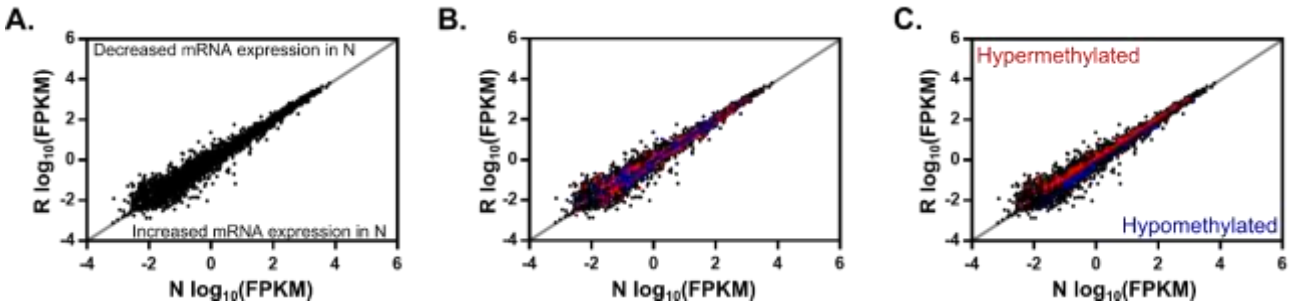

A-C **,** HUVECs were exposed to biomimetic shear stress waveforms, RNA was isolated 6-hours post-FAL, and genome- wide mRNA expression was determined by mRNA-sequencing. Scatter plots indicate relative expression of each gene represented in both non-reversed and reversed conditions and contained in our RRBS dataset (17,227 total). **A,** Indicates all genes corresponding to promoter regions of genes with a methylation ratio difference ≥ |0.10| and FDR<0.1 between non-reversed and reversed conditions. **B**, Contains all 17,227 genes, where genes with significantly hypermethylated promoters in N relative to R are red and hypomethylated genes are blue, corresponding to Table S3. **C,** All 17,227 genes, where significantly hyper- or hypomethylated genes are also downregulated or upregulated, respectively, in N relative to R, corresponding to Table S4 and Table S5. FPKM = fragments per kilobase of transcript per million mapped reads.

Figure S5. Top 50 most significantly overrepresented gene ontology (GO) biological processes.

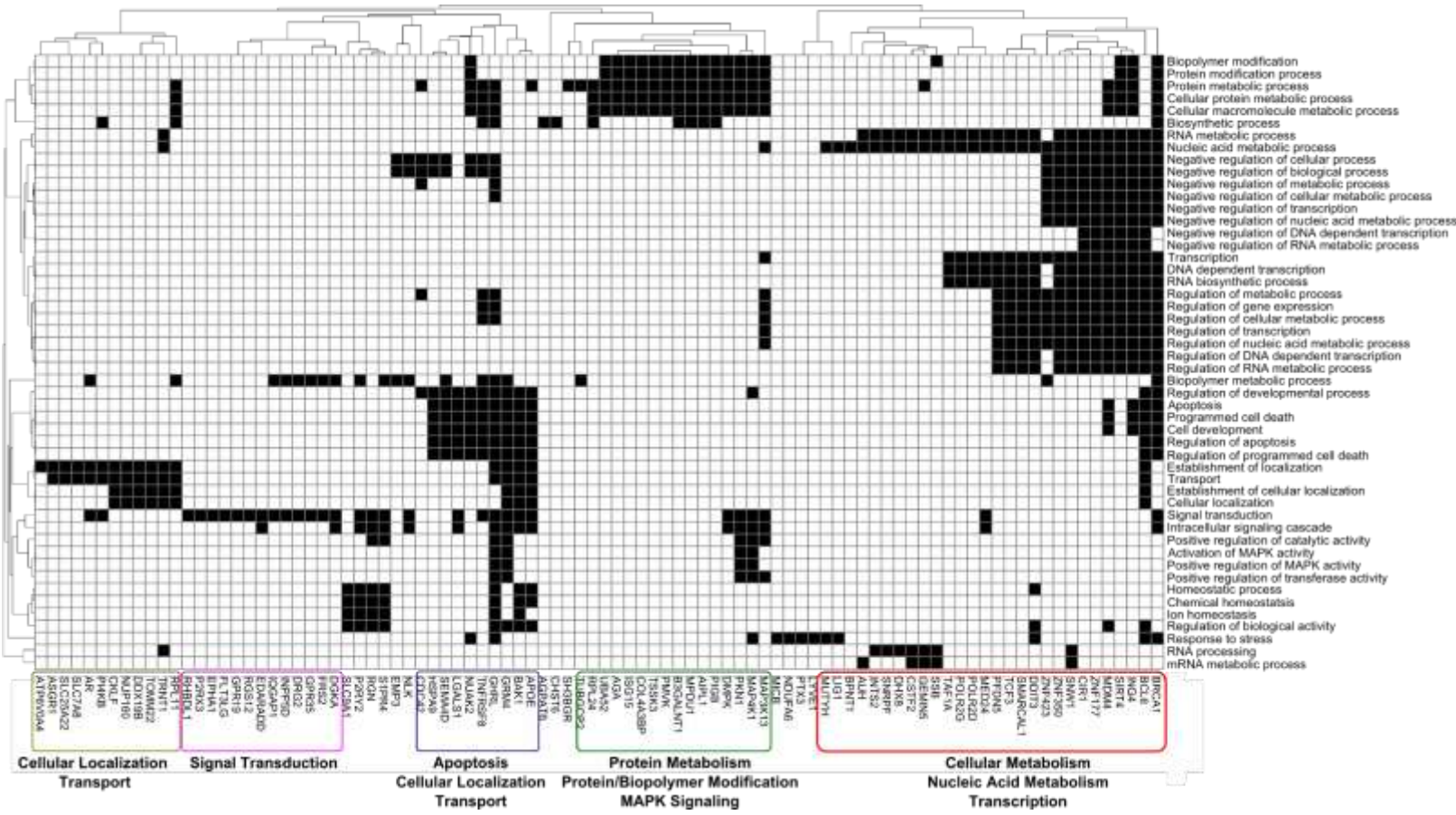

Heat map of the top 50 significantly overrepresented biological process GO terms (columns) for genes with differential changes in expression corresponding to significantly different CpG promoter methylation in non-reversed vs. reversed conditions (i.e. genes that were down-regulated and had a hypermethylated promoter or were up-regulated and had a hypomethylated promoter in non-reversed versus reversed conditions) as listed in Table S4 and Table S5. Black indicates the presence of a gene in a GO process whereas white indicates its absence. Only genes present in at least one GO process are shown.

Figure S6. DNMT1 inhibition also improves the arteriogenic capacity of non-reversed collateral artery segments in Balb/c mice.

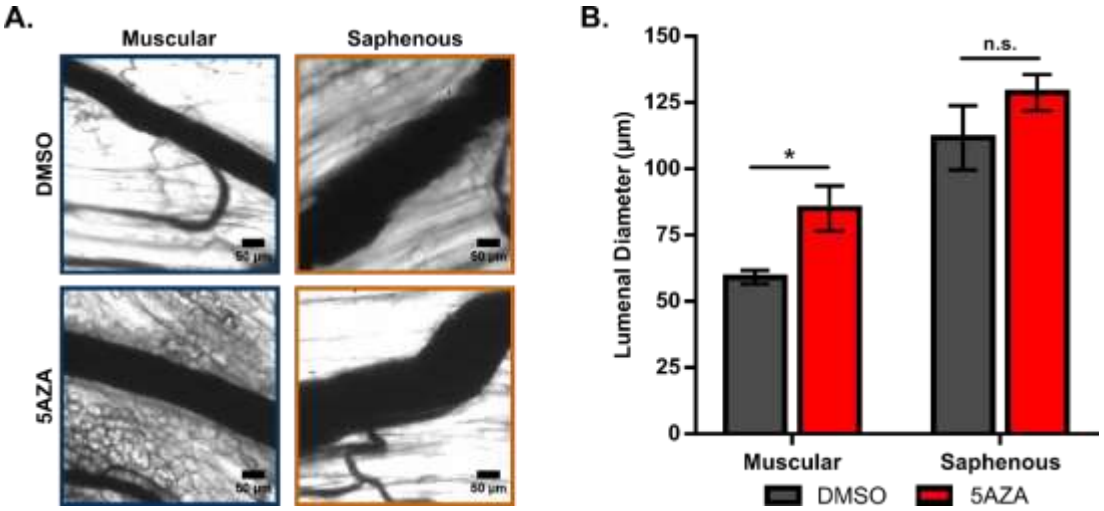

A, Representative vascular cast images from muscular (non-reversed) and saphenous (reversed) collateral artery regions 28 days post-FAL from Balb/c mice treated according to Figure 4A. (Scale Bar = 50µm). **B,** Bar graph of regional lumenal diameter in DMSO or 5AZA treated mice. *$p<0.05$ between DMSO and 5AZA treated mice; Two-way ANOVA followed by a Holm-Sidak multiple comparisons test. Data are mean ± SEM.

Figure S7V. Pericollateral Mac3+ macrophages increased in non-reversed collateral segments with inhibition of DNMT1.

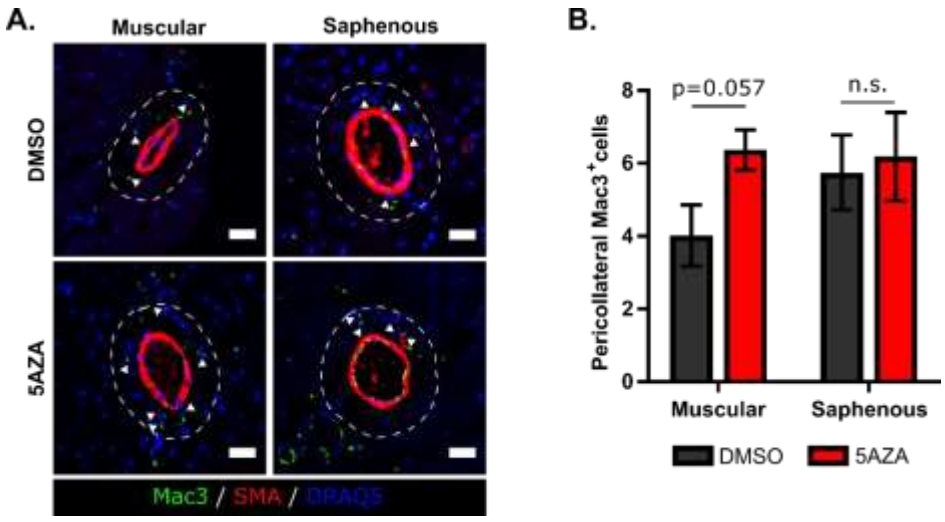

A, Representative cross-sections of gracilis collateral artery regions immunolabeled for macrophage marker, Mac3 (green), smooth muscle alpha actin (SMαA, red), and nuclei (DRAQ5, blue) in C57BL/6 mice treated with 5AZA or DMSO-treated control on day 17 post-FAL according to Figure 4A. Dotted line indicates the pericollateral region (25μm from vessel wall) used for quantification. Arrowheads indicate $Mac3^+$ cells (Scale bar=25μm). **B,** Bar graph of pericollateral $Mac3^+$ cells for 5AZA or DMSO treated mice (n=4). Student's t-test, Data are mean ± SEM.

Figure S8. DNMT1 inhibition leads improves perfusion recovery in aged Balb/c mice.

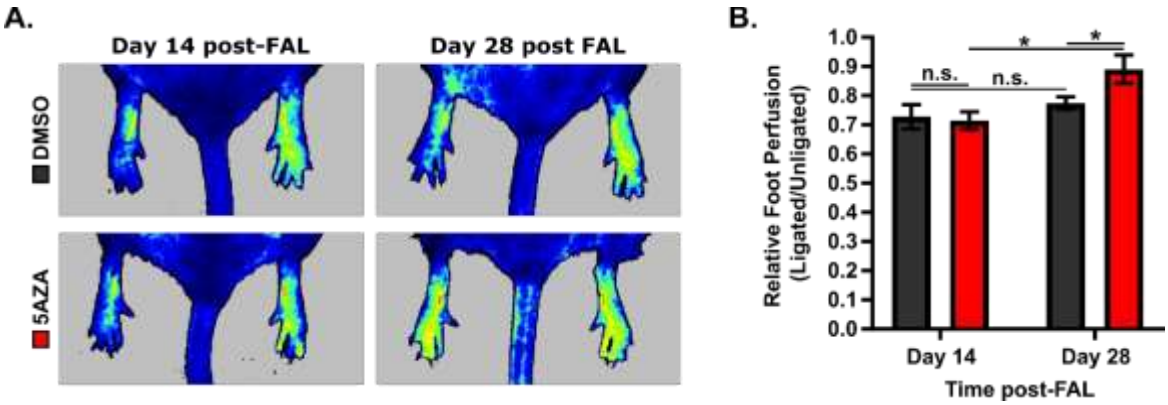

A) Representative images and B) bar graph of relative foot perfusion recovery as assessed by laser Doppler perfusion imaging in 5AZA or DMSO-treated aged (10-11 months old) Balb/c mice. Mice were treated with 5AZA (n=7) or DMSO (n=6) i.p. daily starting at day 14 post-FAL, according to Figure 4A. Two-way ANOVA followed by Holm-Sidak test for multiple comparisons. *$p<0.05$; data are mean ± SEM.